THE EFFECTS OF SPECTRAL ESTIMATION ON MATCHED FILTER DESIGN

by

Kenneth Alan Becker

Thesis submitted to the Faculty of the

Virginia Polytechnic Institute and State University

in partial fulfillment of the requirements for the degree of

Master of Science

in

Electrical Engineering

APPROVED:

A. A. (Louis) Beex, Chairman

Richard L. Moose

Ioannis M. Besieris

May, 1985.

Blacksburg, Virginia

THE EFFECTS OF SPECTRAL ESTIMATION ON MATCHED FILTER DESIGN

by

Kenneth Alan Becker

A. A. (Louis) Beex, Chairman

Electrical Engineering

(ABSTRACT)

Moving-average matched filters (MAMF's) are a class of digital filters used to detect the presence of a known signal in noise. Designing matched filters requires knowledge of the structure of the signal and the noise. If the spectral density of the noise is not known or is changing with time its spectral characteristics must be estimated. Since spectral estimators derive their estimates from a random process realization, the estimates themselves are probabilistic in nature. The performance of MAMF's based on these estimates must, in turn, be distributed in a probabilistic sense.

This thesis investigates the performance of MAMF's designed on the basis of several different spectral estimators. Theoretical aspects of MAMF's and spectral estimators are reviewed and developed. A simulation system is used to exercise the spectral estimators and MAMF's and to provide comparative performance data. A graphical representation, using contour plots, is developed and can be

used to predict the performance of a given MAMF/signal/spectral estimator combination.

Finally, several methods of generating MAMF's whose output performance is relatively insensitive (or robust) to the probabilistic variations caused by the spectral estimators are developed and evaluated. The latter incorporates knowledge of the empirical distribution of the particular spectral estimator used, as well as the freedom of manipulating the signal.

ACKNOWLEDGEMENTS

Gratitude and appreciation are extended to Dr. A. A. Beex, who provided the impetus for this study and for his unbelievable patience in seeing it finished; to Dr. R.L. Moose and Dr. I.M. Besieris who agreed to serve on my committee; and to Jane, my wife, for her support and understanding these past three years.

TABLE OF CONTENTS

LIST OF ILLUSTRATIONS

LIST OF TABLES

1.0 INTRODUCTION

The problem of detecting a known signal in the presence of additive noise has been known for some time [DON]. Both analog designs based on continuous time and discrete components [PAP] [ZHT] and digital designs based on sampled data and digital components [RBG] are possible. Applications for matched filters can be found in radar (the detection of targets) [MIS] and in communications (the detection of digitally coded signals) [ZHT]. This thesis will work with moving-average matched filters (MAMF's), a subset of matched filters for discrete time applications. This is done for several reasons. First, MAMF's can be designed very efficiently by solving a linear Toeplitz system of equations, given a signal and the autocorrelation sequence of the noise [KVM]. Second, they are easy to implement as digital filters [AOS], and are guaranteed to be stable. Finally, the performance of MA, or finite impulse response (FIR) filters, quickly approaches that of other causal digital filters (such as ARMA or infinite impulse response (IIR) filters) as the length of the MA filter increases. For these reasons, a large amount of interest is currently being focused on the design of MAMF's.

Designing a matched filter requires two pieces of information: First, knowledge about the signal in the form

of a continuous- or discrete-time description, or a continuous or discrete spectrum; and second, knowledge about the noise, as either a continuous autocorrelation, a discrete autocorrelation, or a continuous or discrete power spectral density. While the signal information is usually under the control of, and therefore known to the designer, the noise information is in most circumstances not known in advance. Typical examples of such conditions occur in radar or communications systems which move, or can be moved, into different environments with different kinds of noise or interference [AFS] [MIS]. In such cases, the noise spectral information must be continuously estimated. Note that the noise spectral estimates are based on noisy measurements and these estimates are themselves random variables; therefore, MAMF designs based on these estimates will have probabilistic performance descriptors in terms of MAMF output signal-to-noise ratio (SNR). The probabilistic nature of MAMF's using estimated spectral information is not well covered in the literature. This thesis aims at reducing this problem by providing data about the probabilistic nature of MAMF's designed on the basis of estimates for the noise information.

A good deal of work has been done on MAMF systems [CGS] [GMS] [DMB] [RMB] [WBT]. In particular, several authors have, given a particular noise spectral density, determined the signal vector $\underline{s}_{max}$ that will result in a MAMF with

maximum output SNR [JMA] [JAC] [MBT]. Two papers by the author [BEB] [BCB] have discussed the use of this signal vector in a simulation system where the performance of MAMF's using $\underline{s}_{max}$ and various noise spectral estimation schemes were compared. This thesis continues that work in more detail.

Another current area of research involving MAMF's is robust filtering. In robust filtering an attempt is made to design a MAMF whose output SNR is less sensitive in some way to either changes in the noise spectra, distortion of the signal, or both [VPK]. In this thesis, the primary concern will be with errors in the estimation of the noise spectra. While there has been a good deal of work in this area there have also been some apparent limitations. First, several papers have made the assumption that the spectrum of the unknown noise is banded (See Figure 1) [KVP] [HVP] between some upper bound and lower bound functions of frequency. Furthermore, this assumption also assumes that the spectral density exists, that is, the associated autocorrelation is non-negative definite. Many noise spectral estimators generate autocorrelation sequences of the noise. Under the proper circumstances, minor changes in an estimated autocorrelation sequence can cause wide variations in the spectral density of the associated noise ([AOS], pp. 543-548). Second, another paper makes the statement that the estimated noise correlation sequence should be close to the

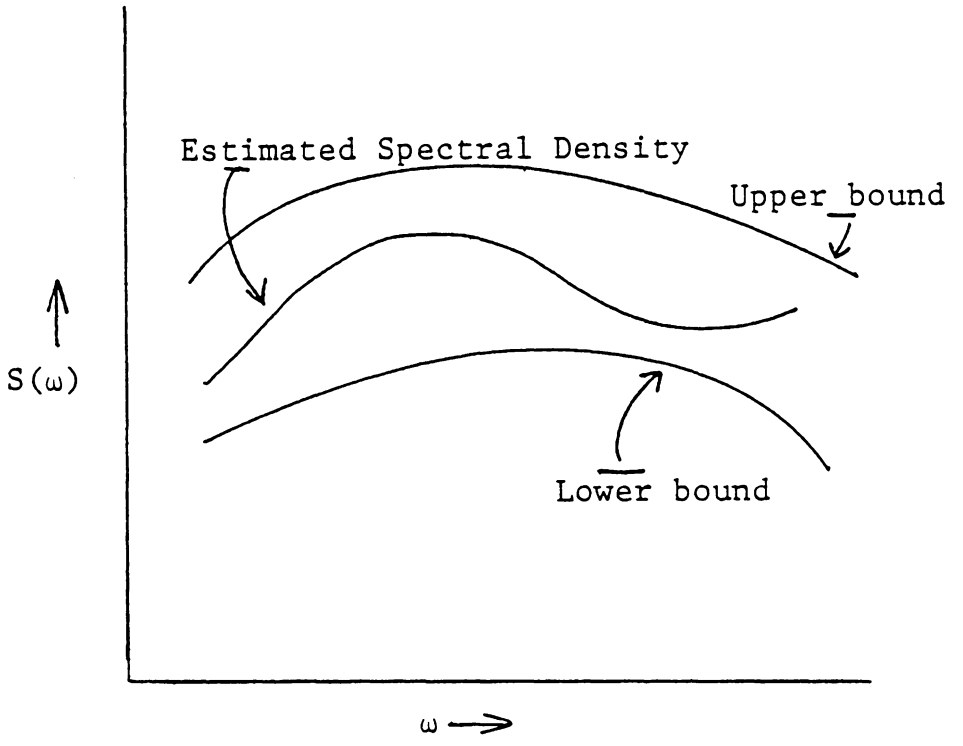

Figure 1. Example of spectral bounds.

actual noise correlation sequence in some respect [VPK]. This may not be true in the case where the noise is non-stationary. Non-stationarity of the noise raises a conflicting design requirement: short data sequences must be used in order to estimate the changing noise spectra. However, these short data sequences increase the variance of the correlation estimates, thereby losing the sought-after closeness. Note that designing a robust matched filter based on spectral bounds usually requires some form of transformation operation on estimated correlation sequences. In a second paper by the author [BCB] and in this thesis, a robust filter design method is investigated which uses information from estimated correlation sequences to directly derive a robust filter. Since this method does not require that the estimated correlation sequences be transformed into spectra, it is expected that this method will generate a more robust matched filter than one based on spectral bounds.

The theoretical development of correlation estimators and MAMF's is covered in Chapter two. Special attention is given in this chapter to the characteristics of symmetric Toeplitz matrices, as the design and performance of MAMF's is bound up in these matrices. In Chapter three several simulation methods used to evaluate the performance of MAMF's in conjunction with different spectral estimators and signals are developed and investigated. Central to this theme is a simulation system that generates colored random noise and

correlation estimates of that noise and a graphical comparison method that allows one to predict the performance of a MAMF/signal combination with a particular correlation estimator. Several methods of generating robust filters and an investigation into the trade-offs between maximum output SNR of a MAMF and robustness are covered in Chapter four. The performance of several robust matched filters is evaluated.

2.0 THEORETICAL DEVELOPMENT.

2.1 PROPERTIES OF SYMMETRIC TOEPLITZ MATRICES.

In this thesis a good deal of attention will be placed on the properties of the correlation matrix, a symmetric, real-valued Toeplitz matrix. A Toeplitz matrix is defined as a matrix in which the elements are identical on any line parallel to the main diagonal. Since the Toeplitz matrices to be worked with have real elements and are symmetric about the main diagonal, they are also in the class of Hermitian matrices. Hermitian matrices have several interesting properties which also apply to Toeplitz matrices.

First, Hermitian matrices are based on the Hermitian form, a real-valued polynomial of the form

$$P_N = \sum_{i=1}^{N} \sum_{j=1}^{N} m_{i,j} x_i^* x_j \qquad (1)$$

which in vector form becomes

$$P_N = [x_1^* \; x_2^* \; \ldots \; x_N^*] \begin{bmatrix} m_{11} & m_{12} & \cdot & \cdot & m_{1N} \\ . & . & . & . & . \\ . & . & . & . & . \\ m_{N1} & m_{N2} & \cdot & \cdot & m_{NN} \end{bmatrix} \begin{bmatrix} x_1 \\ . \\ . \\ x_N \end{bmatrix} \quad (2)$$

$$= \underline{x}^H M_1 \underline{x}$$

where the m_{ij} and x_i are complex numbers, the complex conjugate of x_i is x_i^*, and the complex conjugate transpose of $\underline{x}$ is $\underline{x}^H$. It is easy to show that M_1 must be symmetric about the main diagonal. Since every Hermitian form is assumed to be real-valued, we have

$$\begin{aligned} \underline{x}^H M_1 \underline{x} &= (\underline{x}^H M_1 \underline{x})^* \\ &= \underline{x}^T M_1^* \underline{x}^* \\ &= \underline{x}^H M_1^H \underline{x} \end{aligned} \quad (3)$$

where M_1^* is the complex conjugate of M_1 and M_1^H is the complex conjugate transpose of M_1; hence a matrix M can be found such that

$$\begin{aligned} \underline{x}^H M_1 \underline{x} &= \underline{x}^H M_1 \underline{x}/2 + \underline{x}^H M_1^H \underline{x}/2 \\ &= \underline{x}^H (M_1 + M_1^H) \underline{x}/2 \\ &= \underline{x}^H M \underline{x} \end{aligned} \quad (4)$$

where $M \equiv (M_1 + M_1^H)/2$ [CTC]. It follows immediately that $M = M^H$. Thus, every Hermitian form can be written as $\underline{x}^H M \underline{x}$

with $M = M^H$. A matrix M with the property $M = M^H$ is defined as a Hermitian matrix.

Next it is shown that the eigenvalues of a Hermitian matrix are real. Let λ be an eigenvalue of a Hermitian matrix M and $\underline{e}$ be the eigenvector associated with that eigenvalue. Then,

$$\begin{aligned} \underline{e}^H M \underline{e} &= \underline{e}^H \lambda \underline{e} \\ &= \lambda \underline{e}^H \underline{e} \end{aligned} \tag{5}$$

Since $\underline{e}^H M \underline{e}$ must be a real number (from the definition of a Hermitian matrix), λ must also be a real number.

The Jordan-form representation of a Hermitian matrix is a diagonal matrix. This will be shown by contradiction. To start, suppose that there exists a Hermitian matrix M that has a generalized eigenvector $\underline{e}$ of rank $k \geq 2$. Then, the matrix $(M - \lambda_i I)$ has the property that

$$(M - \lambda_i I)^k \underline{e} = \underline{0} \tag{6}$$

while

$$(M - \lambda_i I)^{k-1} \underline{e} \neq \underline{0} \tag{7}$$

for some eigenvalue λ_i of M. Therefore, for $k \geq 2$, it can be shown that:

$$
\begin{aligned}
0 &= \left[(M - \lambda_i I)^{k-2}\underline{e}\right]^H (M - \lambda_i I)^k \underline{e} \\
&= \underline{e}^H (M - \lambda_i I)^{k-2} (M - \lambda_i I)^k \underline{e} \\
&= \| (M - \lambda_i I)^{k-1} \underline{e} \|^2
\end{aligned} \tag{8}
$$

which implies that

$$
(M - \lambda_i I)^{k-1} \underline{e} = \underline{0} \tag{9}
$$

which contradicts the generalized eigenvector assumption. Therefore, there exists no Jordan block whose order is greater than one. Further, this implies that [CTC] there is a nonsingular matrix P such that

$$
\Lambda = PMP^{-1} \tag{10}
$$

where Λ is a matrix with the eigenvalues of M on the diagonal and zeroes elsewhere.

Finally, it is of interest that the eigenvectors of a Hermitian matrix that correspond to different eigenvalues are orthogonal and can therefore be made orthonormal. To show this, first consider $\underline{e}_i$ and $\underline{e}_j$, the distinct eigenvectors corresponding to the distinct eigenvalues λ_i and λ_j of M, such that $M\underline{e}_i = \lambda_i \underline{e}_i$ and $M\underline{e}_j = \lambda_j \underline{e}_j$. Then,

$$
\underline{e}_j^H M \underline{e}_i = \underline{e}_j^H \lambda_i \underline{e}_i = \lambda_i \underline{e}_j^H \underline{e}_i \tag{11}
$$

and

$$\underline{e}_i^H M \underline{e}_j = \underline{e}_i^H \lambda_j \underline{e}_j = \lambda_j \underline{e}_j^H \underline{e}_i \tag{12}$$

Subtracting Equation 11 from Equation 12 we have

$$(\lambda_i - \lambda_j)(\underline{e}_j^H \underline{e}_i) = 0 \tag{13}$$

Since λ_i and λ_j are distinct, $\underline{e}_j$ and $\underline{e}_i$ must be orthogonal. Second, since the product of an eigenvector and a constant is still an eigenvector, the eigenvectors associated with M can be made orthonormal. Note that if M is real, then the eigenvectors of M will also be real.

Now consider a symmetric Toeplitz matrix M and its set of orthonormalized eigenvectors $\underline{u}_i$. If these vectors are placed into the columns of a rotation matrix U, then multiplying U by its transpose yields

$$U^T U = \begin{bmatrix} \underline{u}_1^T \\ . \\ . \\ . \\ \underline{u}_N^T \end{bmatrix} [\underline{u}_1 \; . \; . \; \underline{u}_N] = I \tag{14}$$

or

$$U^T = U^{-1} \tag{15}$$

Since the matrices U and U^{-1} are those matrices which transform M into its Jordan form representation, we have

$$U^{-1}MU = \Lambda = U^{T}MU \tag{16}$$

where Λ is a matrix with the eigenvalues of M on the diagonal and zeroes elsewhere.

2.2 NON-NEGATIVE DEFINITENESS AND AUTOCORRELATIONS

A critical point in this study is that the autocorrelation sequence for a wide-sense stationary process is non-negative definite, meaning that

$$\sum_i \sum_j x_i x_j \phi_{i-j} = \underline{x}^{T} \Phi \underline{x} \geq 0 \tag{17}$$

where the $\{x_i\}$ are any arbitrary real sequence and Φ is the Toeplitz matrix with first row $[\phi_0 \ \phi_1 \ \cdot \ \cdot \ \phi_{N-1}]$.

First, suppose that a noise power spectral density $S(\omega)$ exists such that

$$S(\omega) \geq 0 \qquad -\infty \leq \omega \leq \infty \tag{18}$$

and

$$S(-\omega) = S(\omega) \tag{19}$$

Then, there exists a function $\phi(\tau)$ such that

$$\phi(\tau) = \int_{-\infty}^{\infty} S(\omega) e^{j\omega\tau} d\omega/2\pi \tag{20}$$

That is, the inverse Fourier transform of the noise spectral density is the autocorrelation function of a wide-sense stationary process [CMG]. Then,

$$\phi(0) = \int_{-\infty}^{\infty} S(\omega) d\omega/2\pi \geq 0 \tag{21}$$

Therefore,

$$\begin{aligned} 0 &\leq \int_{-\infty}^{\infty} S(\omega) \left| \sum_i x_i e^{j\omega\tau i} \right|^2 d\omega/2\pi \\ &= \int_{-\infty}^{\infty} S(\omega) \left[\sum_i x_i e^{j\omega\tau i}\right]\left[\sum_k x_k e^{-j\omega\tau k}\right] d\omega/2\pi \\ &= \sum_i \sum_k x_i x_k \int_{-\infty}^{\infty} S(\omega) e^{j\omega\tau(i-k)} d\omega/2\pi \\ &= \sum_i \sum_k x_i x_k \phi(i-k) \end{aligned} \tag{22}$$

completing the proof [PAP].

The proof in the reverse direction, showing that the Fourier transform of a NND autocorrelation sequence is a nonnegative, even function of ω, is given by Buchner [SBU].

2.3 CORRELATION ESTIMATOR CHARACTERISTICS.

In this study, eight correlation estimators will be used to estimate the correlation matrix Φ. They will be based on short data lengths L to emphasize the differences between the different methods.

2.3.1 DEFINITIONS.

To set the stage for subsequent discussion, we now recall several definitions pertinent to estimators in general.

- An (un)biased correlation estimator is an estimator whose expected value is (not) equal to the actual correlation.

- A consistent correlation estimator is an estimator whose estimates c_i approach the actual correlation ϕ_i as the data length L used to generate that estimate approaches infinity, i.e.

$$\lim_{L\to\infty} P\{|c_i - \phi_i| > \varepsilon\} = 0 \qquad (23)$$

2.3.2 MOVING-AVERAGE ESTIMATORS.

The correlation matrix Φ_x, obtained by method x, will be the symmetric Toeplitz matrix generated by $[\phi_{x,k}]$.

The classical unbiased estimator is given by

$$\phi_{UB,k} = \frac{1}{L-k} \sum_{i=0}^{L-k-1} w_i w_{i+k} \qquad 0 \le k \le L-1 \tag{24}$$

which results in a correlation estimate Φ_{UB}. This estimator requires relatively few computations (on the order of L log(L) [AOS], pp. 155-165), is unbiased, and consistent. However, the correlation sequence estimate $\phi_{UB,k}$ is not necessarily non-negative definite. This will be shown by two methods. First, suppose that a data sequence $\{w_i\}$ exists as follows:

$$\underline{w} = [1 \quad -2 \quad 1] \tag{25}$$

When this data record is operated upon by the classical unbiased estimator, the resulting correlation sequence is

$$\underline{\phi}_{UB} = [2 \quad -2 \quad 1] \tag{26}$$

The Toeplitz matrix Φ_{UB} generated from this sequence is not non-negative definite, since its determinant has a value of minus two. Second, note that $\phi_{UB,k}$ is unbiased, since

$$\begin{aligned} E[\phi_{UB,k}] &= (1/(L-k)) \sum_{i=0}^{L-k-1} E[w_i w_{i+k}] \quad 0 \le k \le L-1 \\ &= \frac{(L-k)}{(L-k)} \phi_k \\ &= \phi_k \end{aligned} \tag{27}$$

Now consider the discrete Fourier transform S_L of the estimated correlation sequence $\{\phi_{UB,m}\}$:

$$S_L(e^{j\omega}) = \sum_{m=-(L-1)}^{L-1} \phi_{UB,m} e^{-j\omega m} \tag{28}$$

The expected value of this estimate is

$$E[S_L(e^{j\omega})] = \sum_{m=-(L-1)}^{L-1} E[\phi_{UB,m}] e^{-j\omega m}$$

$$= \sum_{m=-(L-1)}^{L-1} \phi_m e^{-j\omega m} \tag{29}$$

$$= \sum_{m=-\infty}^{\infty} w_{L,m} \phi_m e^{-j\omega m} \tag{30}$$

where $w_{L,m}$ defines a window sequence

$$w_{L,m} = \begin{matrix} 1 \\ 0 \end{matrix} \begin{cases} |m| < L \\ \text{otherwise} \end{cases} \tag{31}$$

Therefore, the expected value of $S_L(e^{j\omega})$ is the Fourier transform of the product of a rectangular window sequence and

the actual correlation sequence. Hence, $E[S_L(e^{j\omega})]$ can also be found by the convolution of the actual noise spectral density and the Fourier transform of the rectangular window [MGC],

$$R_L(e^{j\omega}) = \frac{\sin(\omega(2L-1)/2)}{\sin(\omega/2)} \tag{32}$$

Note that $R_L(e^{j\omega})$ is a real function that exhibits negative values. Therefore, depending upon the noise spectrum that is to be estimated, it is possible for the expected value of the estimated noise spectrum to be negative. The corresponding estimated correlation sequences must then sometimes not be non-negative definite [SBU].

The classical biased estimator is given by

$$\phi_{CB,k} = (1/L) \sum_{i=0}^{L-k-1} w_i w_{i+k} \qquad 0 \le k \le L-1 \tag{33}$$

which results in a correlation estimate ϕ_{CB}. This estimator, while biased, requires relatively few numerical calculations (on the order of L log(L)), is NND, and becomes consistent as L increases without bound.

To show that it is biased and becomes consistent in the limit, we take expected values and find that

$$E[\phi_{CB,k}] = E[\phi_{UB,k}](L-k)/L \quad 0 \le k \le L-1 \qquad (34)$$
$$= \phi_k(L-k)/L$$

Note that

$$\lim_{L\to\infty} \phi_k(L-k)/L = \phi_k \qquad (35)$$

showing consistency in the limit. The expected value of the CB estimator looks like the product of the actual autocorrelation sequence and a triangular window sequence. Therefore, the expected value of the CB estimator sequence will be non-negative definite, since $T(e^{j\omega})$, the discrete Fourier transform of the triangular window, is

$$T(e^{j\omega}) = \frac{\sin^2(\omega L/2)}{L(\sin(\omega/2))^2} \qquad (36)$$

Since both the spectrum of the noise and the transform of the window sequence are nonnegative for all ω, the expected value of the estimated spectra will also be nonnegative, thus assuring the non-negativity of the expected value of the Fourier transform of the correlation sequence.

It can in fact be shown that every CB estimate is non-negative definite. Upon examination of the correlation estimator, we find that it looks like the convolution of w_k with w_{-k}. That is,

$$\phi_{CB,k} = \frac{1}{L} \sum_{i=0}^{L-i-1} w_i w_{i+k} \qquad 0 \le k \le M-1 \le L$$
$$= \frac{1}{L} w_k^* w_{-k} \tag{37}$$

If we compute $W(e^{j\omega})$, the Fourier transform (FT) of w_k, then the inverse FT of $W(e^{j\omega})W^*(e^{j\omega}) = |W(e^{j\omega})|^2$ corresponds to the linear convolution of w_k with w_{-k}. Since $|W(e^{j\omega})|^2 \ge 0$ for all ω, the inverse Fourier transform, $\phi_{CB,n}$, will be a non-negative definite sequence.

The following four correction methods are based upon the unbiased estimator. They are used to observe the effects of non-negative definiteness upon the output SNR of the moving average matched filters (MAMF's) to be discussed. If a given unbiased autocorrelation sequence estimate is not non-negative definite, then one of the four correction methods is used; otherwise, the sequence is not modified. The four methods discussed below are termed the diagonal correction method, the triangular correction method, the exponential correction method, and the minimum norm correction method.

The diagonal correction method generates Φ_{DC} by

$$\Phi_{DC} = \Phi_{UB} + (\varepsilon - \rho)I \tag{38}$$

where

$$\rho = \min(\lambda_i(\Phi_{UB}),0) \tag{39}$$

Φ_{DC} is non-negative definite since adding a positive constant to the diagonal of Φ_{UB} has the effect of raising the values of all the eigenvalues at once and by that same constant. That is,

$$\begin{aligned}(\Phi_{UB} + kI)\underline{v}_i &= \lambda_i\underline{v}_i + k\underline{v}_i \\ &= (\lambda_i + k)\underline{v}_i\end{aligned} \tag{40}$$

Note that Φ_{DC} is singular if $\varepsilon = 0$ so ε is set slightly greater than zero in order to avoid problems in inverting Φ_{DC}.

The triangular correction method generates Φ_{TC} from

$$\phi_{TC,k} = \begin{cases} \phi_{UB,k}(1-k/W) & 0 \le k < \min(N,W) \\ 0 & \text{otherwise} \end{cases} \tag{41}$$

The window function here is similar to the window used by the biased estimator, but is stronger in the sense that it reduces the variance of the outlying correlation coefficients further at the expense of increased bias.

The exponential correction method generates Φ_{EC} from

$$\phi_{EC,k} = \phi_{UB,k}\, C^k \qquad \begin{cases} 0 < C < 1 \\ 0 \le k \end{cases} \tag{42}$$

This method also biases the correlation estimates away from the NND boundary.

The minimum norm correction method generates Φ_{MC}, where that matrix satisfies

$$\| \Phi_{UB} - \Phi_{MC} \|_E = \text{minimum} \tag{43}$$

subject to

$$\lambda_{min}(\Phi_{MC}) \geq \varepsilon > 0 \tag{44}$$

This method is used in an attempt to retain as much information as is available in the data while placing the correlation estimate matrix Φ_{MC} just inside the NND boundary.

2.3.3 AUTOREGRESSIVE ESTIMATORS.

Another popular estimator is the MEM (maximum entropy) or Burg method. This is an auto-regressive (AR) estimator; that is, given a noise sequence whose spectrum is desired, it generates the parameters for an $(m-1)^{th}$-order filter H(z) that has the form

$$H(z) = \frac{G}{A(z)} \tag{45}$$

where

$$A(z) = 1 + \sum_{k=0}^{m-1} a_k z^{-k} \tag{46}$$

If H(z) has a white noise spectrum at its input, it will generate a spectral estimate of the noise at its output. Note that A(z) is a whitening filter. That is, given the signal whose spectrum is to be estimated as its input, the output of the whitening filter will approach a white noise process. A(z) can be modeled as a lattice filter (Figure 2). The K's are partial correlation coefficients. The $\{a_k\}$ filter coefficients are uniquely related to the K's by the recursive relationship (as m increases from 1 to M-1)

$$\begin{aligned} a_m^m &= K_m \\ a_j^m &= a_j^{m-1} + K_m a_{m-j}^{m-1} \qquad 1 \le j \le m-1 \end{aligned} \tag{47}$$

where a_i^m is the i^{th} coefficient for the m^{th}-order whitening filter.

The lattice filter can be considered as a forward and a backward predictor, where the error e_m of each stage of the lattice filter represents the error for an m-stage one-step forward predictor (Figure 3) and the b_m represents the error for an (m-1)-stage backward predictor (Figure 4).

The objective in whitening the output of the lattice filter (and finding the a_k^m coefficients) is to minimize the

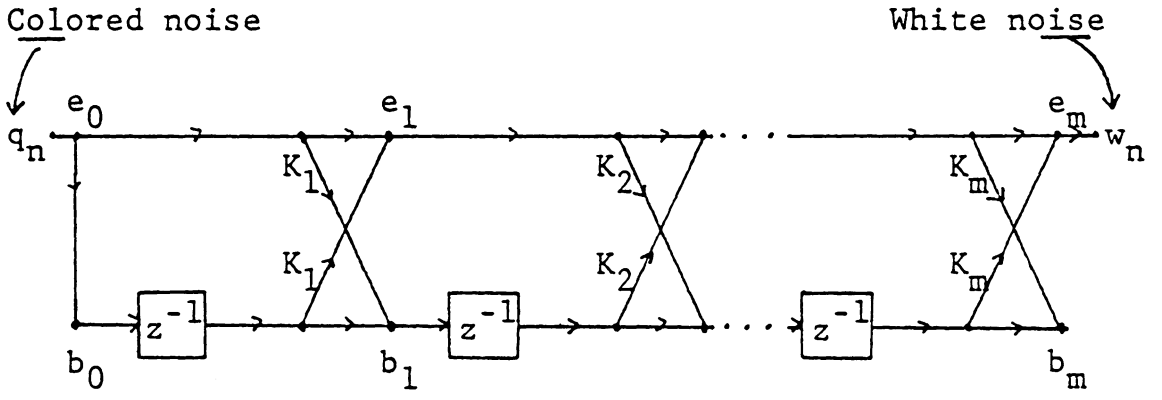

Figure 2. Lattice Filter.

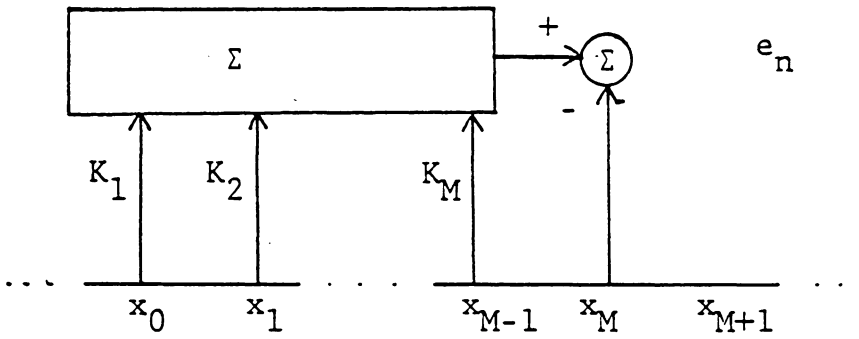

Figure 3. M-1 stage forward predictor.

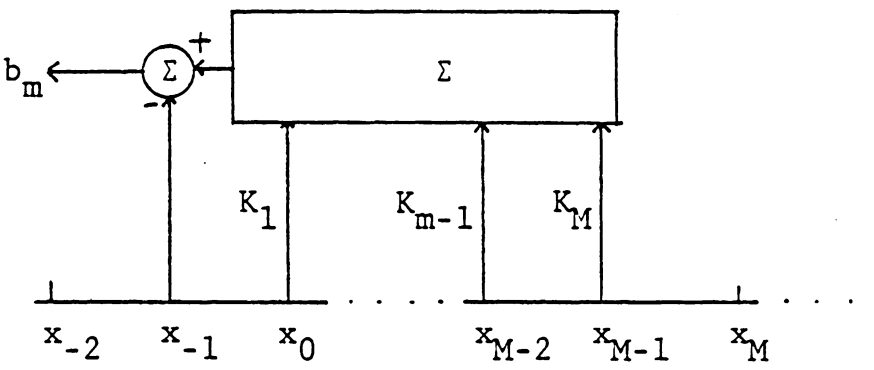

Figure 4. M-1 stage backward predictor.

variance of either the e_m, the b_m, or a combination of both by varying the reflection coefficients K_m [JMB].

In Burg's method, the sum of the above two errors is minimized. We are given that

$$E_m(n) = E[e_m^2(n)] \tag{48}$$

$$B_m(n) = E[b_m^2(n)] \tag{49}$$

$$C_m(n) = E[e_m(n)b_m(n-1)] \tag{50}$$

It is possible to show that

$$E_{m+1}(n) = (1 - K_m^2)E_m(n) \tag{51}$$

and that

$$B_m(n) = (1 - K_m^2)B_{m-1}(n) \tag{52}$$

Then, using Burg's method implies that K_m for each stage is found from

$$K_{m+1} = \frac{-2C_m(n)}{E_m(n) + B_m(n-1)} \tag{53}$$

By taking the derivatives of Equation 51 and Equation 52 with respect to K_m, setting those derivatives equal to zero, and

taking expected values, the equations for $E_m(n)$, $B_m(n)$, and $C_m(n)$ are found to be

$$E_m(n) = \sum_{k=0}^{m} \sum_{i=0}^{m} a_k^m a_i^m \phi(k,i) \tag{54}$$

$$B_m(n-1) = \sum_{k=0}^{m} \sum_{i=0}^{m} a_k^m a_i^m \phi(m+1-k,m+1-i) \tag{55}$$

$$C_m(n) = \sum_{k=0}^{m} \sum_{i=0}^{m} a_n^m a_i^m \phi(k,m+1-i) \tag{56}$$

where $\phi(k,i)$ is the autocorrelation for the noise w_i given by

$$\phi(k,i) = E[w_{n-k} w_{n-i}] \tag{57}$$

In the stationary case used in this thesis, Equation 54 to Equation 56 simplify to

$$E_m = B_m = \sum_{k=0}^{m} \sum_{i=0}^{m} a_k^m a_i^m R(i-k) \tag{58}$$

$$C_m = \sum_{k=0}^{m} \sum_{i=0}^{m} a_k^m a_i^m R(m+1-i-k) \tag{59}$$

and the K_m can be found from

$$K_{m+1} = \frac{C_m}{E_m} = \frac{\sum_{k=0}^{m} a_k^m R(m+1-k)}{(1 - K_m)E_m - 1} \qquad (60)$$

The covariance sequence R(k-i) is calculated by a scaled biased estimator,

$$R_m(k-1) = \sum_{n=m}^{N-1} w_{n-k} w_{n-i} \qquad 0 \le k,i \le m \qquad (61)$$

It can be shown that if the estimated correlation coefficients in Equation 58 to Equation 60 are positive definite then the roots of A(z) will lie within the unit circle [JMB].

Burg's method, as previously noted, is also known as a maximum entropy (MEM) method. The concept of maximum entropy hinges on a rule of statistics that states:

> The Result of any Transformation imposed on the Experimental Data shall incorporate and be consistent with all Relevant Data and be maximally non-committal with regard to Unavailable Data [JGA].

In Burg's context, the transformation in question is the Fourier transform of the correlation sequence to the noise spectral density,

$$S(z) = G^2/(A(z)A^*(1/z)) \qquad (62)$$

and the unavailable data are the correlation sequence values of R(k), $|k| \geq N$, N the length of the noise data record from which the correlation values are estimated. Entropy is defined as a measure of the disorder of a system. By finding correlation values R(k) for k greater than N that maximize the entropy of the estimated spectra, subject to the known correlation values, the above rule is satisfied. It is possible to specify the change in entropy ΔH across a filter in terms of that filter's power spectral density $S(\omega)$ [MSB]:

$$\Delta H = -\int_{-\infty}^{\infty} \log(S(\omega))d\omega \tag{63}$$

Equation 63 is now maximized subject to the constraints

$$\int_{-\infty}^{\infty} S(\omega)e^{-j2\pi\omega n\Delta\tau}d\omega = \phi_n \quad 0 \leq n \leq M-1 \tag{64}$$

where ϕ_n is the estimated correlation at lag $n\Delta\tau$, M is the order of the filter to be found, and τ is the sample time. The spectrum $S(\omega)$ that maximizes Equation 63 can now be found by Lagrangian multiplier techniques and is given as

$$S_{MEM}(\omega) = \frac{\tau/a_0}{\left|\sum_{n=0}^{m} a_n e^{j2\pi\omega n\Delta\tau}\right|^2} \tag{65}$$

where the sequence $\{a_n\}$ is found as the solution to

$$R\underline{a} = [1\ 0\ 0\ \ldots\ 0\ 0]^T \tag{66}$$

where R is the Toeplitz matrix with first row $\phi_{k,M}$. Once the a_k coefficients have been determined, the corresponding correlation estimates may be easily generated [DBS].

The Itakura estimator is similar to the Burg estimator. It differs by the different evaluation procedure for K_m:

$$K_m = -C_m(n)/\sqrt{E_m(n)B_m(n-1)} \tag{67}$$

A property of the Burg and Itakura estimators is the ordering of their respective reflection coefficients:

$$|K_{BG}| \leq |K_{IT}| \leq 1 \tag{68}$$

This implies that the poles of the estimation filter derived from the Itakura estimator can be closer to the unit circle (and the correlation sequence derived from that filter closer to the NND boundary) than those for the corresponding Burg estimator. This will have consequences to be seen later in this thesis.

2.4 MOVING-AVERAGE MATCHED FILTERS.

A moving average matched filter (MAMF) is designed to maximize the signal-to-noise ratio (SNR) at the filter output

at some time n_0 (Figure 5). In Figure 5, w_n is noise, s_n is the known signal to be detected, x_n is the signal corrupted by noise, and y_n is given by

$$y_n = \sum_{i=0}^{N-1} h_i x_{n-i} \tag{69}$$

where the sequence $\{h_i\}$ is the impulse response of the filter. In the remainder of this thesis, n_0 is set to N-1. Due to the principle of superposition for linear systems, the signal and noise at the output of the filter can be evaluated separately. The signal power at time N-1 is determined under the condition that no noise is present at the input and is given by

$$(y_{N-1})^2 = \left(\sum_{i=0}^{N-1} s_i h_{N-1-i}\right)^2 = (\underline{s}^T \underline{h})^2 \tag{70}$$

where

$$\underline{s}^T = [s_{N-1}\ s_{N-2}\ \cdot\ \cdot\ s_0] \tag{71}$$

and

$$\underline{h}^T = [h_0\ h_1\ \cdot\ \cdot\ h_{N-1}] \tag{72}$$

The noise power is determined from the expected value of y_{N-1} with no signal present:

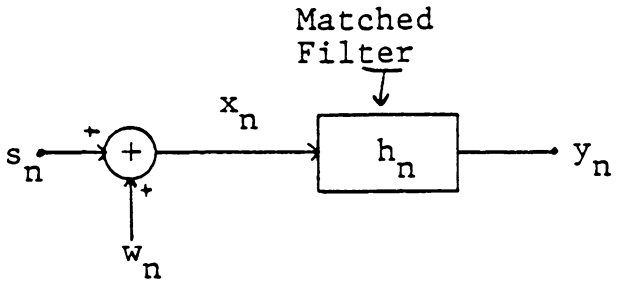

Figure 5. MAMF block diagram.

$$E[(y_{n-1})^2] = E[(h_n * w_n)^2]$$

$$= E\left[\sum_{i=0}^{N-1}\sum_{j=0}^{N-1} h_i w_{N-1-i} h_j w_{N-1-j}\right]$$

$$= \sum_{i=0}^{N-1}\sum_{j=0}^{N-1} h_i h_j E[w_{N-1-i} w_{N-1-j}] \qquad (73)$$

$$= \sum_{i=0}^{N-1}\sum_{j=0}^{N-1} h_i h_j \phi_{i-j}$$

$$= \underline{h}^T \Phi \underline{h} \qquad (74)$$

where the ϕ_i are the noise autocorrelations and Φ is the Toeplitz matrix with first row $[\phi_0\ \phi_1\ .\ .\ \phi_{N-1}]$. Φ, as shown before, is non-negative definite, i.e., $\underline{x}^T \Phi \underline{x} \geq 0$ for all $\underline{x}$. The SNR at the output of the MAMF is then given by

$$\text{SNR} = \frac{(\underline{s}^T \underline{h})^2}{\underline{h}^T \Phi \underline{h}} \qquad (75)$$

It will be of interest to note that multiplying $\underline{h}$ by some arbitrary constant k does not change the output SNR. This is seen as follows:

$$\frac{(\underline{s}^T k\underline{h})^2}{(k\underline{h}^T \Phi k\underline{h})} = \frac{k^2(\underline{s}^T\underline{h})^2}{k^2(\underline{h}^T\Phi\underline{h})} \tag{76}$$

$$= \frac{(\underline{s}^T\underline{h})^2}{(\underline{h}^T\Phi\underline{h})}$$

We now seek to maximize the SNR at the output of the MAMF using Lagrangian multiplier techniques. To do this, we take Equation 75, set $\underline{h}^T\Phi\underline{h} = K$ where K is some fixed constant, and attempt to maximize $\underline{s}^T\underline{h}$. The Lagrangian equation becomes

$$I(\underline{h}) = \sum_{i=0}^{N-1} s_{N-1-i}h_i + \left(\sum_{i=0}^{N-1}\sum_{j=0}^{N-1} h_i h_j \phi_{i-j} - K\right) \tag{77}$$

Taking the partial derivative of Equation 77 with respect to $\underline{h}$ and setting it to zero results in

$$\underline{0} = \frac{\partial(I(\underline{h}))}{(\partial\underline{h})} \tag{78}$$
$$= \underline{s} - 2\lambda\Phi\underline{h}$$

Since multiplying $\underline{h}$ by a constant does not change the SNR, λ may be set to any convenient value. Setting it equal to 0.5 and solving for $\underline{h}$ [BEB] results in

$$\underline{h} = \Phi^{-1}\underline{s} \tag{79}$$

The optimum output SNR is then given as

$$\begin{aligned} SNR &= \frac{(\underline{s}^T \Phi^{-1} \underline{s})^2}{\underline{s}^T \Phi^{-1} \Phi \Phi^{-1} \underline{s}} \\ &= \underline{s}^T \Phi^{-1} \underline{s} \end{aligned} \tag{80}$$

The optimum SNR varies with both Φ and $\underline{s}$. To see this, note that as Φ is NND and has real components it may be factored (from Section 2.1):

$$\Phi = U \Lambda U^T \tag{81}$$

with

$$\Lambda = \begin{bmatrix} \lambda_0 & & 0 \\ & \lambda_1 & \\ & \ddots & \\ 0 & & \lambda_{N-1} \end{bmatrix} \tag{82}$$

where the λ_i are the eigenvalues of Φ and can be ordered to satisfy the property that

$$\lambda_0 \geq \lambda_1 \geq \ldots \geq \lambda_{N-1} \geq 0 \tag{83}$$

U is the matrix of orthonormal eigenvectors

$$U = [\underline{u}_0 \ \underline{u}_1 \ \ldots \ \underline{u}_{N-1}] \tag{84}$$

associated with each λ_i. Note that the $\underline{u}_i$ are real since Φ is real. If $\underline{s}$ is set equal to $\underline{u}_{N-1}$ and the above factorization is substituted into Equation 80, the SNR becomes

$$\begin{aligned} SNR &= \underline{u}_{N-1}^T U \Lambda^{-1} U^T \underline{u}_{N-1} \\ &= \underline{u}_{N-1}^T [\underline{u}_0\ \underline{u}_1 \cdots \underline{u}_{N-1}] \begin{bmatrix} 1/\lambda_0 & & & 0 \\ & 1/\lambda_1 & & \\ & & \ddots & \\ 0 & & & 1/\lambda_{N-1} \end{bmatrix} \begin{bmatrix} \underline{u}_0^T \\ \vdots \\ \underline{u}_{N-1}^T \end{bmatrix} \underline{u}_{N-1} \\ &= 1/\lambda_{N-1} \end{aligned} \tag{85}$$

This is the maximum value of SNR, designated SNR^m. The minimum value of SNR is achieved when $\underline{s} = \underline{u}_0$ and its value is $1/\lambda_0$.

All of these calculations are based on the assumption that the noise correlation matrix Φ is known. This may, in fact, not be the case. If the spectral information must be estimated, then the SNR based on the estimated correlations becomes

$$SNR = \frac{(\underline{s}^T \Phi^{-1} \underline{s})^2}{\underline{s}^T \Phi^{-1} \Phi_a \Phi^{-1} \underline{s}} \tag{86}$$

where $\hat{\Phi}$ is the estimated autocorrelation matrix and Φ_a is the actual autocorrelation matrix. Note that when $\hat{\Phi} = \Phi_a$, Equation 86 reduces to Equation 80.

While the maximum for Equation 86 is still SNR^m, the minimum is no longer $1/\lambda_0$. To show this, consider the inverse of a Toeplitz matrix, A:

$$A^{-1} = B/\Delta \tag{87}$$

where B is the transpose of the matrix of cofactors of A and Δ is the determinant of A. In general, B will be symmetric about the major diagonal but will not be Toeplitz [JMA]. If Equation 87 is applied to $\hat{\Phi}$ in Equation 86 , the determinant terms will factor out leaving

$$SNR = \frac{(\underline{s}^T \Psi \underline{s})^2}{\underline{s}^T \Psi \Phi_a \Psi \underline{s}} \tag{88}$$

where Ψ is the transpose of the cofactors of $\hat{\Phi}$. Since $\hat{\Phi}$ is an estimate, neither it, nor its inverse, is restricted to being NND. Therefore, it is easy to show that there exist Ψ and $\underline{s}$ such that

$$\underline{s}^T \Psi \underline{s} = 0 \tag{89}$$

while

$$\Psi \underline{s} \neq \underline{0} \tag{90}$$

In this case, the SNR in Equation 88 will be zero, since Φ_a in the denominator of that equation is still non-negative definite for all $\underline{x}$.

Another characteristic of Equation 86 is the invariance of the SNR to changes in the magnitude of Φ. To show this, let $\Phi = T[\phi]$. Let $\underline{\phi}$ be multiplied by some non-zero constant k such that Φ becomes $k\Phi$ and Φ^{-1} becomes Φ^{-1}/k. Then, after substitution into Equation 86, we have

$$SNR = \frac{((\underline{s}^T \Phi^{-1} \underline{s})^2)/k^2}{(\underline{s}^T \Phi^{-1} \Phi_a \Phi^{-1} \underline{s})/k^2}$$

$$= \frac{(\underline{s}^T \Phi^{-1} \underline{s})^2}{\underline{s}^T \Phi^{-1} \Phi_a \Phi^{-1} \underline{s}} \tag{91}$$

Finally, it is of interest that, with an estimated Φ, SNR^m may occur at points besides $\Phi = \Phi_a$. To show this, consider Equation 75. When $\Phi = \Phi_a$, $\underline{h}$ is at its optimum value, which we shall call $\underline{h}_{opt}$. Note that $\underline{h}_{opt}$ is obtained from

$$\underline{h}_{opt} = \Phi^{-1} \underline{s} \tag{92}$$

and, further, that $\underline{s}$ and $\underline{h}_{opt}$ are both the same eigenvector $\underline{u}_{N-1}$ of Φ_a, differing only by a constant k such that

$$\underline{s} = k\underline{h}_{opt} \tag{93}$$

where in this case $k = 1/\lambda_{N-1}$, as seen in Equation 85. Since multiplying $\underline{h}_{opt}$ by a constant will not change the SNR (Equation 76), we need only find an estimated matrix Φ where

$$\Phi^{-1}\underline{u}_{N-1} = k\underline{h}_{opt} \tag{94}$$

where k is any constant. This matrix Φ will always exist. The proof is as follows: First, the eigenvectors $\underline{u}_i$ of a symmetric Toeplitz matrix are either symmetric where

$$\underline{v}_i = [v_{i,0}\ v_{i,1}\ \cdot\ \cdot\ v_{i,1}\ v_{i,0}] \tag{95}$$

or are skew symmetric where

$$\underline{v}_j = [v_{j,0}\ v_{j,1}\ \cdot\ \cdot\ -v_{j,1}\ -v_{j,0}] \tag{96}$$

[JMA]. Now, let $\underline{v}_i$ be the symmetric eigenvector of a matrix Φ_a (the skew-symmetric case is similar). We wish to show that there exist many matrices $\Phi = T[1\ \phi_1\ \phi_2\ \cdot\ \cdot\phi_{N-1}]$ with

the same eigenvector $\underline{v}$ but with different eigenvalues λ. We begin with

$$\Phi\underline{v} = \lambda v$$

$$= \begin{bmatrix} 1 & \phi_1 & \cdot & \cdot & \phi_{N-2} & \phi_{N-1} \\ \phi_1 & 1 & \cdot & \cdot & \phi_{N-3} & \phi_{N-1} \\ \cdot & \cdot & \cdot & \cdot & \cdot & \cdot \\ \cdot & \cdot & \cdot & \cdot & \cdot & \cdot \\ \phi_{N-2} & \phi_{N-3} & \cdot & \cdot & 1 & \phi_1 \\ \phi_{N-1} & \phi_{N-2} & \cdot & \cdot & \phi_1 & 1 \end{bmatrix} \begin{bmatrix} v_0 \\ v_1 \\ \cdot \\ \cdot \\ v_1 \\ v_0 \end{bmatrix} = \lambda \begin{bmatrix} v_0 \\ v_1 \\ \cdot \\ \cdot \\ v_1 \\ v_0 \end{bmatrix} \qquad (97)$$

Since $\underline{v}$ is symmetric, this system of equations can be rewritten into the form

$$\begin{bmatrix} v_0 & v_1 & v_2 & \cdot & \cdot & v_1 & v_0 \\ v_1 & v_0+v_2 & v_3 & \cdot & \cdot & v_0 & 0 \\ \cdot & \cdot & \cdot & \cdot & \cdot & \cdot & \\ v_1 & v_0+v_2 & v_3 & \cdot & \cdot & v_0 & 0 \\ v_0 & v_1 & v_2 & \cdot & \cdot & v_1 & v_0 \end{bmatrix} \begin{bmatrix} 1 \\ \phi_1 \\ \cdot \\ \phi_{N-2} \\ \phi_{N-1} \end{bmatrix} = \begin{bmatrix} v_0 \\ v_1 \\ \cdot \\ v_1 \\ v_0 \end{bmatrix} = \lambda \begin{bmatrix} v_0 \\ v_1 \\ \cdot \\ v_1 \\ v_0 \end{bmatrix} \qquad (98)$$

$$= V\underline{\phi} = \lambda\underline{v}$$

Note that there will be N/2 identical rows in V if N is even and (N-1)/2 identical rows in V if N is odd. Therefore,

solving Equation 98 for a correlation vector $\underline{\phi}$ is equivalent to solving a linear underdetermined system of [(N+1)/2] equations in N-1 unknowns. Such systems of equations have an infinite number of solutions for N greater than two. Therefore, there are many different $\hat{\phi}$ matrices with the same eigenvector $\underline{v}$.

3.0 SIMULATION

3.1 SIMULATION DESIGN

In this chapter, graphical and simulation techniques will be used to investigate the effects of estimation of spectra, different noise spectra, and signal vector choice upon the output SNR of a MAMF. This SNR is given by

$$\text{SNR} = \frac{(\underline{s}^T \hat{\Phi}^{-1} \underline{s})^2}{\underline{s}^T \hat{\Phi}^{-1} \Phi_a \hat{\Phi}^{-1} \underline{s}} \tag{99}$$

where $\underline{s}$ is a signal vector, $\hat{\Phi}$ is a Toeplitz matrix with an estimated correlation sequence $[c_0\ c_1\ .\ .\ c_N]$ as its first row, and Φ_a is a Toeplitz matrix with the actual correlation sequence $[\phi_0\ \phi_1\ .\ .\ \phi_N]$ as its first row.

Unless explicitly stated otherwise, three-point correlation sequences based on five-point noise sequences will be used in the discussions to follow. This is done to make the results more amenable to display and to emphasize the differences between methods. We note, however, that the results and conclusions to be found may be extended to higher dimensions. Three types of noise spectra will be used: white, lowpass, and bandpass. Each type of noise will be generated by passing white gaussian noise generated by the

IMSL subroutine GGNML [IML] through a digital filter (Figure 6). The gain of these filters has been adjusted so that the correlation at lag zero will have a value of one. A white noise sequence is generated by removing the digital filter from Figure 6. The three point correlation sequence of the white noise is

$$\underline{\phi}_{WH} = [1.0 \quad 0.0 \quad 0.0]^T \tag{100}$$

A digital Butterworth lowpass filter, derived via the bilinear z-transform method from a 3^{rd}-order analog filter is used to generate the lowpass noise sequence. Its cutoff frequency is $3\pi/8$ radians. Its transfer function and correlation sequence are

$$H_{LP}(z) = \frac{.1373 + .4118z^{-1} + .4118z^{-2} + .1373z^{-3}}{1 - .7224z^{-1} + .4772z^{-2} + 0.752z^{-3}} \tag{101}$$

$$\underline{\phi}_{LP} = [1 \quad .7514 \quad .2523]^T \tag{102}$$

Its magnitude plot is shown in Figure 7. A digital Butterworth bandpass filter is used to generate a bandpass noise sequence. It is derived by means of a frequency transformation ([AOS], pp. 230) from the above lowpass

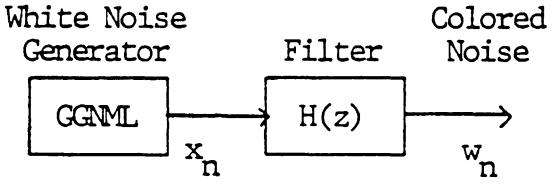

Figure 6. Colored noise generation.

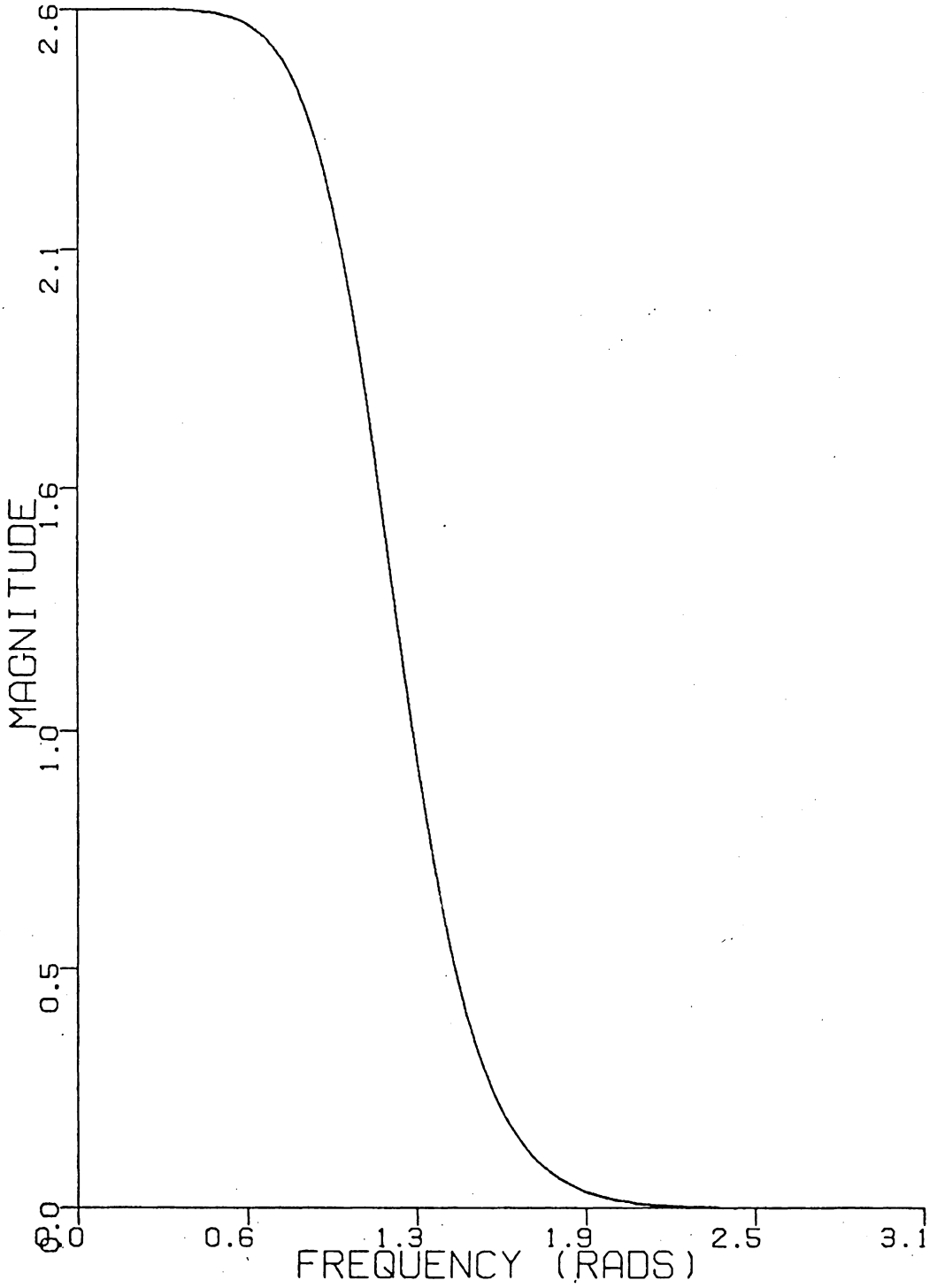

Figure 7. Lowpass filter magnitude response.

filter. Its cutoff frequencies are $\pi/8$ and $5\pi/8$ radians. Its transfer function and correlation sequence are

$$H_{BP}(z) = \frac{.2357-.7071z^{-2}+.7071z^{-4}-.2345z^{-6}}{1-1.624z^{-1}+.9763z^{-2}-.5721z^{-3}+.5286z^{-4}-.1804z^{-5}} \quad (103)$$

$$\underline{\phi}_{BP}(z) = [1 \quad .33073 \quad -.43211]^T \quad (104)$$

The corresponding magnitude plot is shown in Figure 8.

As was shown in Section 2.4, the output SNR of a MAMF is a function of the estimated correlation sequence used to generate that MAMF. A graphical analysis technique, using two types of contour plots, is used to investigate this dependence. The first type of contour plot presents the values of normalized SNR (NSNR) versus c_1 and c_2, where NSNR is generated from

$$NSNR = \frac{(\underline{s}^T \Phi^{-1} \underline{s})^2}{(\underline{s}^T \Phi^{-1} \Phi_a \Phi^{-1} \underline{s}) SNR^m} \quad (105)$$

where

$$\Phi = T[1 \quad c_1 \quad c_2] \quad (106)$$

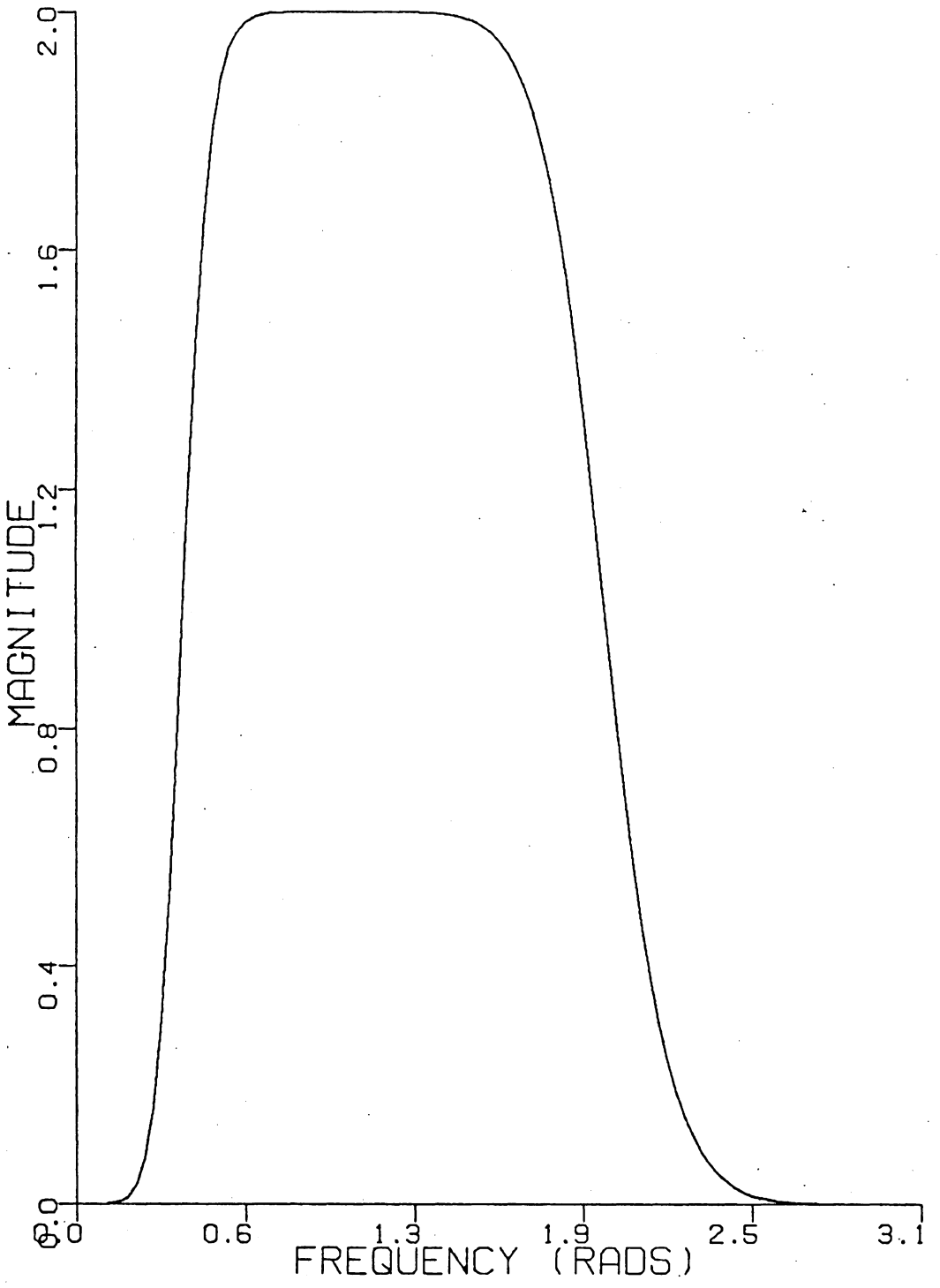

Figure 8. Bandpass filter magnitude response.

Φ_a is the actual Toeplitz matrix associated with one of the noise processes; $\underline{s}$ is a signal vector with an l_2-norm of one; and SNR^m is the maximum possible SNR given Φ_a and $\underline{s}$ (Equation 80) and is found from

$$SNR^m = \underline{s}^T \Phi_a^{-1} \underline{s} \tag{107}$$

The second type of contour plot is a scaled two-dimensional histogram of 8092 normalized estimated correlation sequences. These many sequences were found to result in a histogram that was relatively smooth. Three-point non-normalized correlation sequences $\underline{c}_{nn}$ are obtained by operating one of the eight estimator/correction methods discussed in Section 2.2 on 8092 independent five-point colored noise sequences generated by the system shown in Figure 6. The non-normalized correlation sequences are then used to generate normalized correlation sequences $\underline{c}_n$ using the relation

$$c_{n,i} = c_{nn,i}/c_{nn,0} \qquad 0 \le i \le 2 \tag{108}$$

Note that $c_{n,0}$ always has a value of one. Further note that if a $\underline{c}_n$ and a $\underline{c}_{nn}$ were used to design two MAMF's, their output SNR's would not differ (Equation 91). The 8092 $\underline{c}_n$ are then sorted into a 51 by 51 bin histogram in $c_{n,1}$ and $c_{n,2}$ where bx_i and by_j are the coordinates of a bin and

$$-1.2 \leq bx_i \leq 1.2$$
$$-1.2 \leq by_j \leq 1.2 \tag{109}$$

and

$$\Delta bx = \Delta by = 0.048 \tag{110}$$

where Δbx and Δby are the increments of the bin grid in the x and y direction, respectively. Note that the sum of the values $H_{i,j}$ in the bins satisfies

$$\sum_i \sum_j H_{i,j} = 8092 \tag{111}$$

The histogram to be plotted should have scaled values p_{ij} that approximate the actual probability density function $p(c_1,c_2)$ where

$$\int_{-1.2}^{1.2} \int_{-1.2}^{1.2} p(c_1,c_2)\, dc_1\, dc_2 = 1 \tag{112}$$

and

$$p_{ij}\Delta bx\Delta by = \int_{bx_i-\Delta bx/2}^{bx_i+\Delta bx/2} \int_{by_j-\Delta by/2}^{by_j+\Delta by/2} p(c_1,c_2)\, dc_1\, dc_2 \tag{113}$$

and where

$$\sum_i \sum_j p_{ij} \Delta bx \Delta by = 1.0 \tag{114}$$

Upon comparison of Equation 111 with Equation 114, it is found that

$$p_{ij} = \frac{H_{ij}}{8092(\Delta bx)(\Delta by)} \tag{115}$$

Both the p_{ij} and NSNR are plotted against c_1 and c_2 using the contour plotting subroutine GCONTR [WVS].

3.2 SIMULATION RESULTS AND ANALYSIS.

The signals and the SNR^m associated with the three noise systems are given in Table 1. In this chapter, $\underline{s}$ will be set equal to the eigenvector associated with the minimum eigenvalue of Φ_a. This results in a maximal SNR^m (Equation 85). The actual correlation sequences ϕ_{WH}, ϕ_{LP}, and ϕ_{BP} are summarized in Table 2. The value of C given in Equation 42 on page 20 is set to 0.8.

The SNR contour plots for the white, lowpass, and bandpass noise processes are shown in Figure 9, Figure 10, and Figure 11, respectively. The correlation histogram contour plots are shown in Figure 12 through Figure 35.

Table 1. Signals that cause SNR^m.

SYSTEM	SIGNAL	SNR
Lowpass	-.4696 0.7476 -.4696	17.8
Bandpass	0.5957 -.5381 0.5957	3.72
White	0.5774 0.5774 0.5774	1.00

Table 2. Actual correlation sequences.

SYSTEM	CORRELATION SEQUENCE
Lowpass	1 0.7514 0.2523
Bandpass	1 0.3307 -.4321
White	1 0 0

On each plot, the actual correlation point Φ_a is marked with a pair of crossed lines and the nonnegative definite region is delineated with a thick line.

3.2.1 ESTIMATOR CHARACTERISTICS.

The correlation histograms clearly show the characteristics of the various estimators. The biased estimator plots (Figure 12, Figure 20, and Figure 28) show that its estimates are bounded away from the NND boundary. The unbiased estimator plots (Figure 13, Figure 21, and Figure 29) place estimates on both sides of the NND boundary. The Burg and Itakura estimators (Figure 18, Figure 19, Figure 26, Figure 27, Figure 34, and Figure 35) also place their estimates inside the NND boundary, as do the various correction schemes based on the unbiased estimator.

3.2.2 CONTOUR PLOTTING PROBLEMS.

Some of the correlation histograms that should be entirely inside the NND region (such as the Burg estimates plotted in Figure 26) appear to have estimates outside the NND region. This perceived inconsistency is due to the discretization of the data points used to generate the histogram plot and the contour plotting program used. An illustration of this problem is shown in Figure 36. In Figure 36, let points p_1

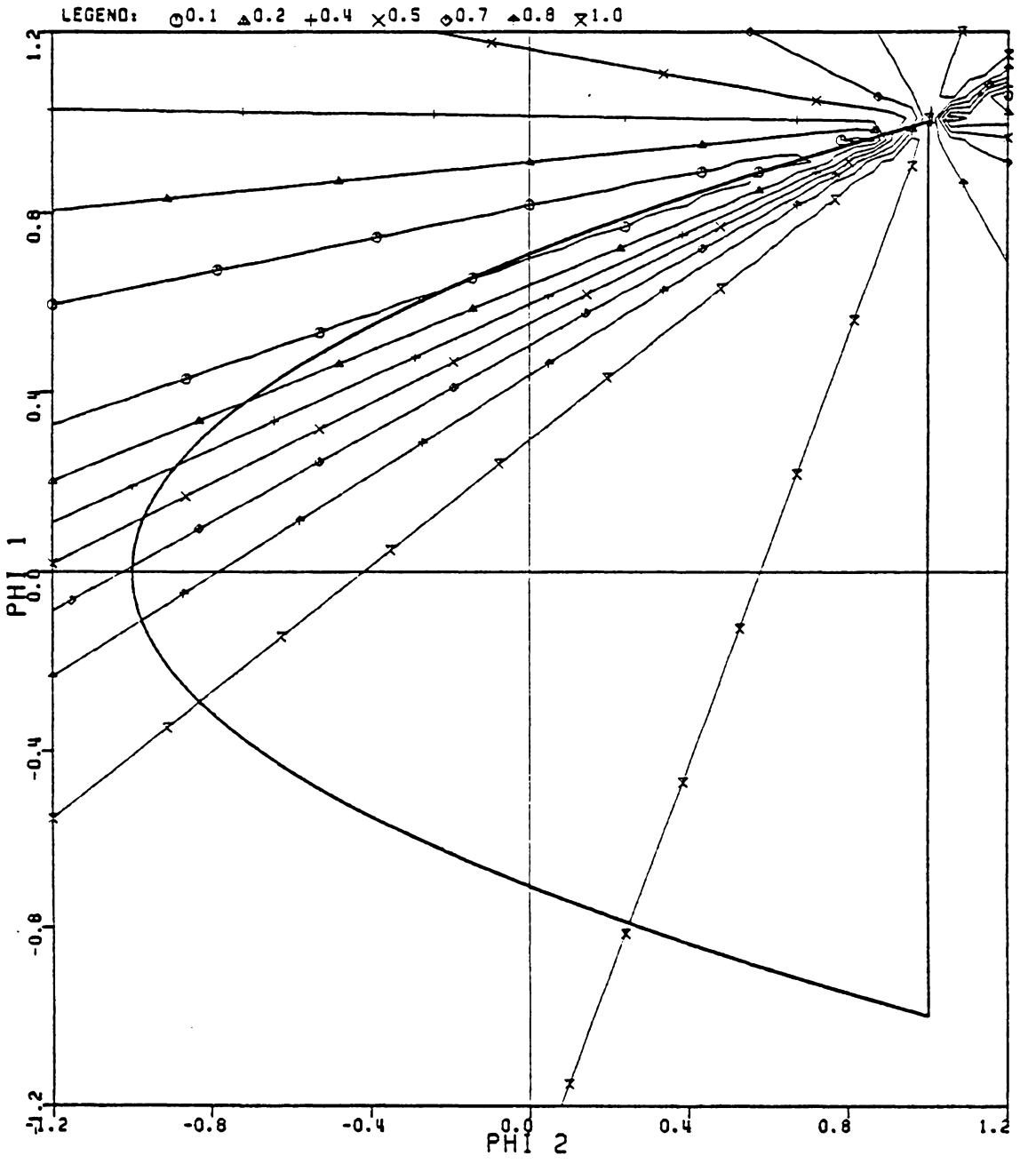

Figure 9. Normalized SNR, white system.

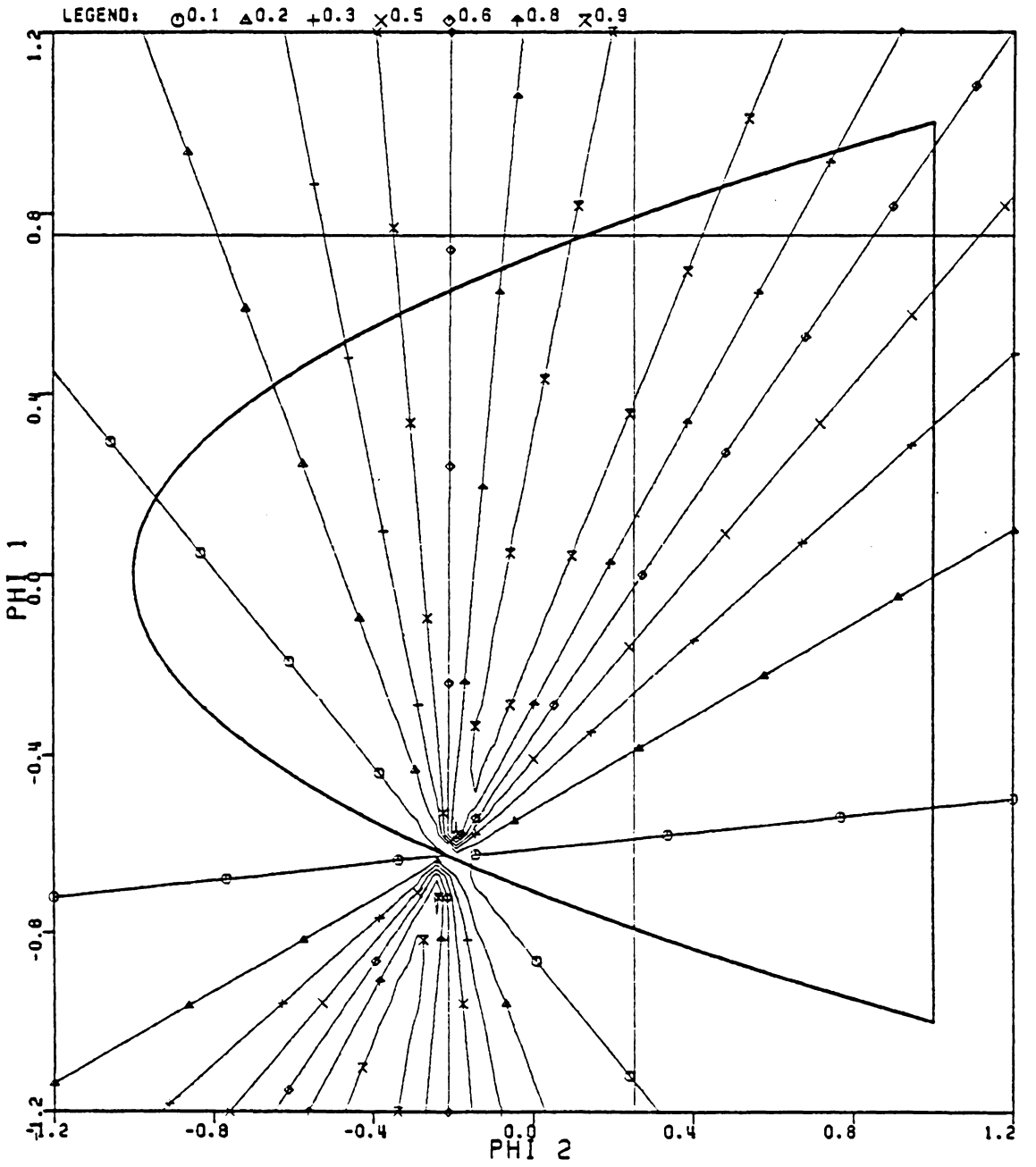

Figure 10. Normalized SNR, lowpass system.

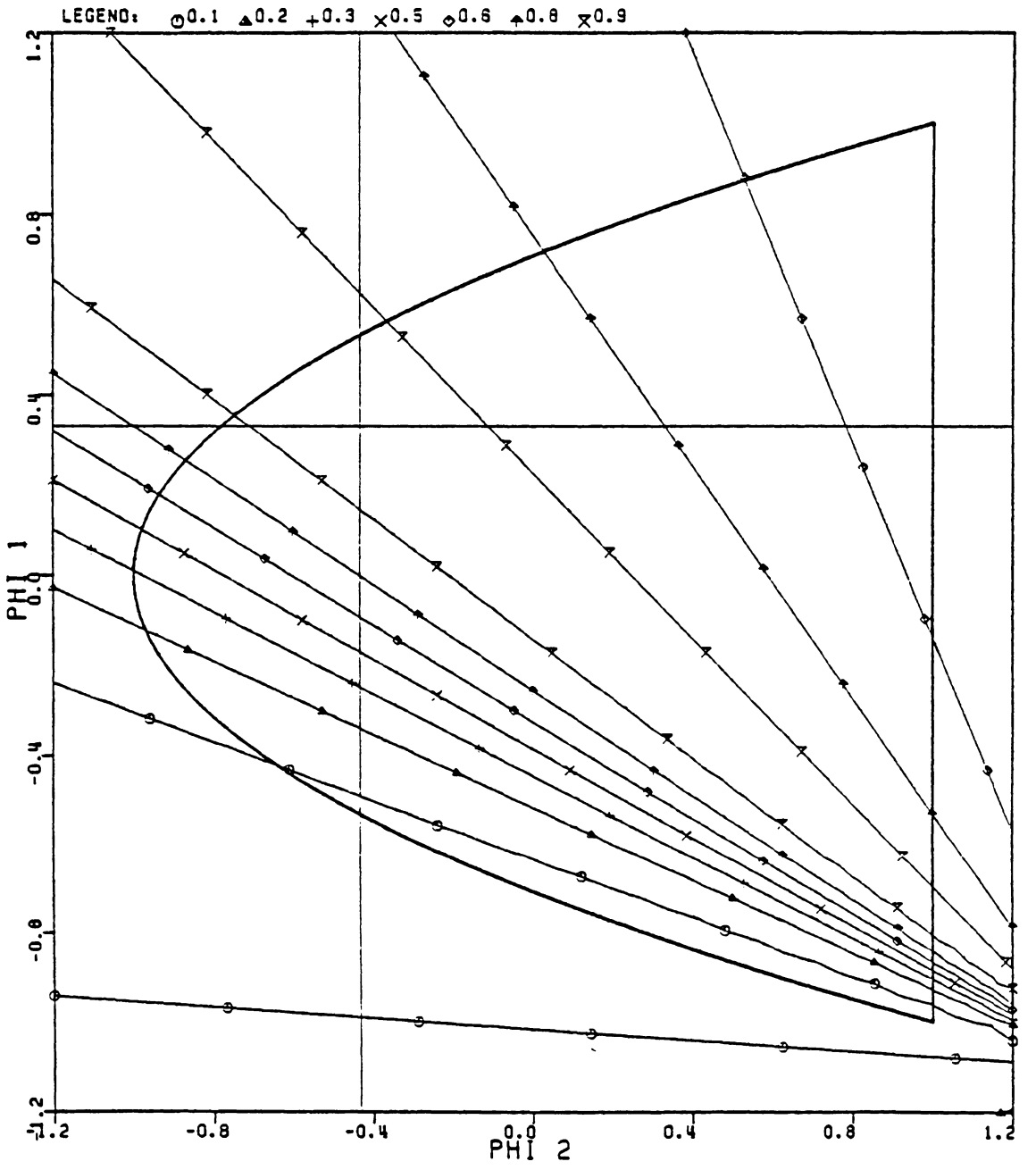

Figure 11. Normalized SNR, bandpass system.

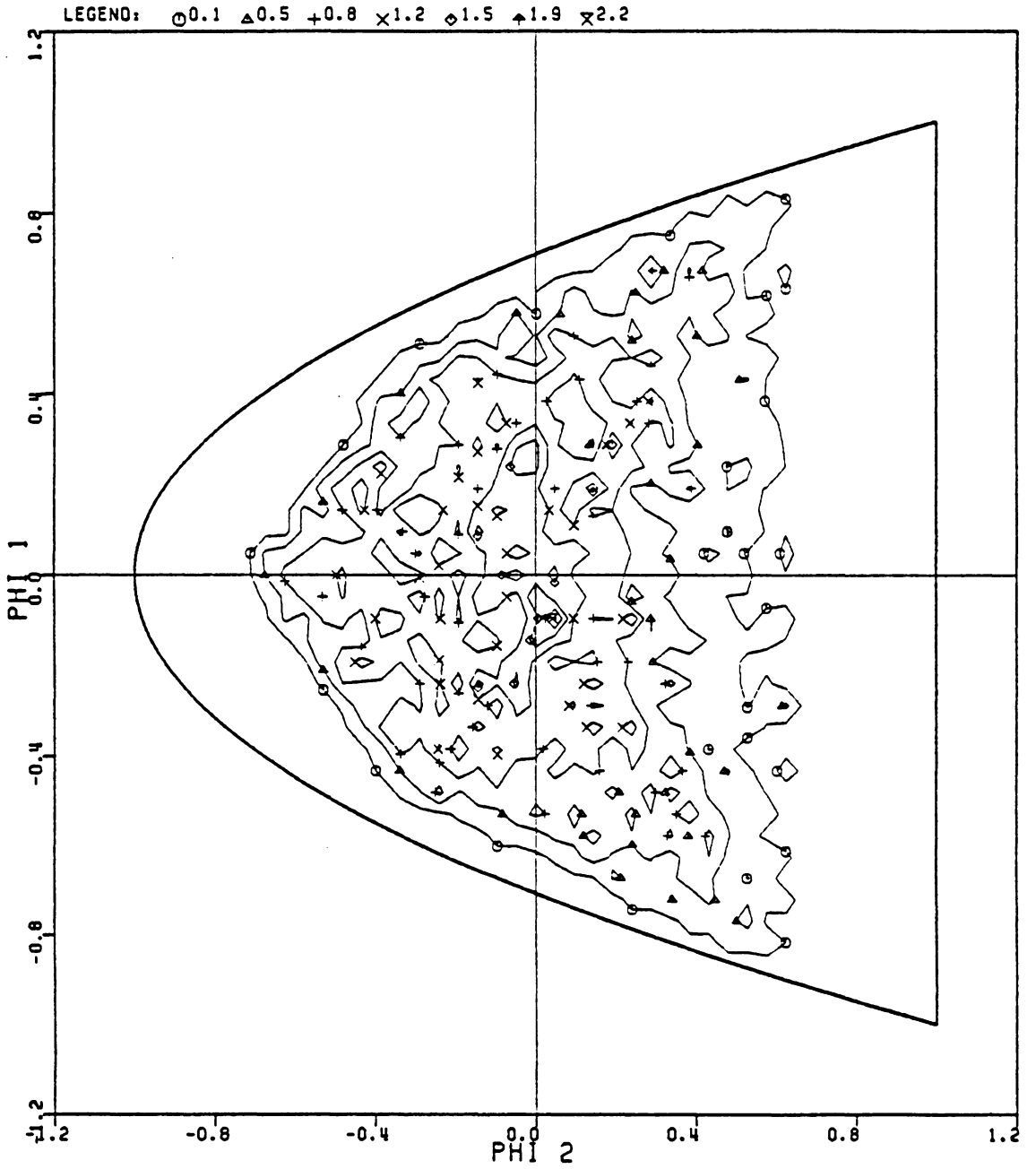

Figure 12. Biased estimator, white system.

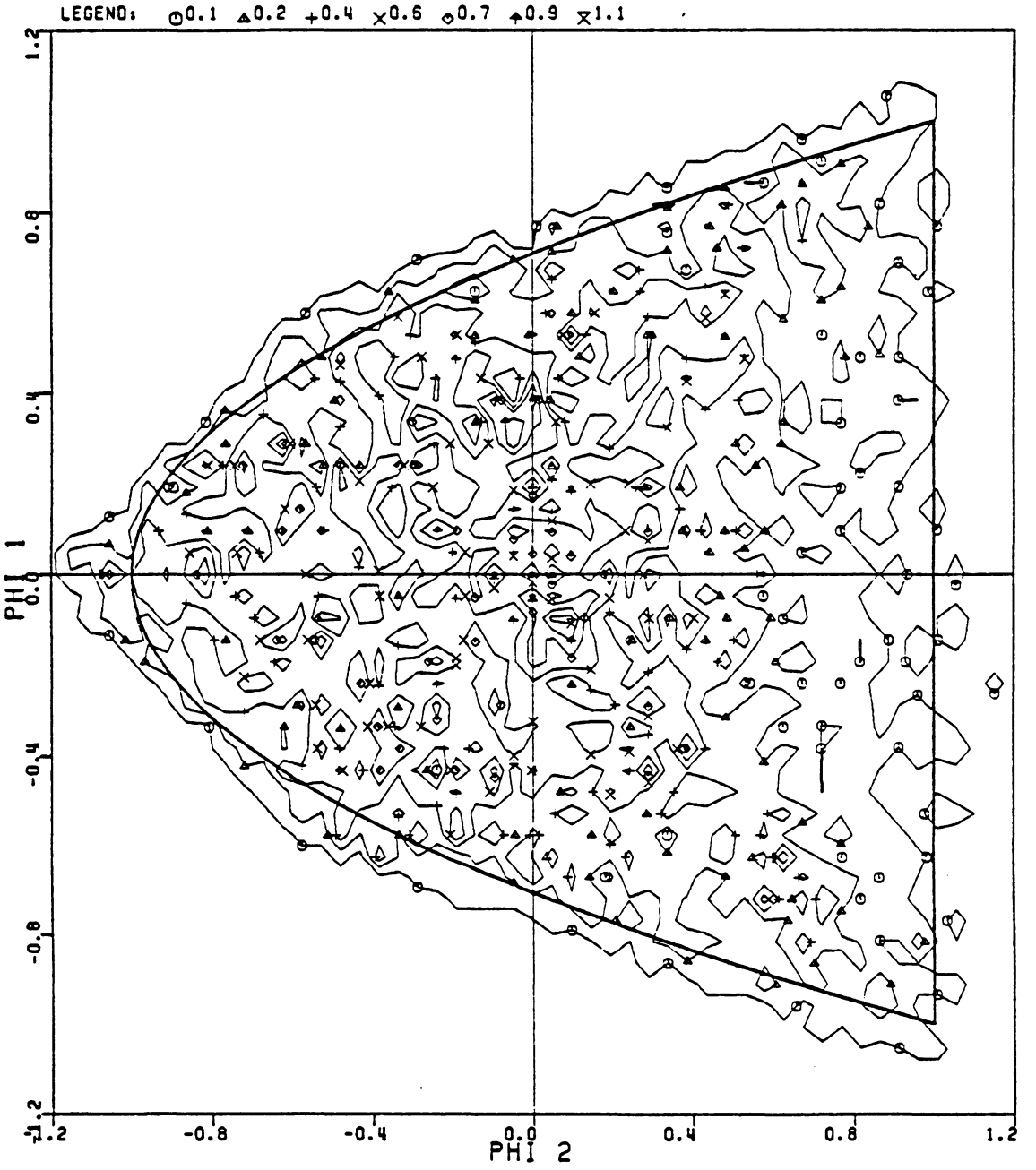

Figure 13. Unbiased estimator, white system.

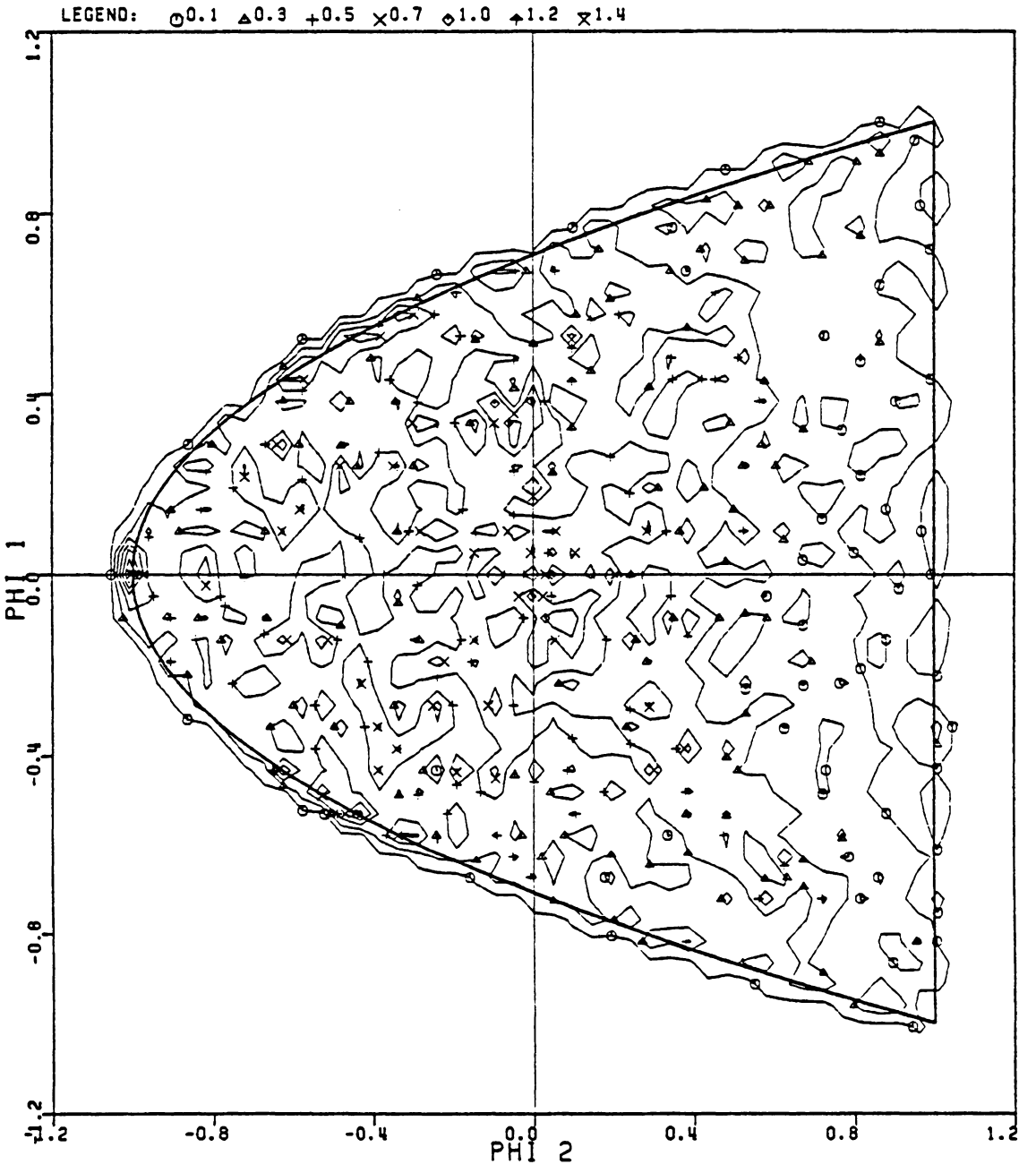

Figure 14. Diagonal correction, white system.

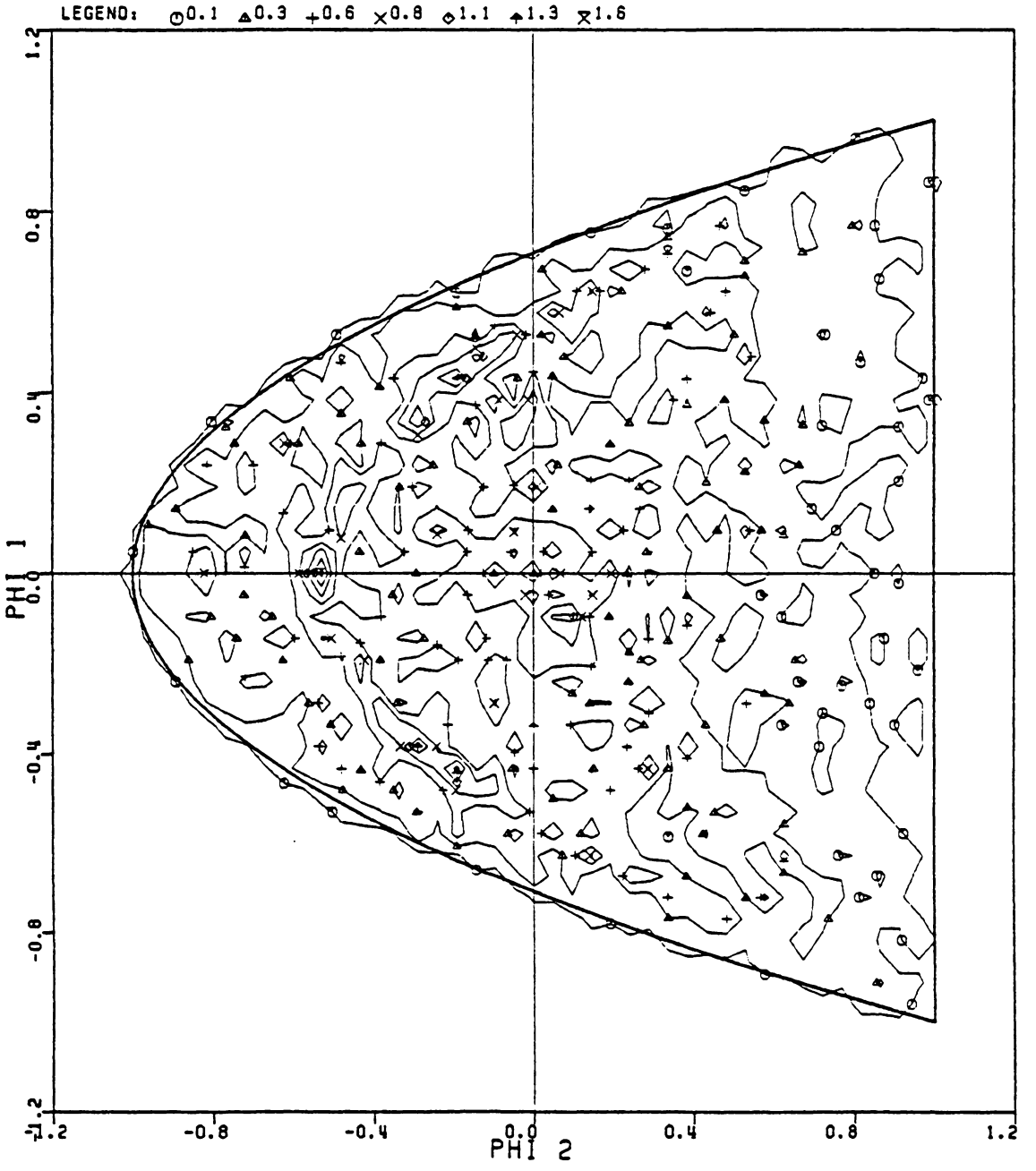

Figure 15. Triangular correction, white system.

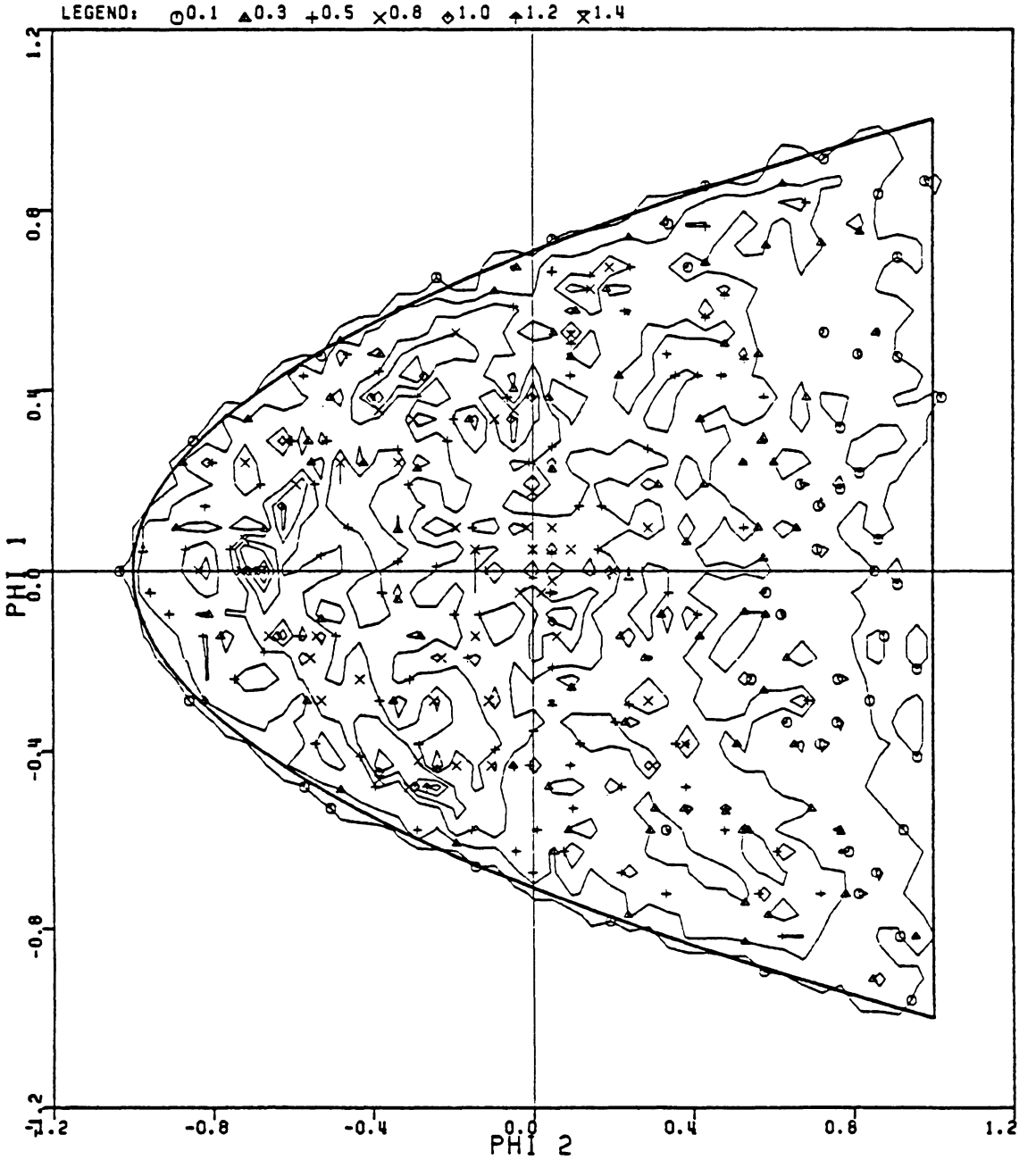

Figure 16. Exponential correction, white system.

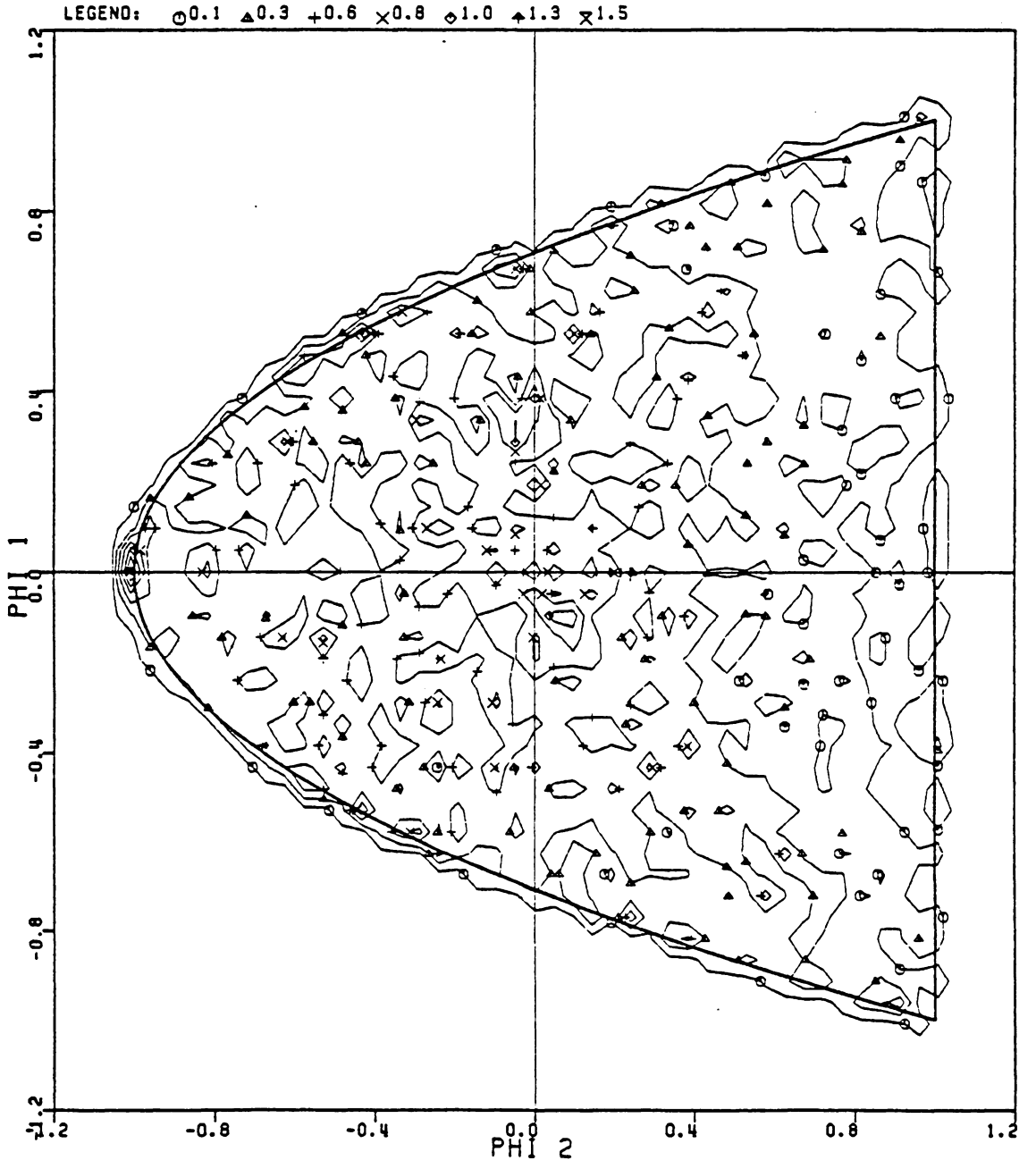

Figure 17. Minimum norm correction, white system.

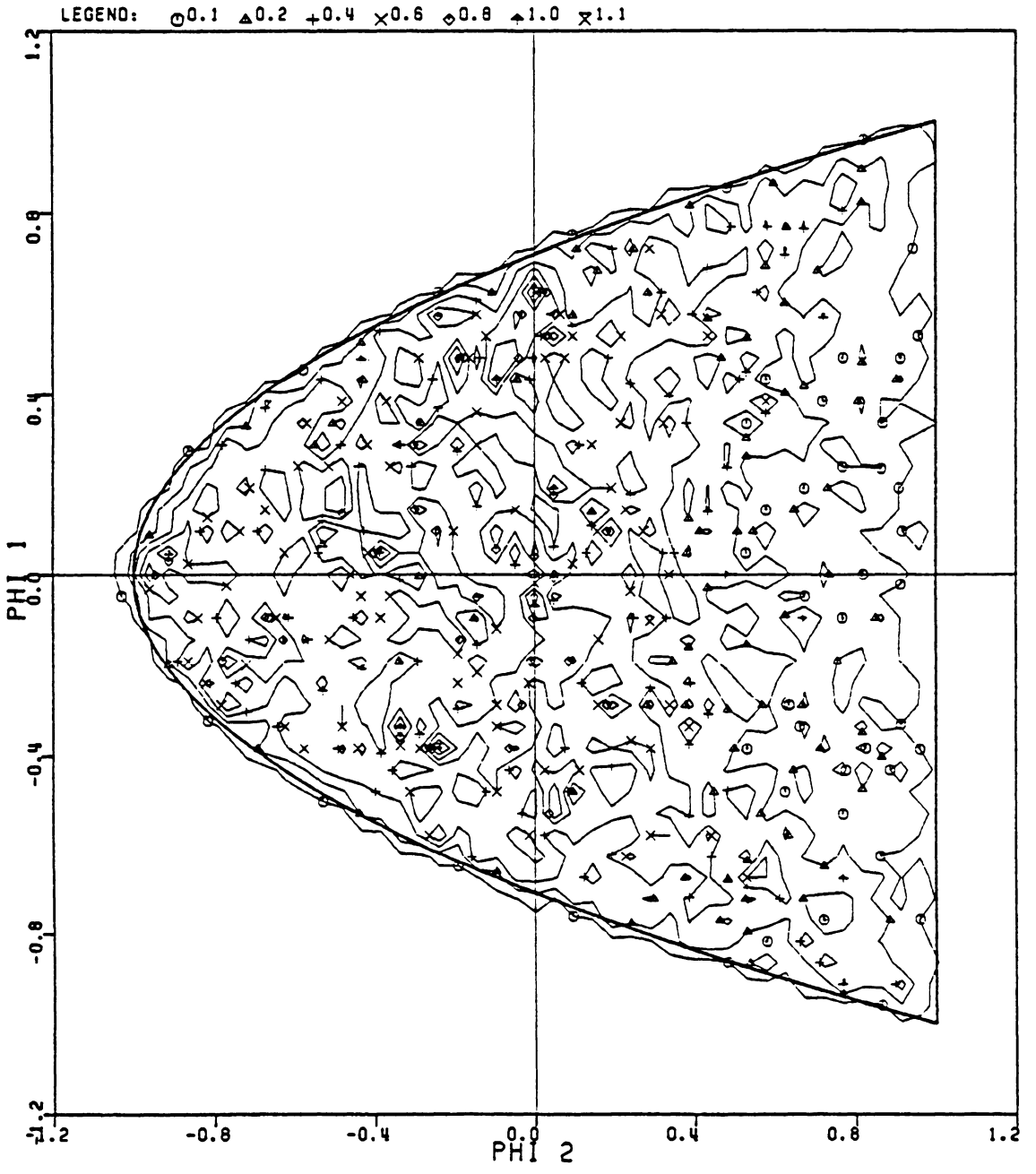

Figure 18. Burg estimator, white system.

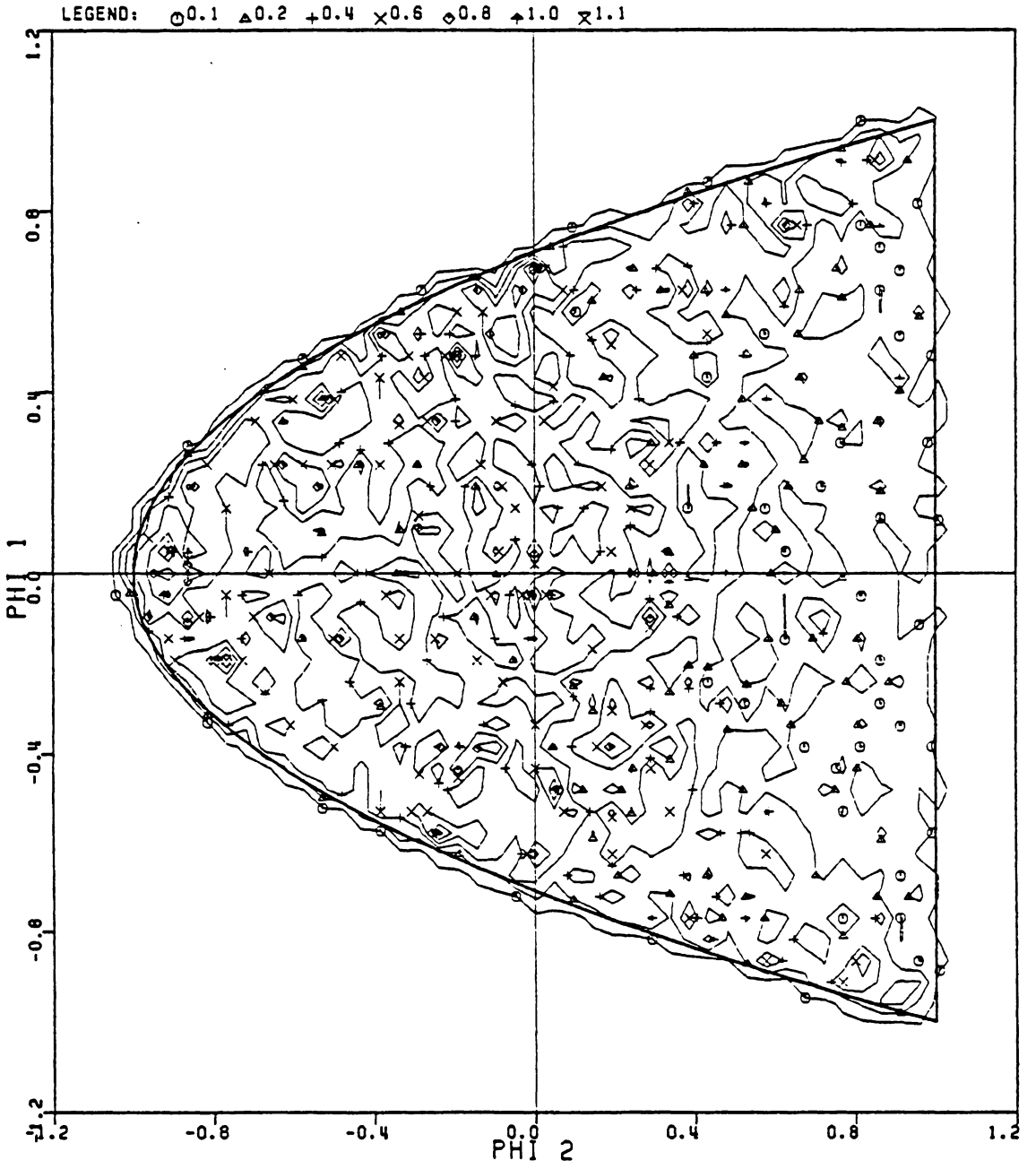

Figure 19. Itakura estimator, white system.

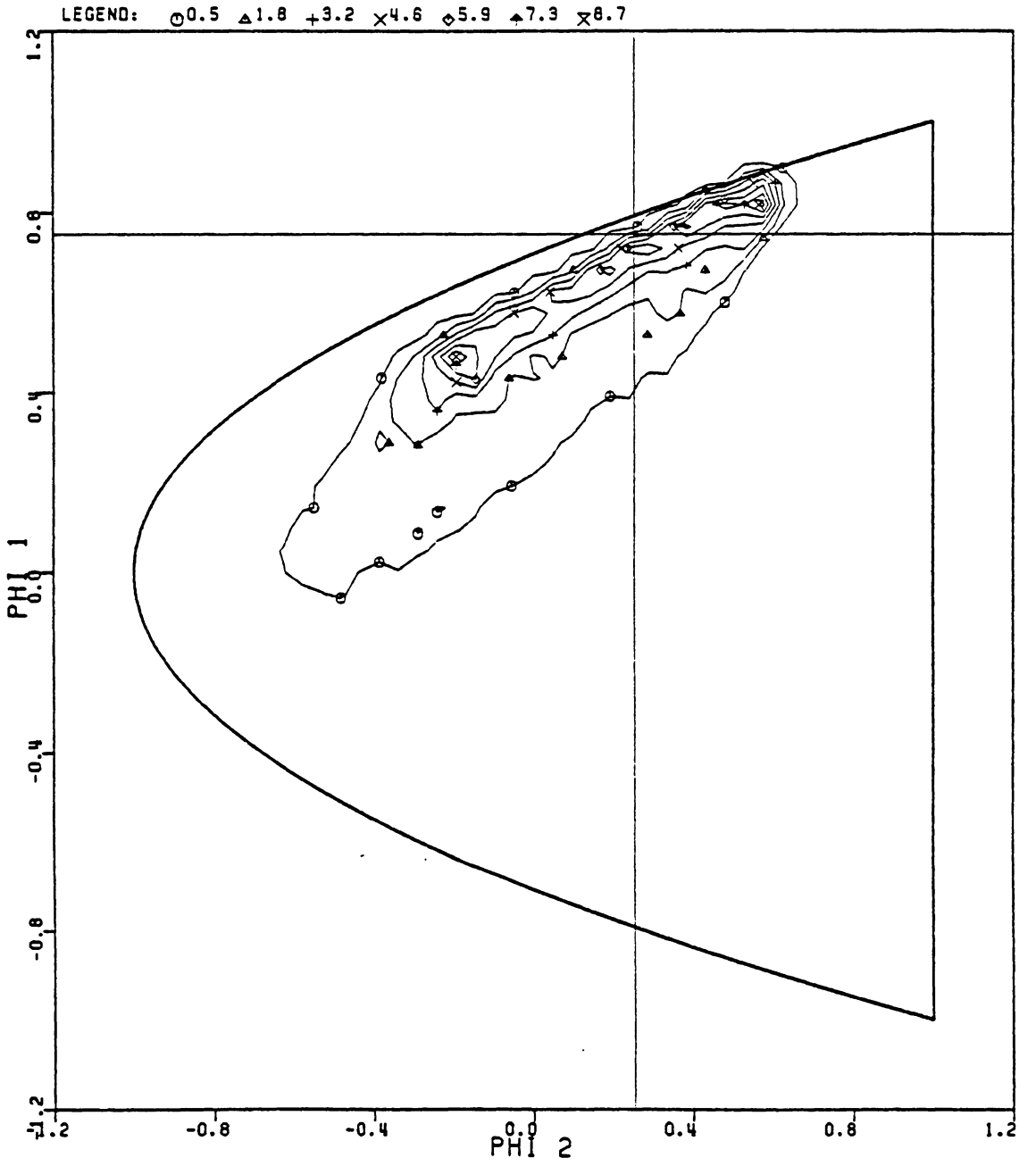

Figure 20. Biased estimator, lowpass system.

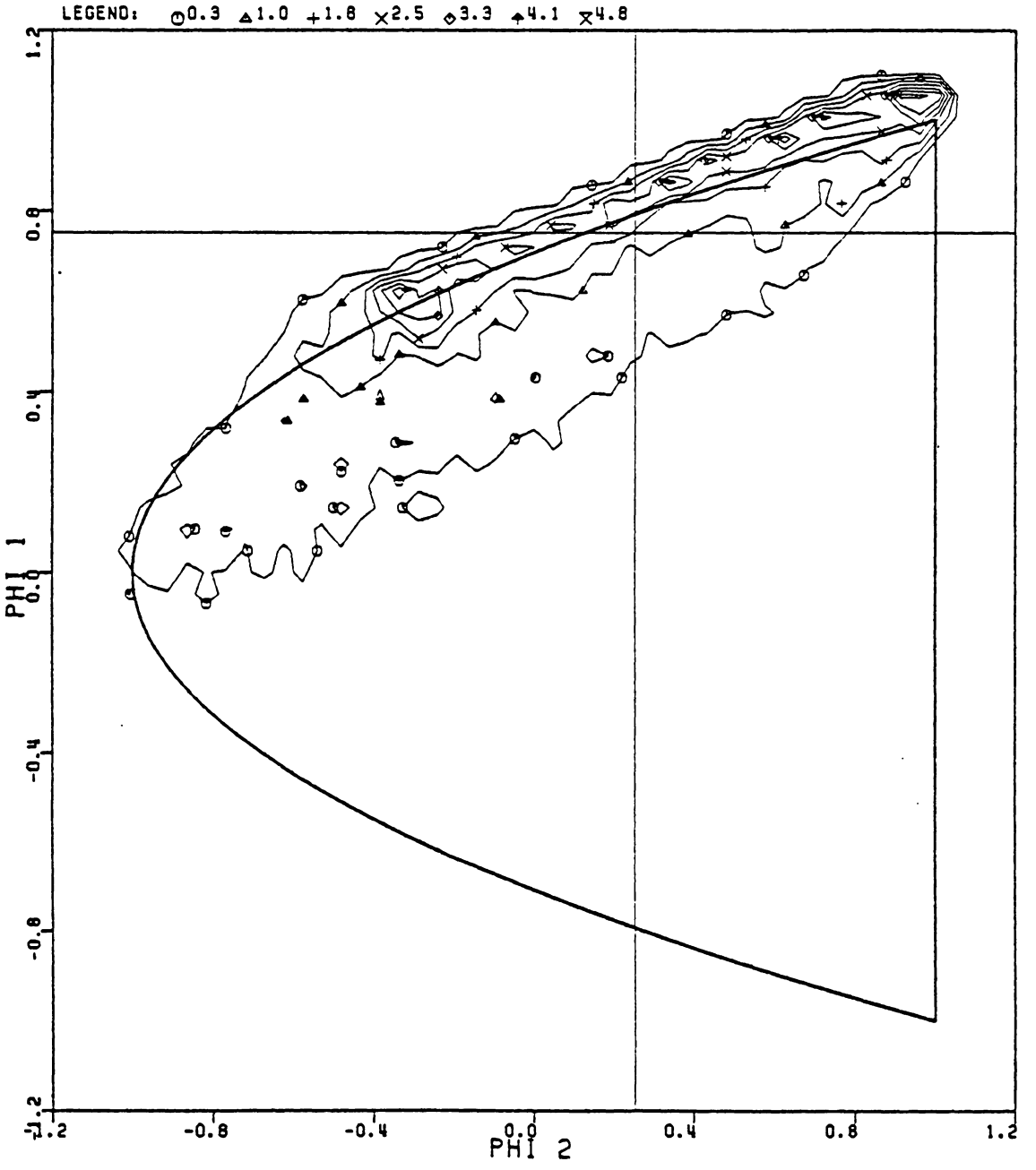

Figure 21. Unbiased estimator, lowpass system.

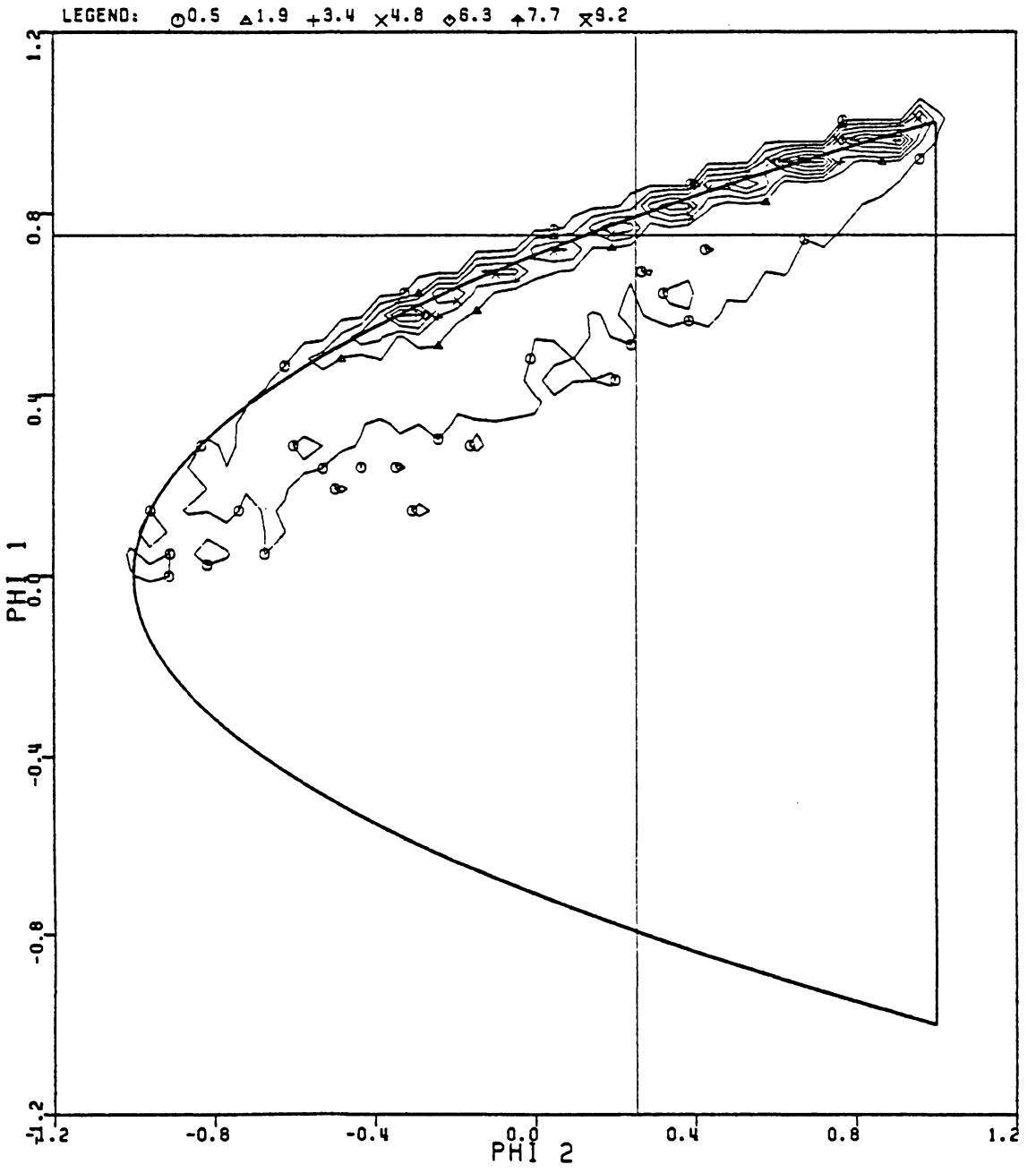

Figure 22. Diagonal correction, lowpass system.

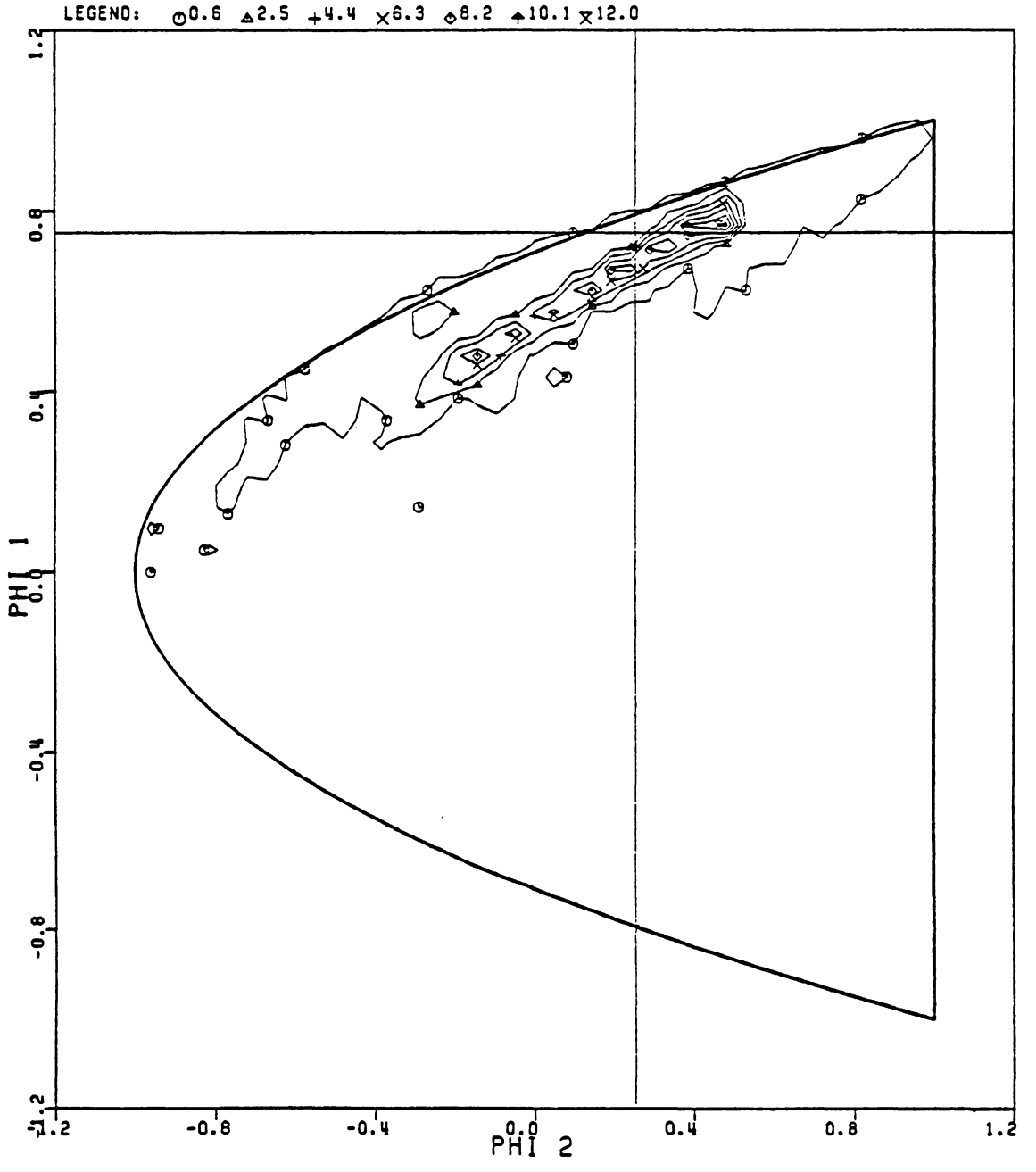

Figure 23. Triangular correction, lowpass system.

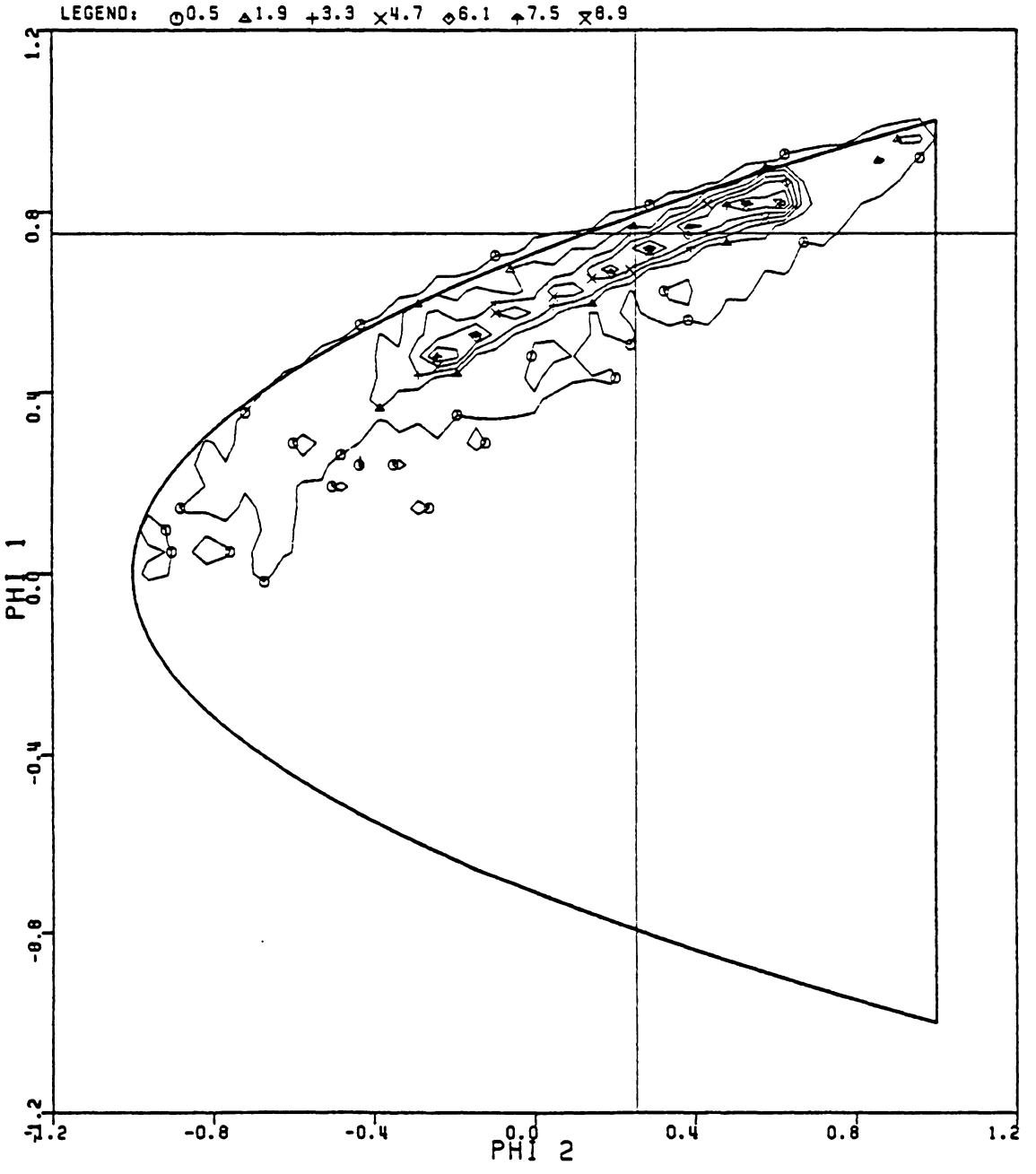

Figure 24. Exponential correction, lowpass system.

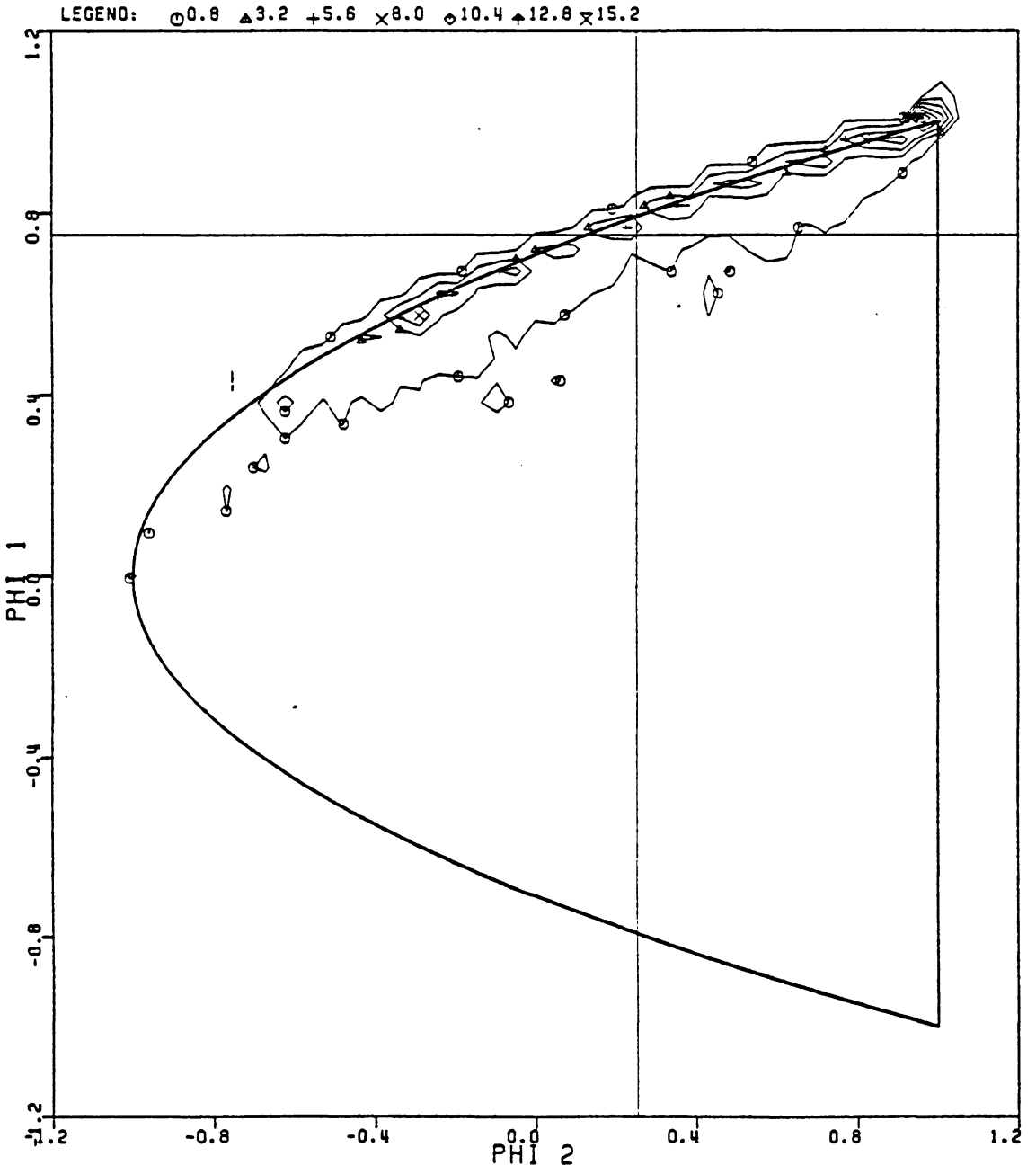

Figure 25. Minimum norm correction, lowpass system.

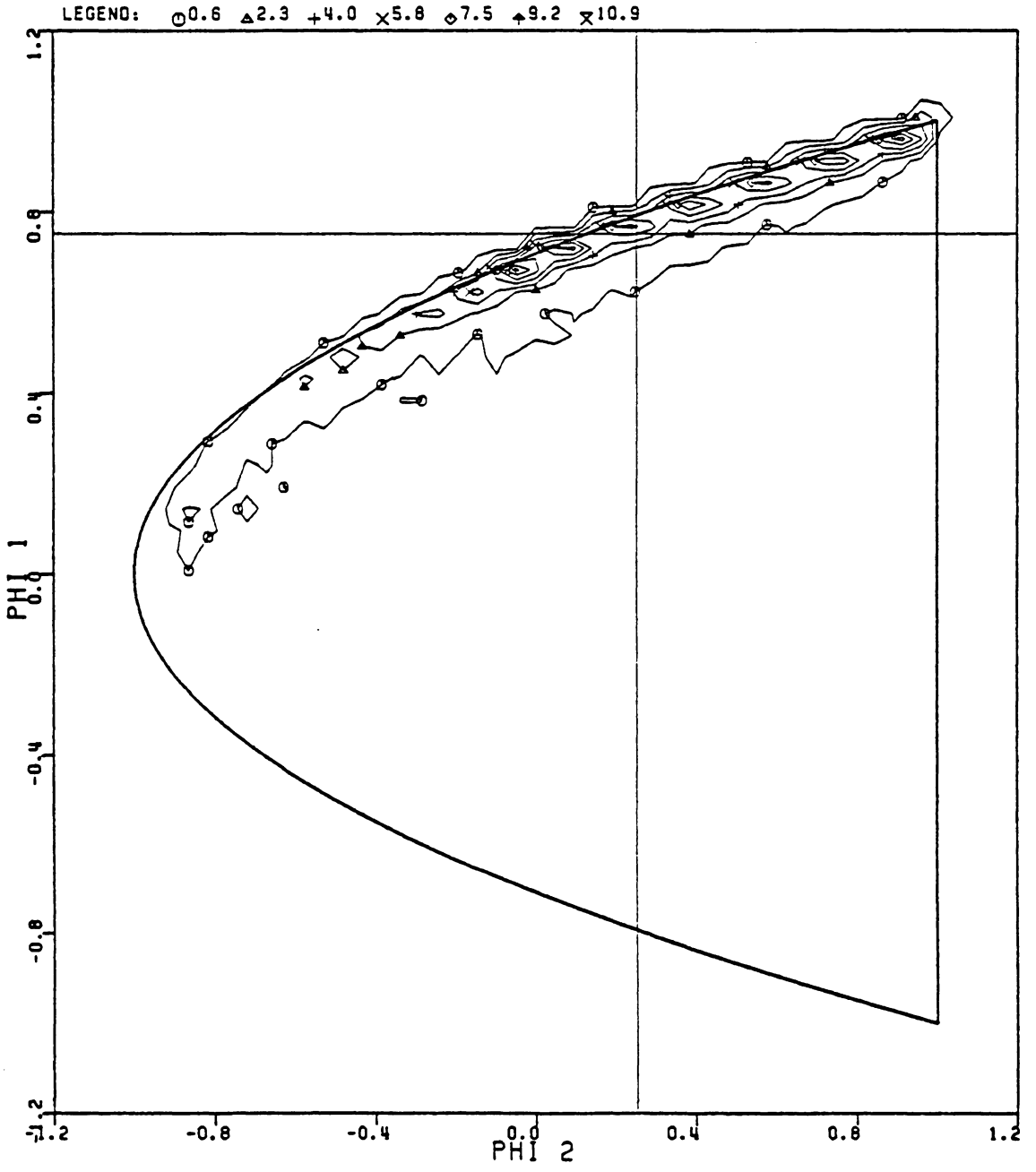

Figure 26. Burg estimator, lowpass system.

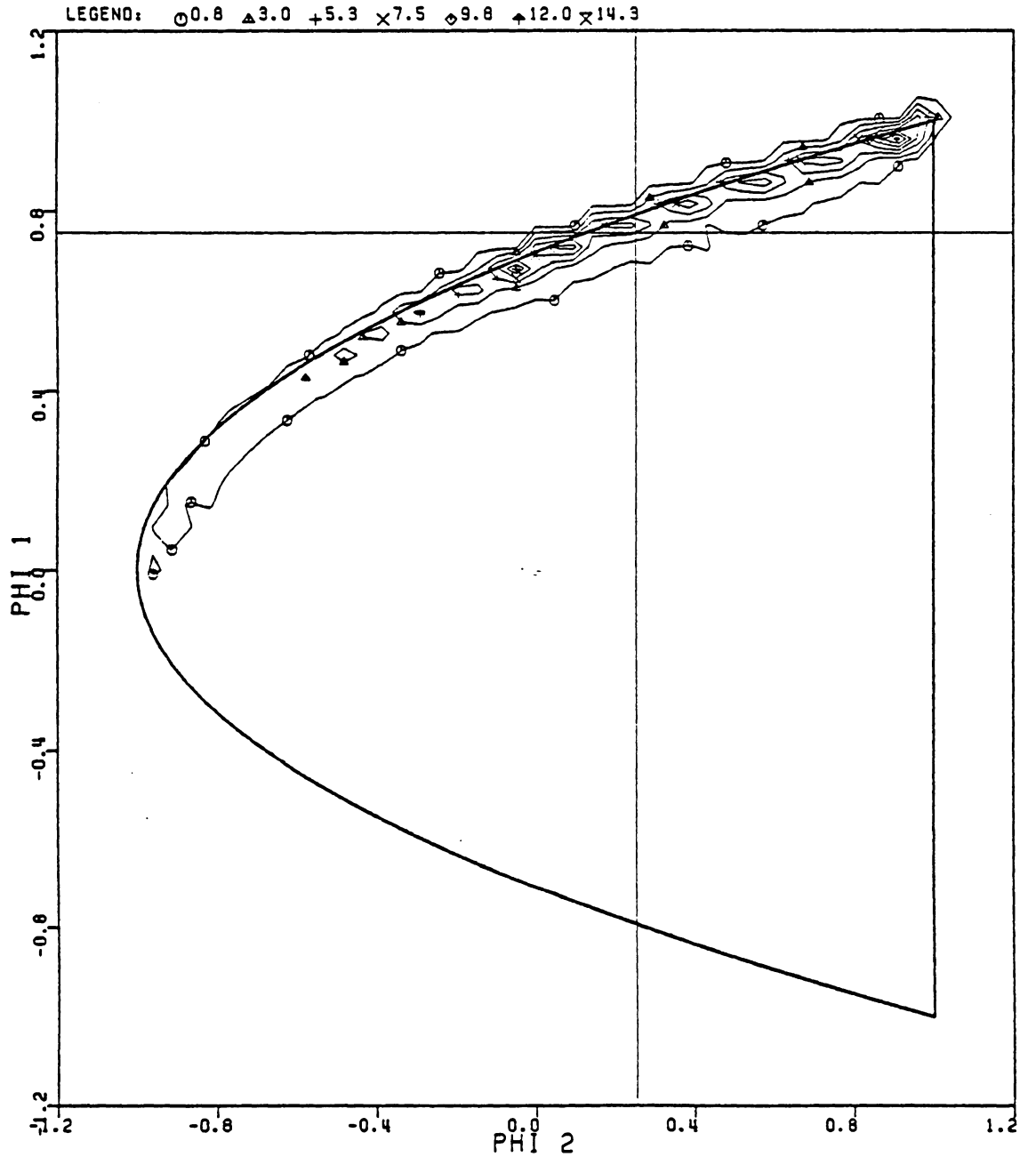

Figure 27. Itakura estimator, lowpass system.

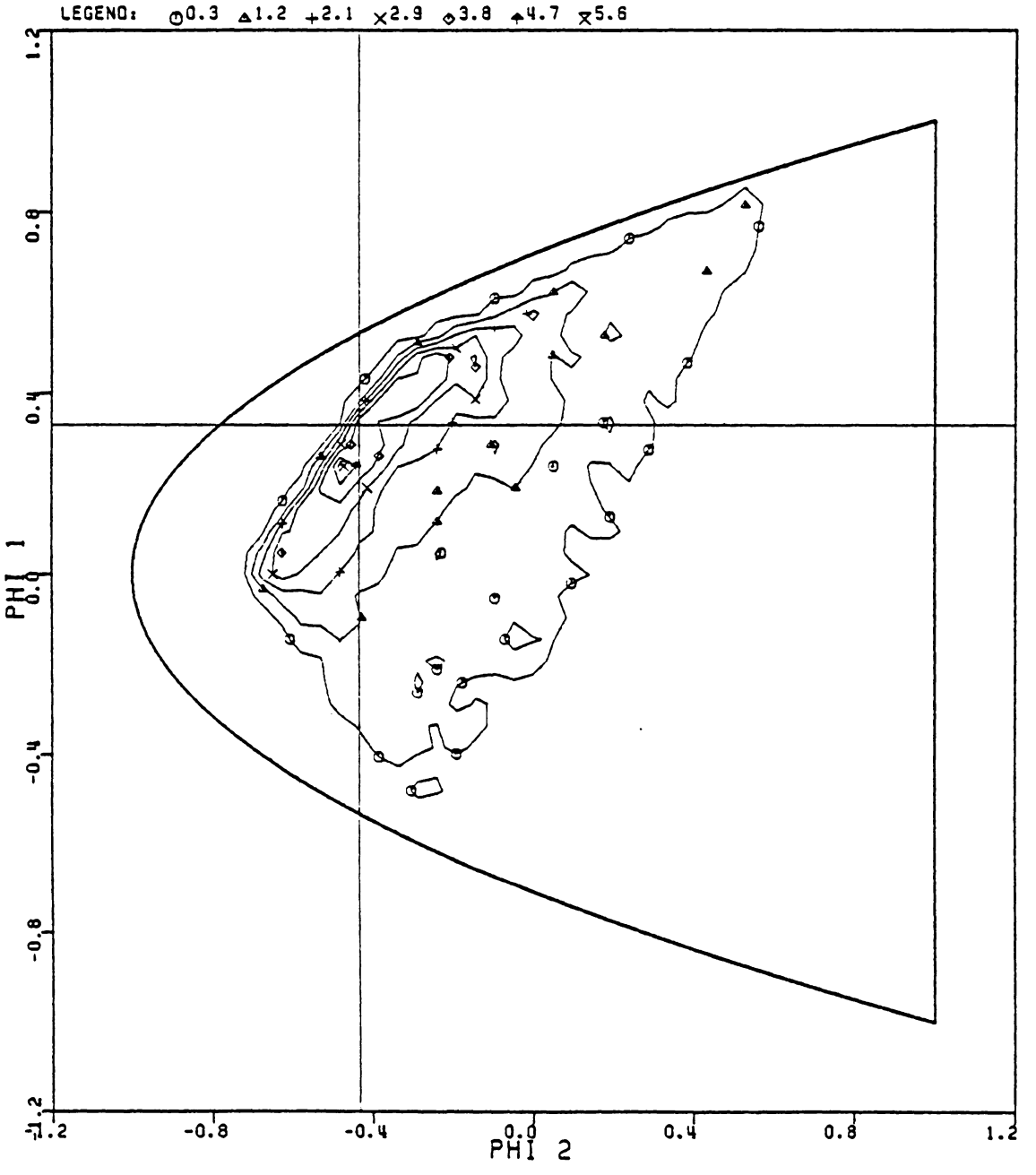

Figure 28. Biased estimator, bandpass system.

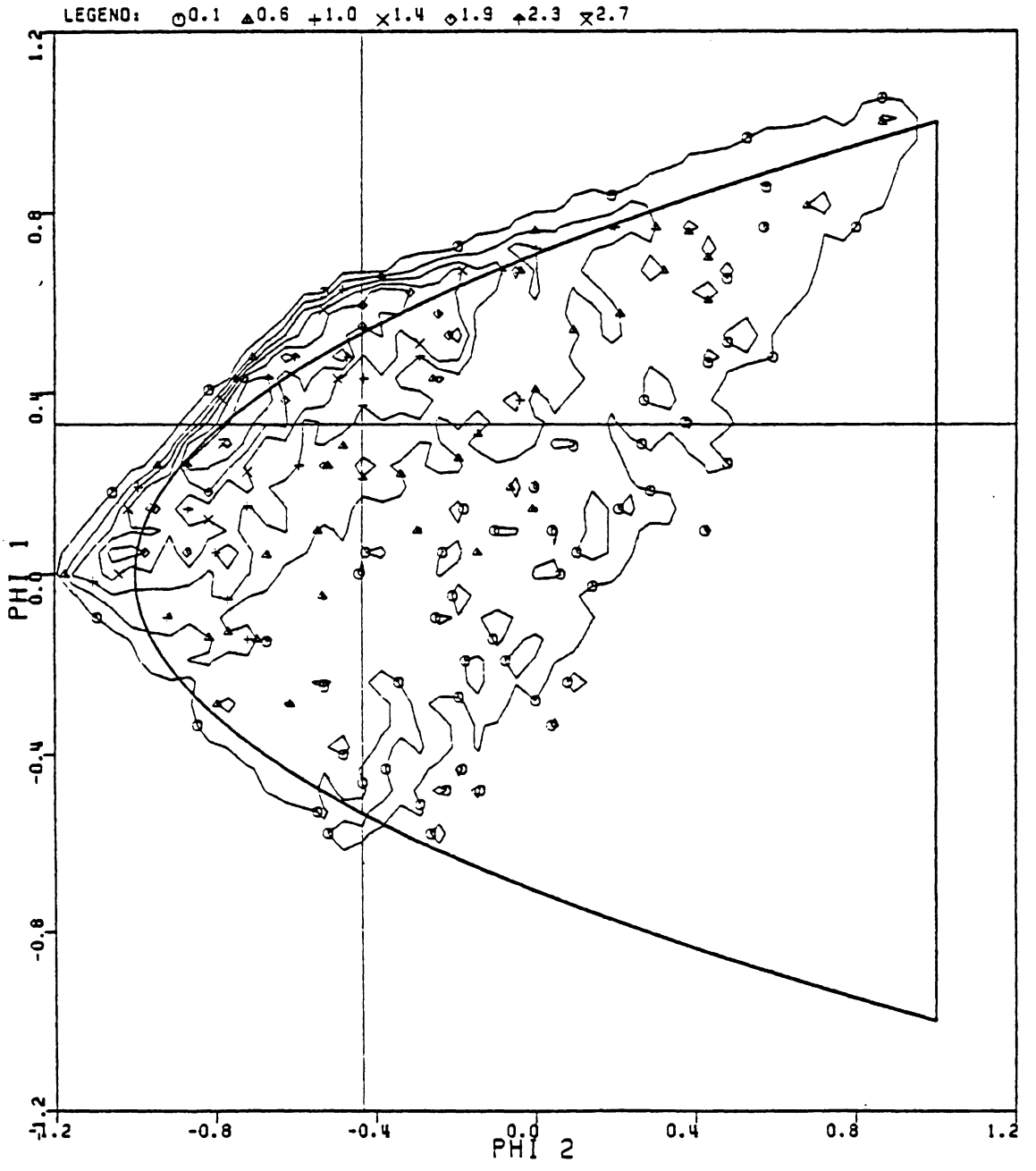

Figure 29. Unbiased estimator, bandpass system.

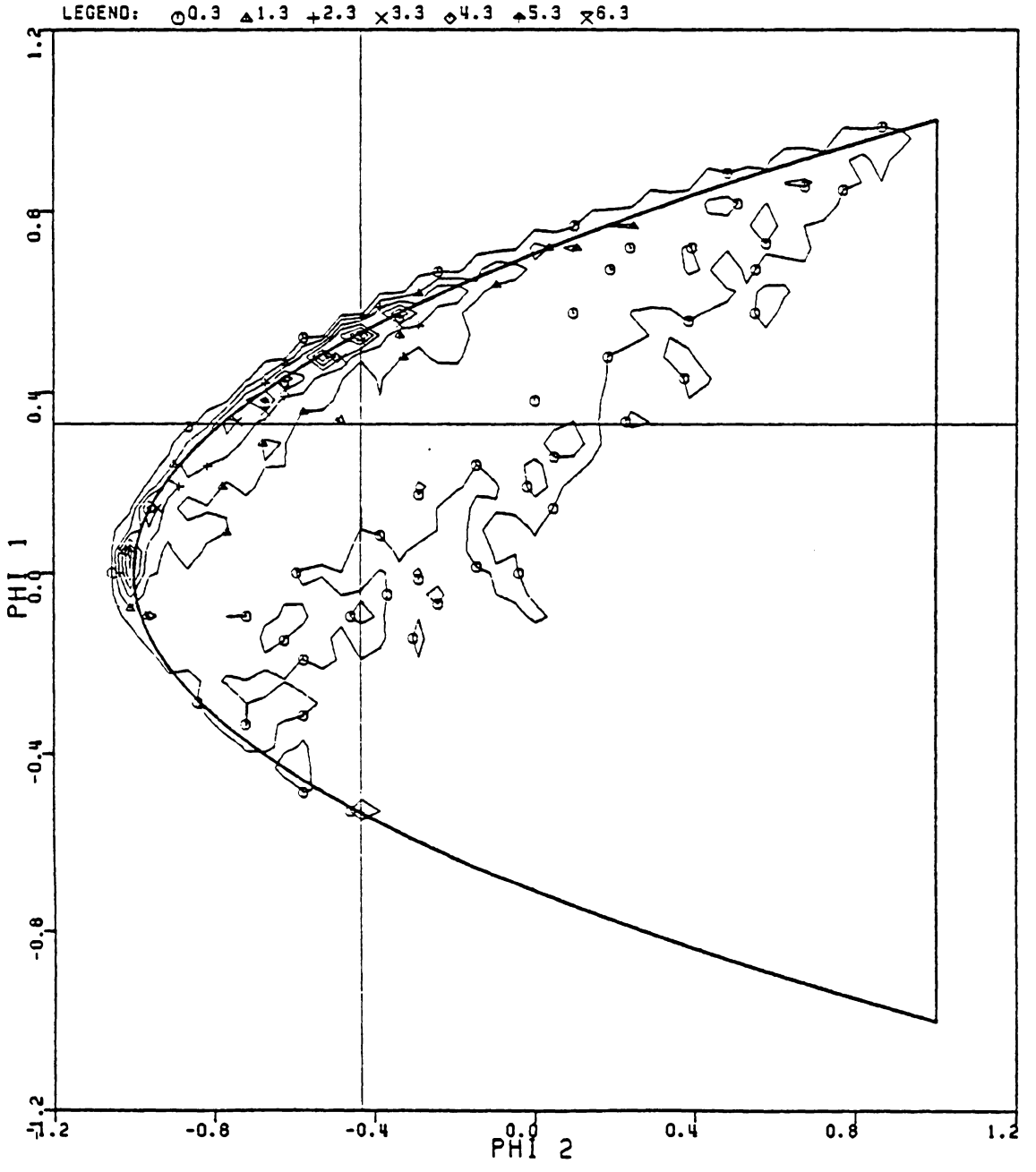

Figure 30. Diagonal correction, bandpass system.

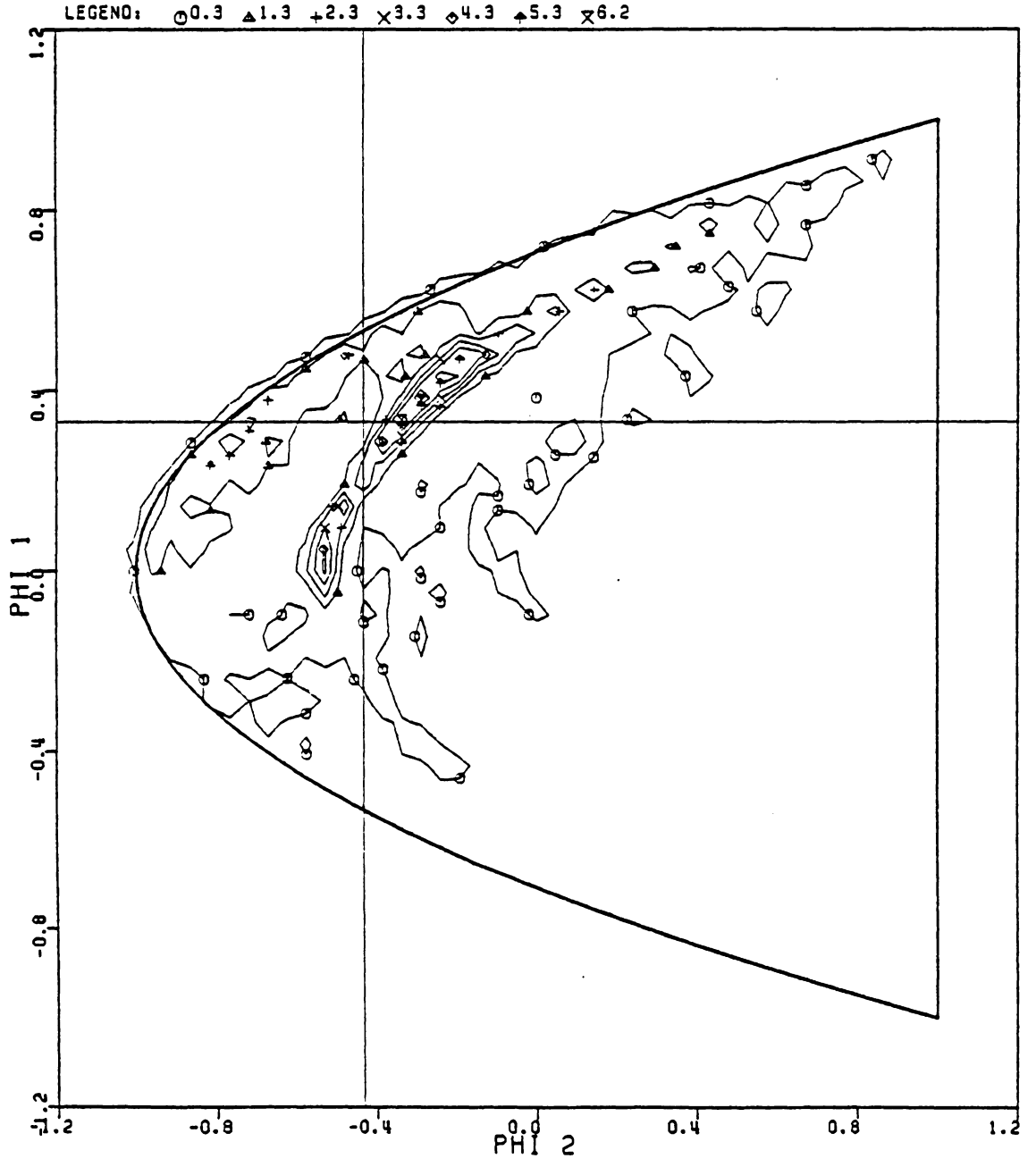

Figure 31. Triangular correction, bandpass system.

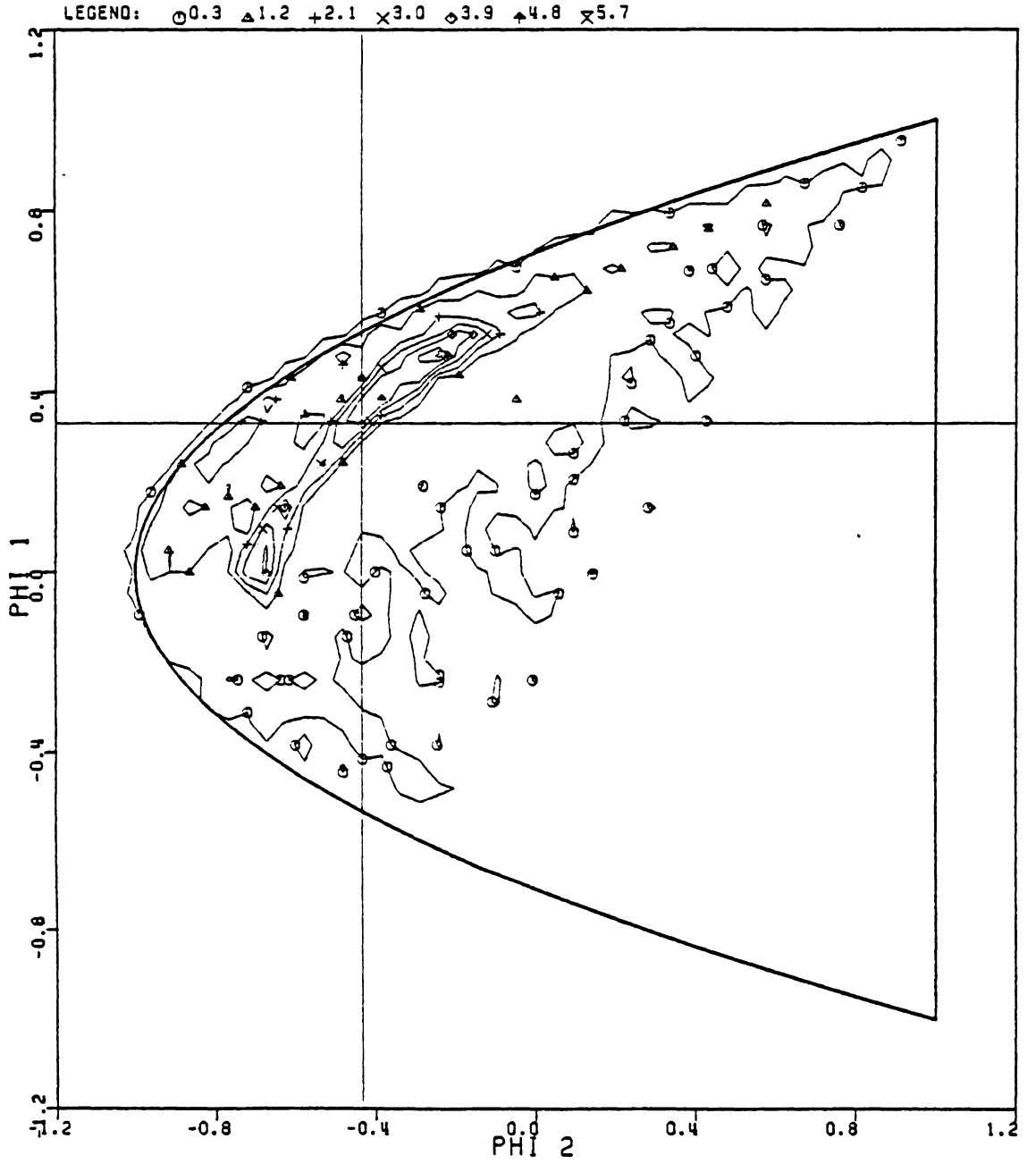

Figure 32. Exponential correction, bandpass system.

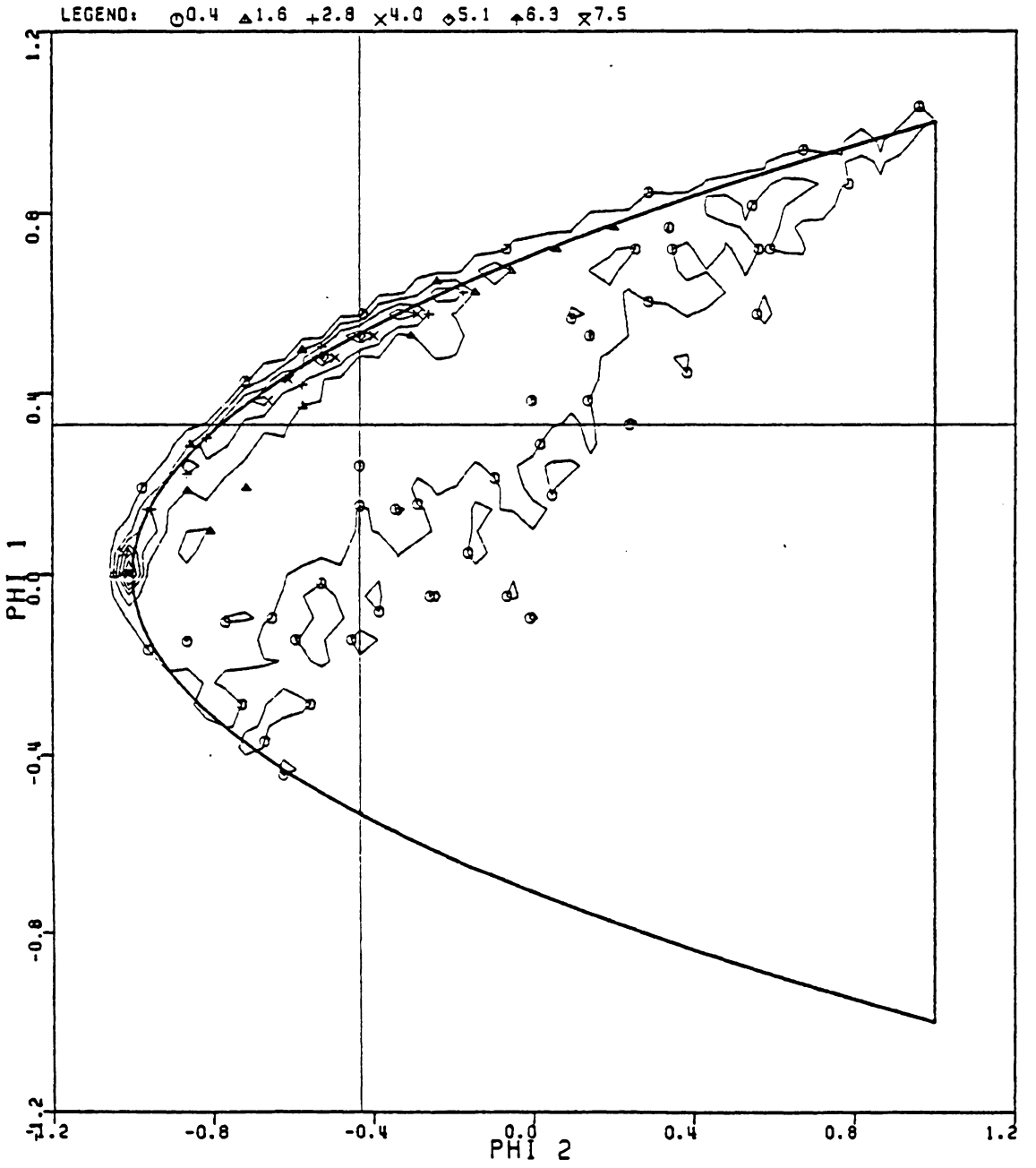

Figure 33. Minimum norm correction, bandpass system.

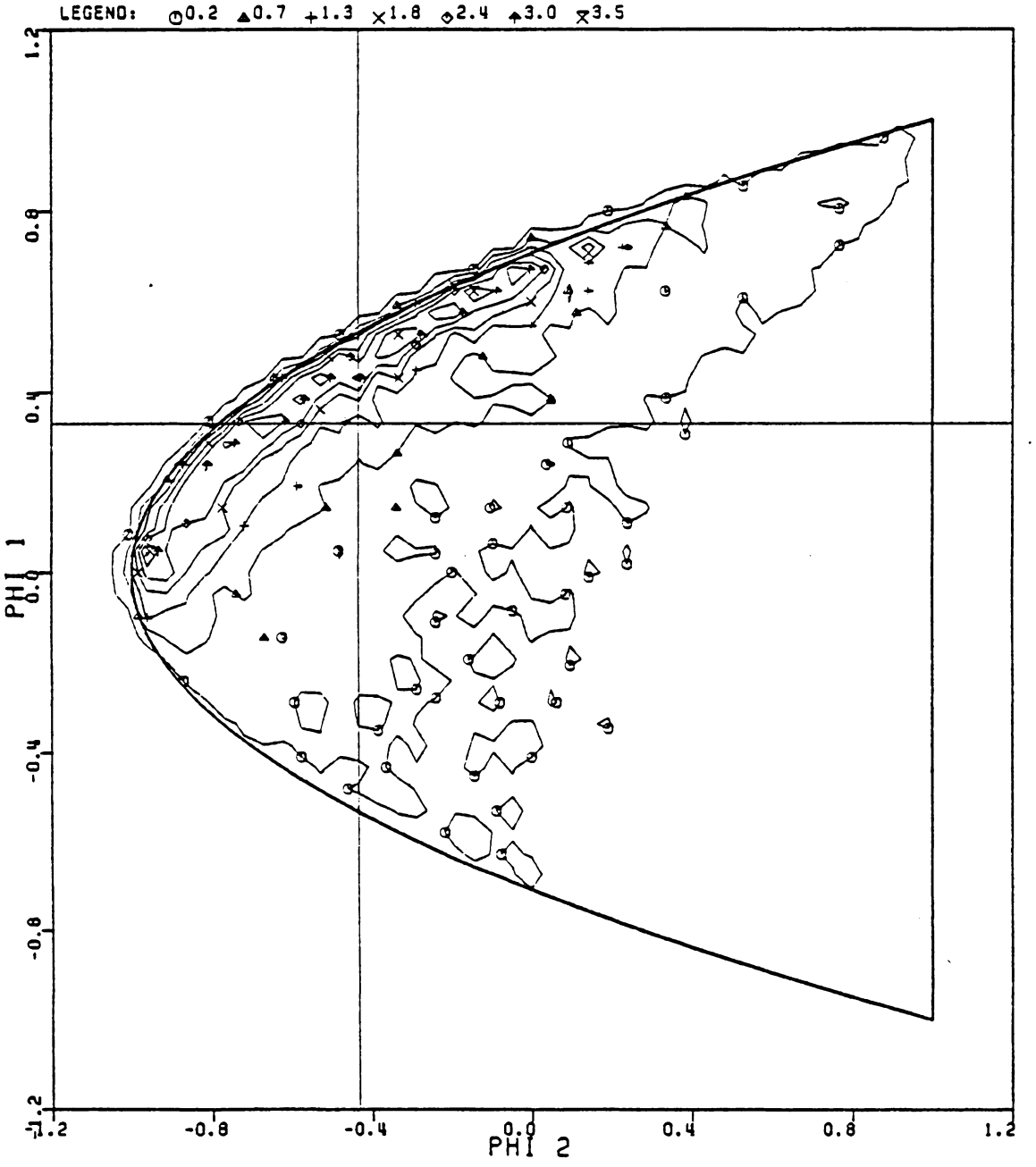

Figure 34. Burg estimator, bandpass system.

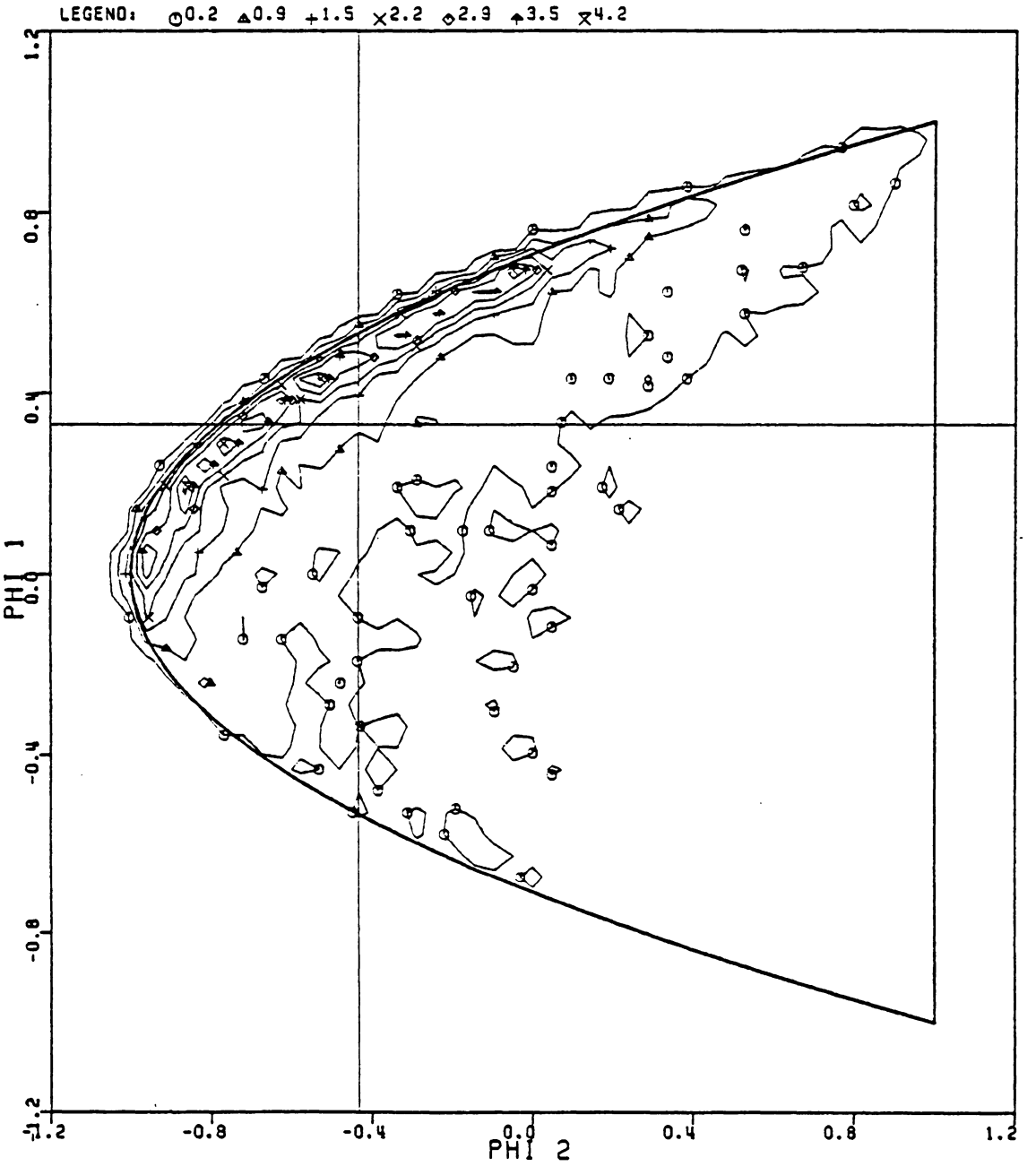

Figure 35. Itakura estimator, bandpass system.

through p_4 be histogram data points with values of 0, 0, 10, and 10, respectively, and let the value 5 be a contour level. Further, let the actual NND boundary pass close to the pair of points p_3 and p_4. The contour plotting program GCONTR will then place the contour line associated with the value 5 equidistant between the pairs of points p_1-p_3 and p_2-p_4, causing an apparent error. This apparent error can be reduced by increasing the number of points used to generate the histogram. Unfortunately, this would also greatly increase numerical processing time and computer memory requirements, and was therefore not done.

3.2.3 MAMF PERFORMANCE.

Each of the 8092 correlation estimates mentioned above was applied to the MAMF design process resulting in a sequence of 8092 MAMF's for each estimator. The normalized SNR (NSNR) for each of the 8092 MAMF's was determined using Equation 105, and the mean m, and standard deviation σ, of the NSNR sequence were found for each estimator, as given in Table 1 on page 51. Table 3 summarizes these results. Note that the mean and σ in Table 3 are relative to the SNR^m for each case.

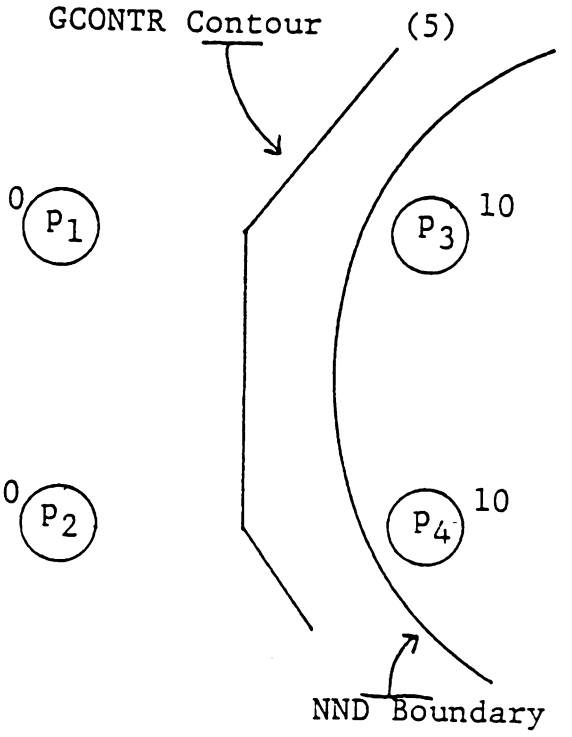

Figure 36. GCONTR apparent error example.

Table 3. NSNR performance of estimators.

	NOISE PROCESS					
	WHITE		LOWPASS		BANDPASS	
ESTIMATOR	m	σ	m	σ	m	σ
Biased	.848	.126	.803	.220	.849	.171
Unbiased	.748	.218	.697	.274	.751	.258
Diagonal	.743	.229	.676	.300	.717	.296
Triangular	.769	.192	.748	.273	.781	.232
Exponential	.763	.201	.721	.284	.758	.258
Min. Norm	.746	.224	.685	.278	.738	.271
Burg	.764	.190	.729	.275	.752	.245
Itakura	.740	.208	.721	.275	.736	.255

The relative performance for the combination of a given estimator, signal, and noise process can be predicted by mentally overlaying the deterministic NSNR contour plot and one of the correlation histograms for the particular noise process. Consider, for example, Figure 37, where the NSNR contour plot and the histograms for the biased, unbiased, and Burg estimators for the white noise process have been gathered for convenience. Of the three estimators shown, the unbiased estimator histogram (part b of Figure 37) is spread over the largest area. When that histogram and the NSNR contour plot are overlaid it can be seen that a good many of the correlation estimates correspond to MAMF's with relatively low values of SNR. Therefore, the values of output SNR for MAMF's designed with correlation estimates from an unbiased estimator will vary widely. This is confirmed in Table 3, where the unbiased estimator for the white noise case has a low NSNR m and high σ. The Burg estimator (part c of Figure 37) is somewhat more compact, giving a higher NSNR m and lower σ. Finally, the biased estimator (part d of Figure 37) is the most compact about Φ_a and therefore has the highest NSNR m and lowest σ.

The dangers of using estimators that place estimates close to the NND boundary can now be seen. In Figure 9, a trough of low NSNR can be seen adjacent to the upper NND boundary. Estimators like the diagonal or minimum norm correction methods that place correlation points on that boundary will

result in MAMF's that have low SNR. This is borne out in Table 3, where the minimum norm and diagonal correction methods have the lowest NSNR m and highest σ of all the estimators. Furthermore, the Itakura estimator (Figure 19) places its estimates closer to the NND boundary than the Burg estimator; as Table 3 shows, this lowers the performance of that estimator. Similar results are obtained for the bandpass noise case; see Table 3 and Figure 38.

In Table 3, the means and standard deviations for the lowpass noise case are lower and higher, respectively, than those for either the white noise or bandpass noise cases. Again, these results can be predicted by examining the noise histograms and NSNR contour plots. In part a of Figure 39, it can be seen that there is a low-SNR trough that runs from center left to lower right, with a break in its center. Further, in parts b, c, and d of Figure 39 the estimator histograms have a ridge-like structure that does not run parallel to the high-NSNR ridge in part a of Figure 39. These characteristics result in MAMF's with low average NSNR. Furthermore, these MAMF NSNR values will have high standard deviation. An estimator like the biased estimator (part d of Figure 39) which concentrates its estimates close to Φ_a still gives improved performance compared to estimators that are more widely distributed (parts b and c of Figure 39). It is of interest that the unbiased estimator for the bandpass system (part b of Figure 38) is nearly as good as

the Burg estimator (part d of Figure 38). The Burg estimator is more compact; however, it tends to place its estimates along a slope that falls rapidly into regions of low SNR, yielding results similar to those from the unbiased estimator.

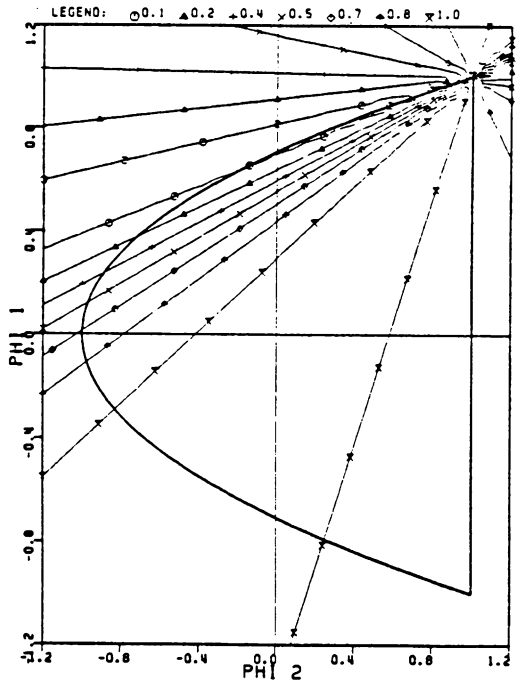

a. NSNR contour plot.

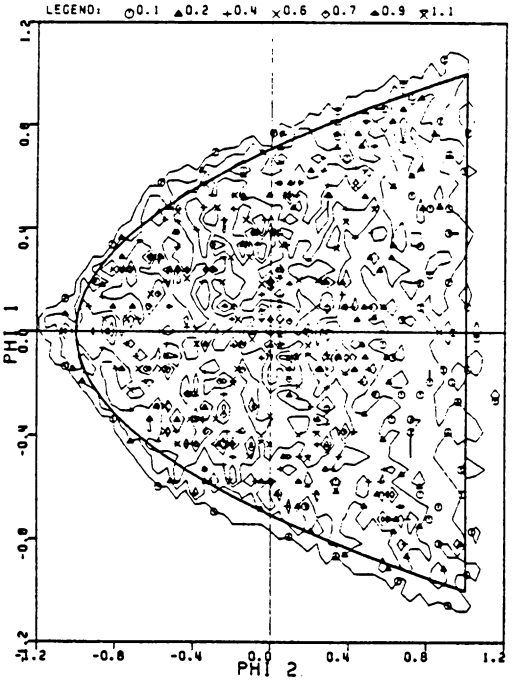

b. Unbiased estimator.

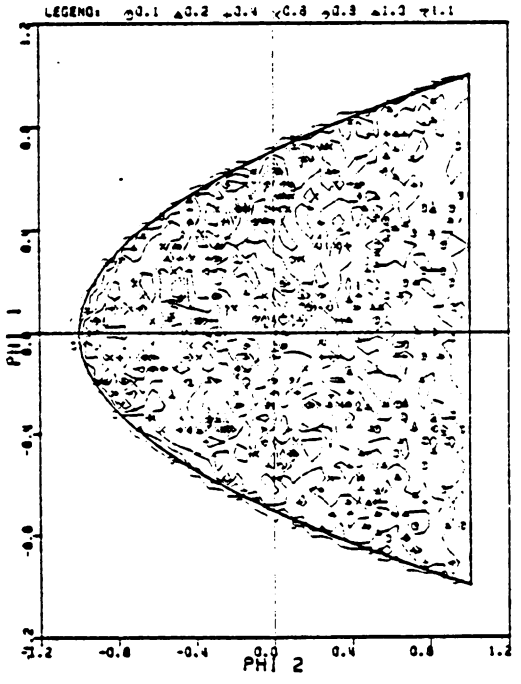

c. Burg Estimator.

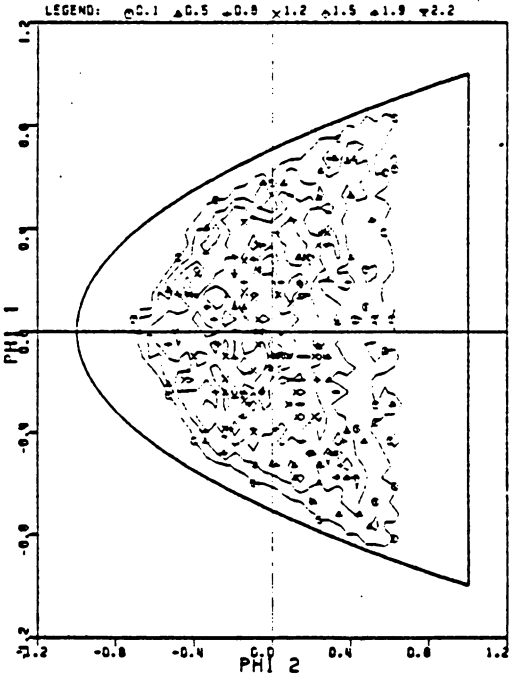

d. Biased estimator.

Figure 37. White noise system estimator comparison.

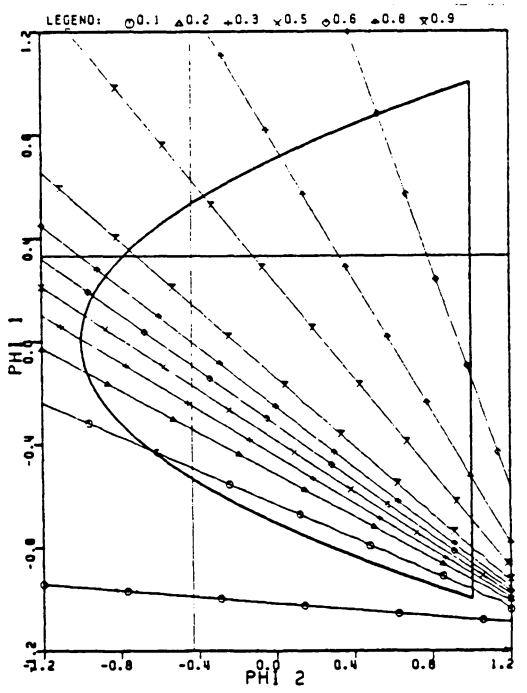

a. NSNR contour plot.

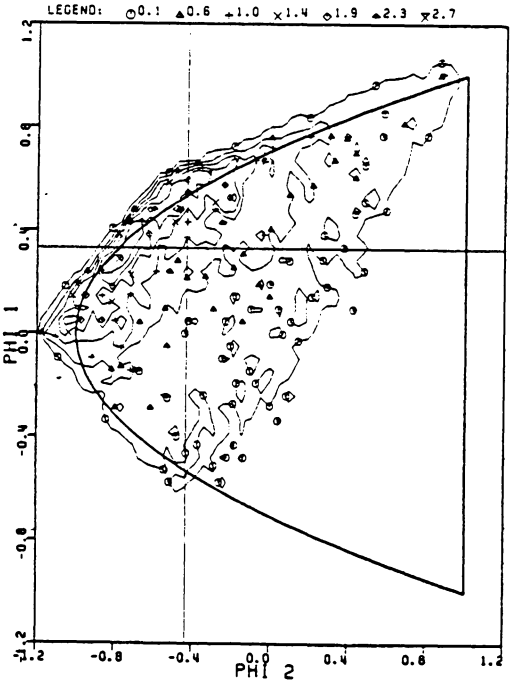

b. Unbiased estimator.

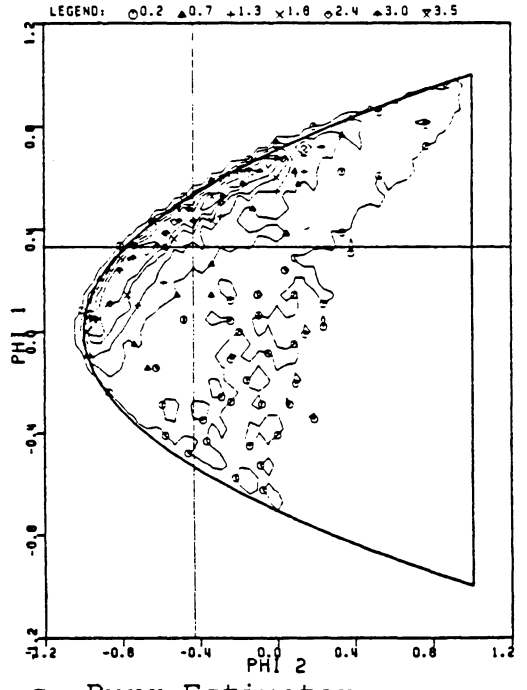

c. Burg Estimator.

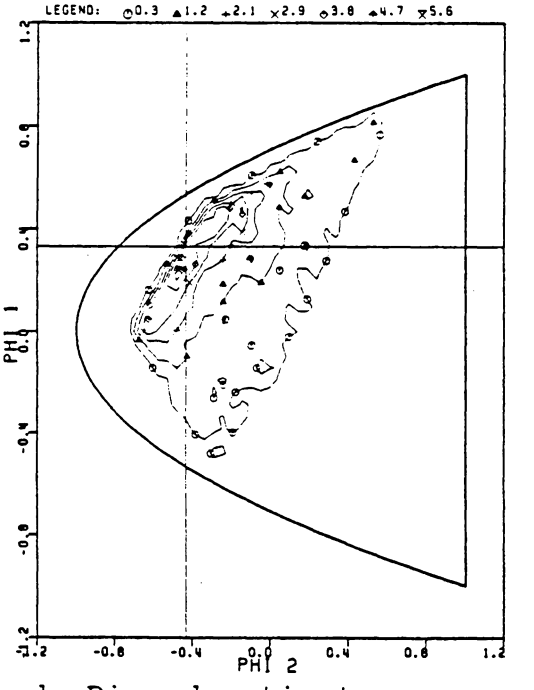

d. Biased estimator.

Figure 38. Bandpass noise system estimator comparison.

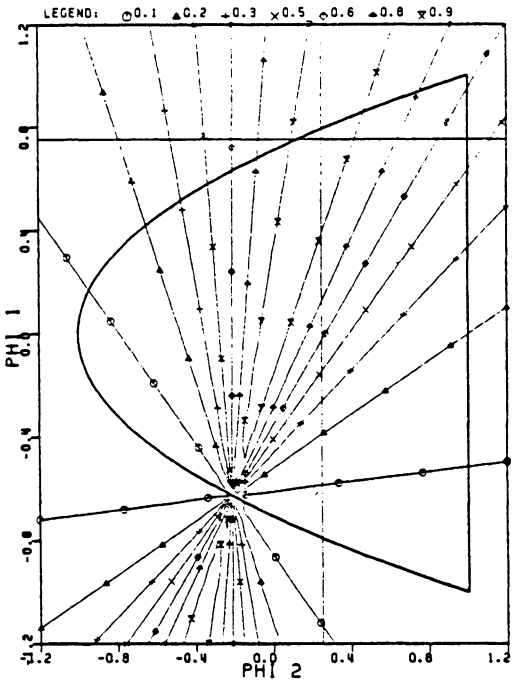

a. NSNR contour plot.

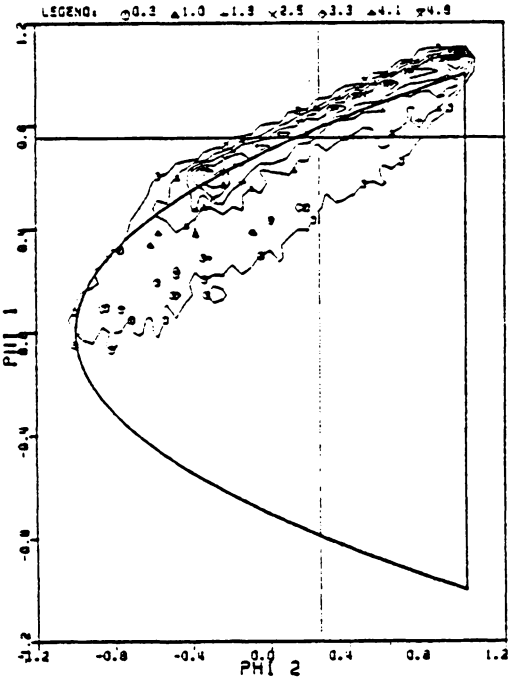

b. Unbiased estimator.

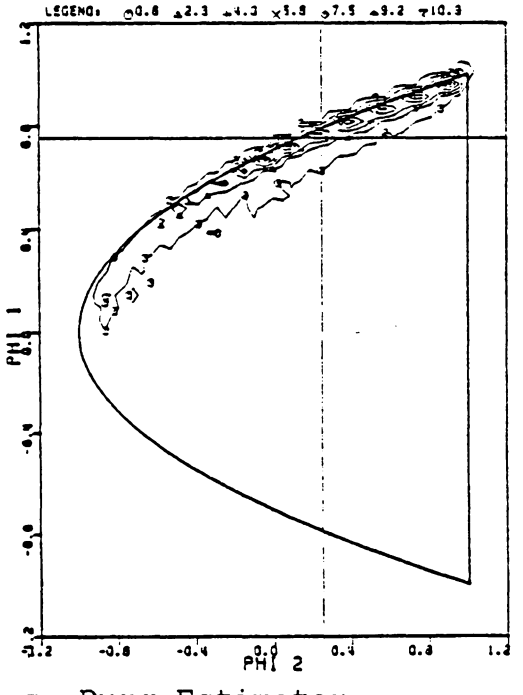

c. Burg Estimator.

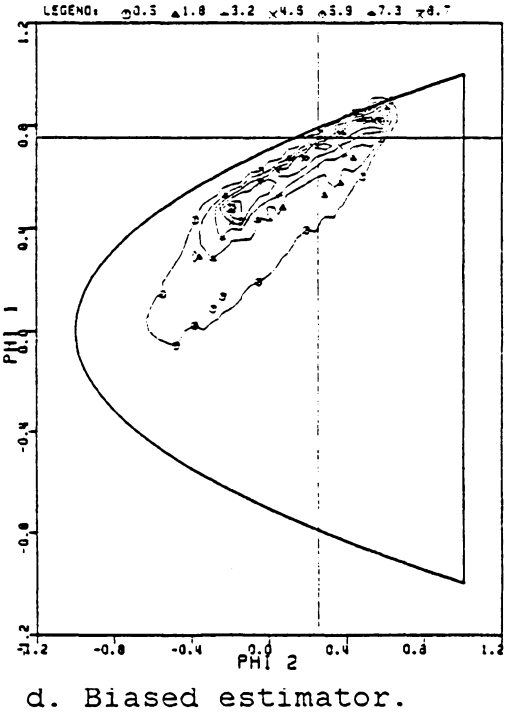

d. Biased estimator.

Figure 39. Lowpass noise system estimator comparison.

4.0 GENERATING ROBUST FILTERS.

4.1 INTRODUCTION.

As the deterministic NSNR plots show, the SNR of the MAMF's considered so far decreases rapidly in certain directions as the estimated correlation ϕ moves away from ϕ_a. The NSNR contour plots are functions of the signal vector $\underline{s}$, the actual correlation ϕ_a, and the estimated correlation ϕ. Since ϕ_a and ϕ are beyond the control of a designer, it behooves us to modify $\underline{s}$ in an attempt to increase the robustness of the MAMF's by reducing the change in MAMF output SNR for estimated correlations near ϕ_a.

Since changing $\underline{s}$ away from that signal vector that gives the maximum SNR will reduce SNR^m, finding an $\underline{s}$ to improve the robustness of the MAMF becomes a nonlinear problem where SNR^m is traded off against robustness.

4.2 FORMULATIONS FOR ROBUST PERFORMANCE.

Several forms of information about the MAMF system are available:

- the correlation histogram;

- Φ_a; and

- the SNR contour plot for a given signal.

Given these data, it was decided to use nonlinear programming techniques to generate a signal vector that would result in some desired degree of robustness. The following discussion describes the general approach used. First, a function is derived from the correlation histogram for use as a weighting function. Second, the output SNR's of a MAMF designed using some signal vector $\underline{s}$ are evaluated at the correlation histogram grid points. Next, the output SNR's of the MAMF and the weighting function are combined to form one of several cost functions. Finally, these cost functions are minimized or maximized using a nonlinear programming technique that varies $\underline{s}$ to achieve MAMF's with a desired degree of robustness. The MAMF's designed by this technique are then evaluated for their performance.

The weighting function will now be discussed. Two undesirable characteristics of histograms reduce their effectiveness as a weighting function. First, the histogram values may vary over a range of 100:1; second, the outliers of the histogram are irregular and highly variable. If the histogram is used directly as a weighting function, the first characteristic will weight the cost function solution towards those few points on the histogram with maximum value, thus

reducing the robustness of the filter to be generated. The second characteristic causes a problem in the opposite direction. Since the outliers of the correlation histogram correspond to correlation estimates that are rarely encountered and may correspond to NSNR points that are low (Figure 9), including them in the cost function would weight the cost function away from a filter with high SNR^m. To reduce these problems, a smoothed version of the histogram was developed to serve as a weighting function. The first step taken was to reduce the number of outliers. Let

$$\sum_{i=1}^{N_1} \sum_{j=1}^{N_2} p_{ij} = \text{Max} \tag{116}$$

where

$$N_1 + N_2 = N \tag{117}$$

where the p_{ij} are the values of the histogram and $N_1 + N_2 = N$ is the number of non-zero histogram values. The lowest level Q_{min} is then found that generates a reduced set of histogram values q_{ij} where

$$\sum_{i=1}^{M_1} \sum_{j=1}^{M_2} q_{ij} \leq (0.95)\text{Max} \tag{118}$$

and

$$q_{ij} = p_{ij} \qquad p_{ij} \geq Q_{min} \tag{119}$$

where p_{ij} that are less than Q_{min} are discarded from the q_{ij} set and $M_1 + M_2 = M$ is the number of q_{ij} in the reduced set. Note that this method effectively removes the outliers of the histogram. The problem of extreme variability in the new histogram described by the q_{ij} is now addressed. It is desired to generate a weighting function $w(q_{ij})$ with a maximum value of one and a minimum value of W_{min}. This is simply done using a linear transformation

$$w(q_{ij}) = \frac{q_{ij} - Q_{min}}{Q_{max} - Q_{min}} (1 - W_{min}) + W_{min} \tag{120}$$

where

$$Q_{max} = \sup_{i,j}(q_{ij}) \tag{121}$$

and

$$Q_{min} = \min_{i,j}(q_{ij}) \tag{122}$$

The cost functions will now be discussed. Note that in the following discussion a given cost function may be either maximized, minimized, or combined with another cost function

in order to generate a signal vector $\underline{s}$ that can be used to design a robust filter.

The first cost function to be discussed is F_{dif}, which is given by

$$F_{dif} = \sum_{i=1}^{M_1} \sum_{j=1}^{M_2} |w(q_{ij}) - SNR_{ij}/SNR^m| \tag{123}$$

where

$$SNR_{ij} = \frac{(\underline{s}^T C_{ij}^{-1} \underline{s})^2}{\underline{s}^T C_{ij}^{-1} \Phi_a C_{ij}^{-1} \underline{s}} \tag{124}$$

and

$$SNR^m = \underline{s}^T \Phi_a^{-1} \underline{s} \tag{125}$$

$\underline{s}$ is some signal vector; $C_{ij} = T[c_0 \; c_{1,ij} \; c_{2,ij}]$ where $c_0 = 1$ and $c_{1,ij}$ and $c_{2,ij}$ describe a grid point of the reduced histogram with value q_{ij}; Φ_a is the actual noise correlation matrix for the system being used; and SNR^m is the maximum possible MAMF output SNR given $\underline{s}$. Note that F_{dif} is varied by changing $\underline{s}$. F_{dif} is the sum of the absolute values of the difference between a surface described by $w(q_{ij})$ and a surface described by the NSNR contour plot. Minimizing F_{dif} changes the NSNR contour plot to closely match the

surface described by the $w(q_{ij})$. This can increase the NSNR m and reduce NSNR σ. If, for example, W_{min} (Equation 120) is set to one, the NSNR surface may, in certain of the problems to be considered, be forced flat. This would result in an NSNR m of one and a σ of zero.

F_{snr} is given by

$$F_{snr} = \sum_{i=1}^{M_1} \sum_{j=1}^{M_2} SNR_{ij} w(q_{ij}) \tag{126}$$

where the SNR_{ij} is as given in Equation 124. F_{snr} is the weighted sum of the SNR's taken over the grid described above. By maximizing this function of $\underline{s}$ it is apparent that a signal vector would be generated resulting in the maximum average SNR for the probability mass distribution $w(q_{ij})$. If the set of SNR's generated all reach some maximal value, the NSNR m would be expected to rise and σ to decrease.

F_{del} is given by

$$F_{del} = \sum_{i=1}^{M_1} \sum_{j=1}^{M_2} \left(\sum_{k=0}^{2} \left[\frac{\partial SNR_{ij}}{\partial c_{k,ij}} \right]^2 \right) w(q_{ij}) \tag{127}$$

F_{del} is the weighted sum of the sum of squares of the gradients of the three-dimensional SNR surface taken over the reduced histogram grid. By minimizing this function, it is expected that the SNR surface would become flatter over the

reduced set of correlation points. If the surface became flat, the NSNR m would increase and σ would decrease.

The following combinations of two of the above three functions were used:

$$F_1 = C(F_{dif} + 1) + (1 - C)F^*_{snr}/F_{snr} \qquad (128)$$

and

$$F_2 = C(F_{del} + 1) + (1 - C)F^*_{snr}/F_{snr} \qquad (129)$$

where $0 \leq C \leq 1$ and F^*_{snr} is a constant, such that F_1 or $F_2 = 1$ when C is zero. A signal vector $\underline{s}$ is found by minimizing F_1 or F_2. The constant C allows a weighted solution vector $\underline{s}$ to be generated somewhere between the solutions given by F_{snr} and F_{dif} or F_{del}. A value of one was added to F_{del} and F_{dif} in Equation 128 and Equation 129 to make minimizing these terms somewhat more tractable, as it is possible for them to have a value of zero.

4.2.1 NUMERICAL PROBLEMS AND SOLUTIONS.

While attempting to numerically find the minima or maxima of the functions listed above, several problems were encountered and overcome. The following paragraphs will discuss these problems and their current solutions.

F_{snr} may be maximized or F_{del} may be minimized by reducing the l_2 norm of the signal vector $\underline{s}$, as this reduces the signal energy. The final result of this undesired action would be the zero vector $\underline{0}$. To remove this problem, a signal vector $\underline{s}$ of l_2 norm one was derived from the working vector $\underline{x}$, used in the minimization software, where

$$\underline{s} = \underline{x}/\|\underline{x}\| \tag{130}$$

The FORTRAN minimization subroutine used to generate the signal vectors that minimize or maximize the above functions (VA10AD from the Harwell Subroutine Library [MJH]) works more efficiently and reliably if an initial starting vector is supplied that is close to the final solution. Therefore, 124 $\underline{x}$ vectors that generated 124 $\underline{s}$ vectors on an l_2 ball of one were made; the $\underline{x}$ vector that resulted in a minimal function value was then used as an initial starting vector.

Because $\underline{s}$ is a normalized version of $\underline{x}$, there are an infinite number of $\underline{x}$ that will result in the same $\underline{s}$. Routines like VA10AD and others like it (LMDIF in the MINPAK subroutine library [GHM] and LEQT1F in the IMSL subroutine library [IML]) that use discrete derivative approximations to approach a solution have trouble with this and will occasionally give solution vectors which do not correspond to minimal function values. A solution to this problem is to fix one of the elements x_i and to allow the minimization

routine to vary the remaining elements. This method has given reliable results. The following algorithm was used:

> Given a starting vector $\underline{x}$, x_0 is fixed and x_1 and x_2 are varied to give a minimum function. If the starting vector has an x_0 that is zero, x_1 is fixed and x_0 and x_1 are varied. If the starting values of x_0 and x_1 are zero, then x_2 is fixed and x_0 and x_1 are allowed to vary.

Note that $x_0 = x_1 = x_2 = 0$ is excluded as a possible starting vector due to the requirement that the signal norm have a value of one.

The minimization of F_2 when C was not zero or one was found to be numerically difficult. The reasons for this are as follows: let $\underline{s}_{del}$, $\underline{s}_{snr}$, and $\underline{s}_{dif}$ be the signal vectors associated with a minimum F_{del}, a maximum F_{snr}, and a minimum F_{dif} respectively. It turns out that $F_{del}(\underline{s}_{snr})$ is approximately 10^{10}, while $F_{snr}(\underline{s}_{del})$ is approximately ten. Under these conditions and with the resolution of double precision numbers in FORTRAN, the $\underline{s}$ that minimizes F_1 for any value of C slightly more than zero becomes $\underline{s}_{del}$. F_{dif} was created as an alternative to F_{del} because of this problem. F_{dif} has several desirable characteristics as compared to F_{del}:

1. $F_{dif}(\underline{s}_{snr}) \approx 100$, allowing for a smoother change in the solution vector $\underline{s}$ as C is varied.

2. If W_{min} is set to 1.0, $\underline{s}_{dif} = \underline{s}_{del}$ and both functions will have a minimum value of zero for the three noise processes investigated.

4.3 ROBUST FILTER RESULTS.

To recapitulate, the hypothesis in this chapter is that the robustness of a MAMF, measured by increased normalized NSNR m and decreased NSNR σ can be traded off against maximum SNR. The three following test cases will show this.

Note that in the discussions to follow, the Burg correlation estimator was used to generate the $w(q_{ij})$. The Burg estimator was used for two reasons. First, the correlation estimates it generates are non-negative definite. Second, the Burg estimator has relatively poor performance compared to the biased estimator (See Table 3) and it was thought interesting to see how much improvement in its performance could be obtained.

The first test case found the signal vectors $\underline{s}$ that minimized F_{dif} for eleven values of W_{min}, $0.0 \leq W_{min} \leq 1.0$ for the lowpass system. See Table 4 for the signal vectors. Then, for each $\underline{s}$, SNR^m and the normalized NSNR mean m and standard deviation σ for a simulated system as described in Section 3.2.2 was generated. See Figure 40 for a plot of SNR^m, normalized NSNR m and NSNR σ versus W_{min}.

Table 4. Lowpass signal vectors for different W_{min}

W min	Signal Vectors		
0.0	0.4825	0.1517	-.9873
0.1	-.0780	0.0098	-.9969
0.2	-.2056	-.1273	-.9703
0.3	-.3142	-.2588	-.9134
0.4	-.7821	-.3925	-.4841
0.5	-.6685	-.4699	-.5764
0.6	-.6036	-.5164	-.6075
0.7	-.5890	-.5504	-.5917
0.8	-.5761	-.5799	-.5761
0.9	-.7026	0.0160	0.7114
1.0	-.7071	0.0	0.7071

The two large tick marks on the left vertical axis correspond to the NSNR m and σ for the signal vector $\underline{s}_{max}$ used in Table 3. Note the transition of SNR^m from 6.3 to 1.3 as m increases and σ decreases. A high m and low σ implies that a MAMF is robust and indifferent to changes in the estimated correlation. Therefore, Figure 40 directly shows the trade-off between SNR^m and robustness. As mentioned previously, it is possible to have a system where the NSNR m is near one and σ near zero, as shown in Figure 40 for $W_{min} = 0$. The drawback of this system is, of course, the very low SNR^m.

As previously shown, the NSNR contour plots can be used to predict the relative performances of a MAMF/spectral estimator pair using a particular signal vector. In Figure 41, Figure 42, and Figure 43, the NSNR contour plot for the lowpass case using the first, fourth, and eleventh signal vectors of Table 4 are shown. Note from the first two figures that the robustness of the MAMF improves as the high NSNR ridge overlaps more with the correlation histogram ridge shown in Figure 26 on page 71. In Figure 43 the NSNR contour plot has become flat, corresponding to the case in Figure 40 where W_{min} is one, the NSNR m is one, and the NSNR σ is zero.

In the second and third test cases, the signal vectors $\underline{s}$ were found that minimized F_1 for eleven values of C, $0 \leq C \leq 1$, with W_{min} set to 0.75, for the lowpass and bandpass systems. See Table 5 and Table 6 for the signal

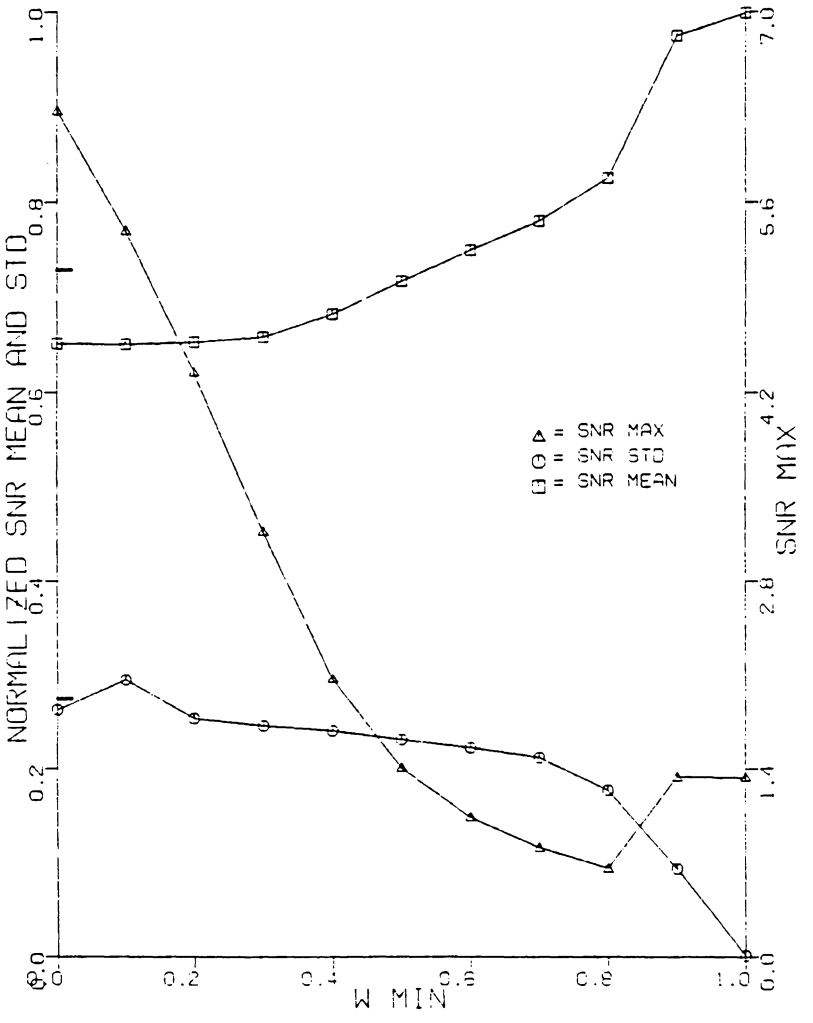

Figure 40. Lowpass performance as W_{min} is varied.

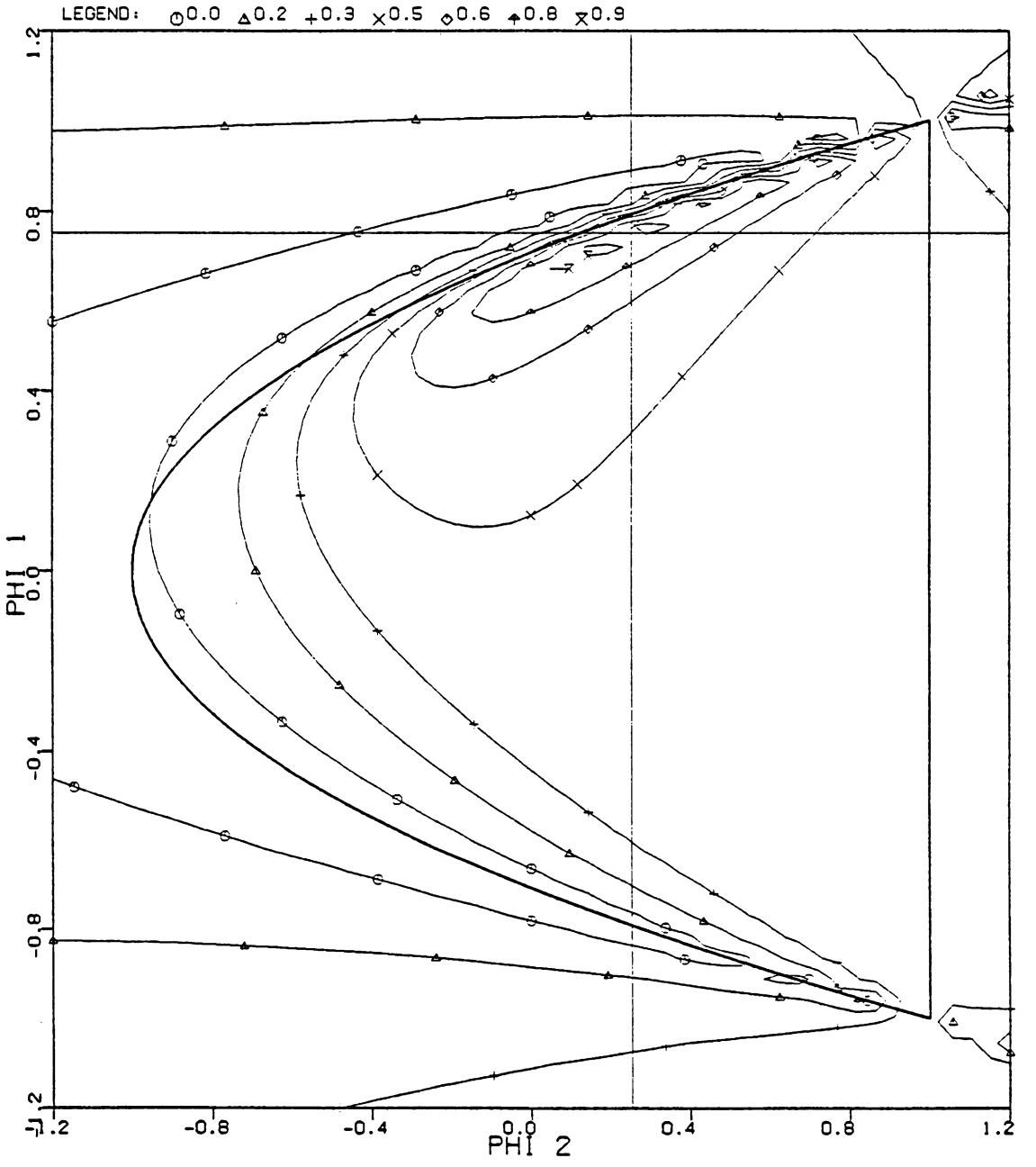

Figure 41. Lowpass for W_{min}, 1st signal vector.

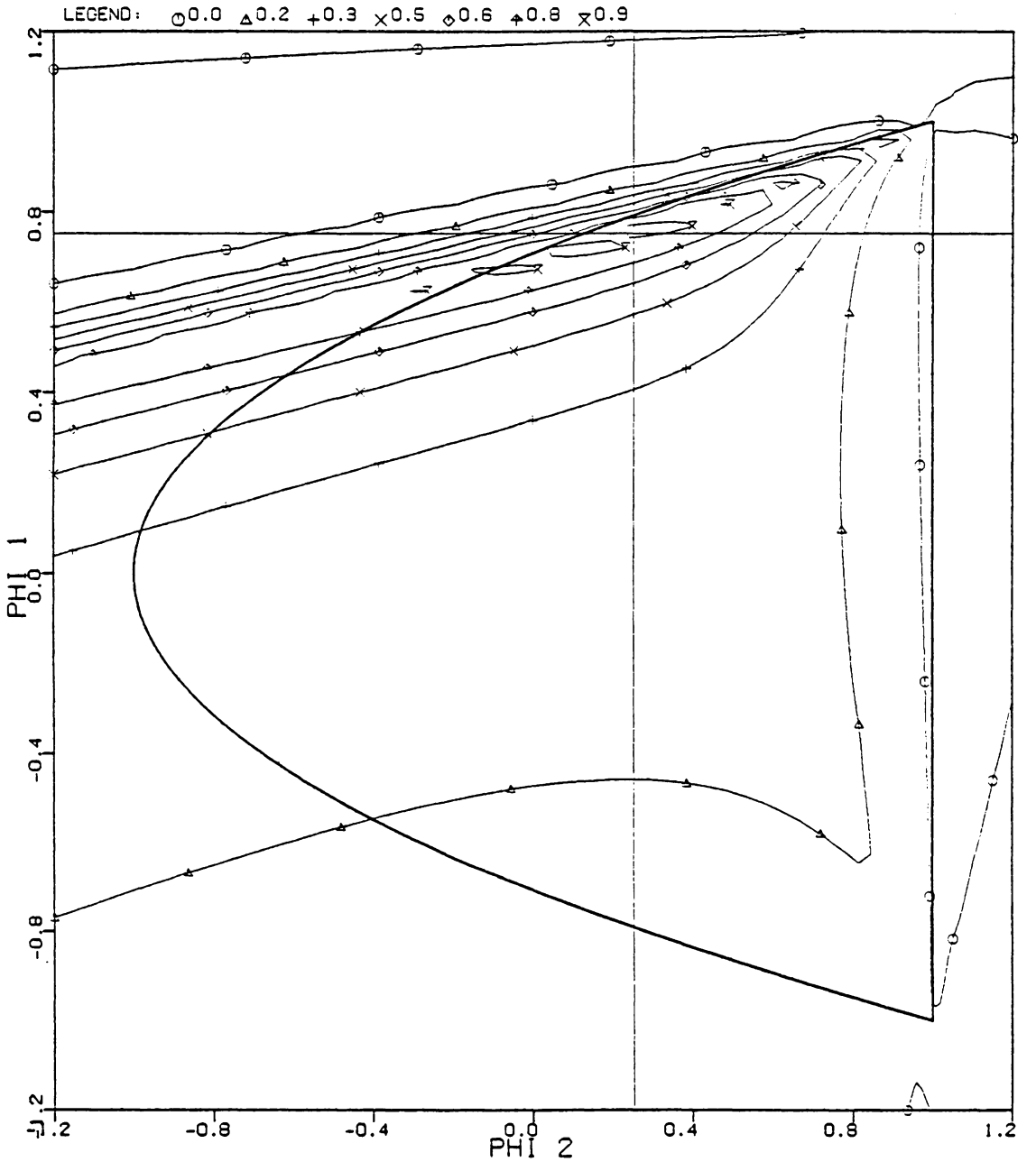

Figure 42. Lowpass for W_{min}, 4th signal vector.

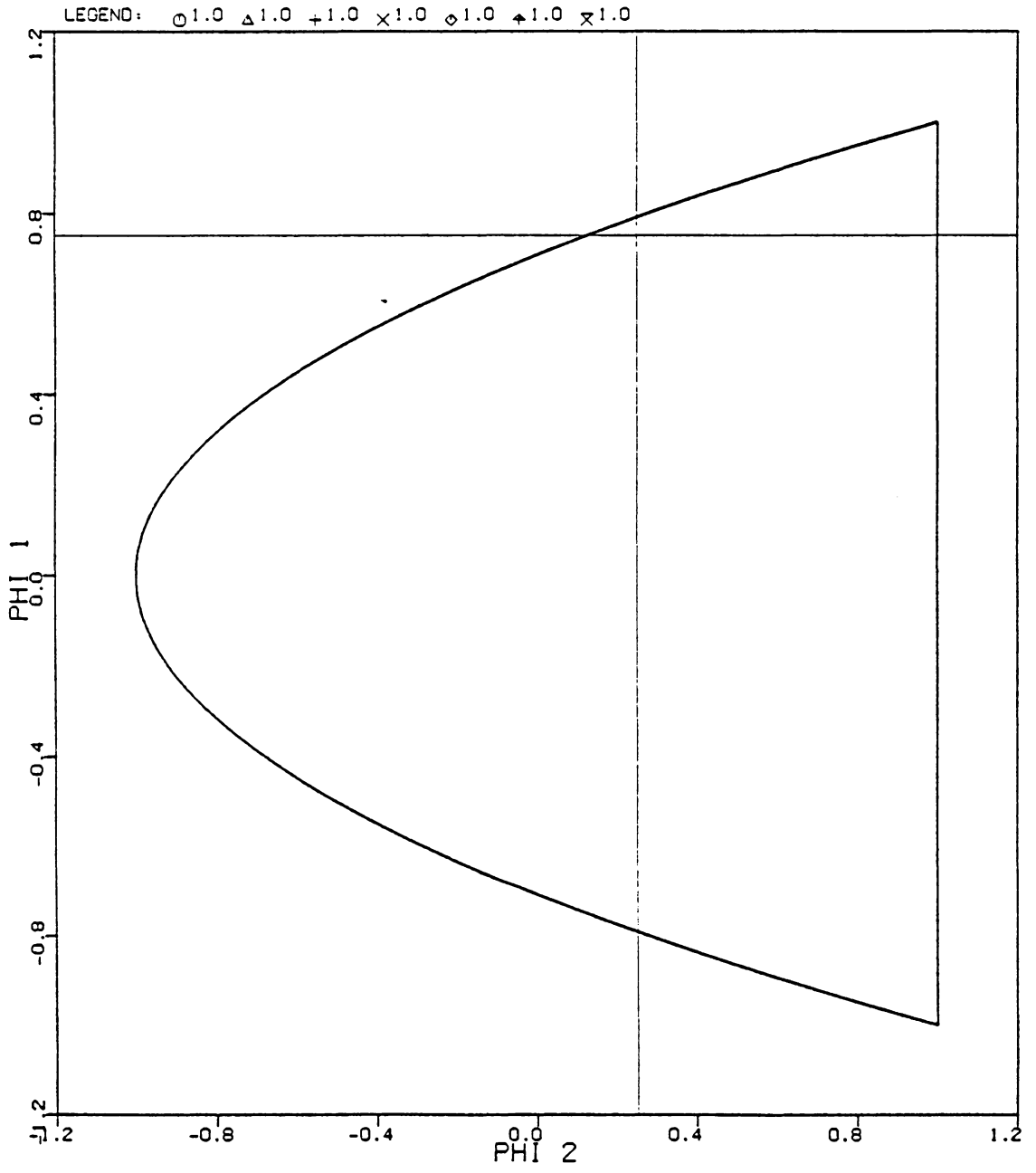

Figure 43. Lowpass for W_{min}, 11th signal vector.

vectors. SNR^m, NSNR m, and NSNR σ were found for each $\underline{s}$ and the data plotted versus C (Figure 44 and Figure 45). Figure 46 to Figure 48 and Figure 49 to Figure 51 show the NSNR contour plots for the first, fourth, and eleventh signal vectors of Table 5 and Table 6 for the lowpass and bandpass systems, respectively. As seen in Figure 44 and Figure 45, SNR^m decreases, NSNR m increases, and NSNR σ decreases as C increases, again showing the trade-off between robustness and performance. The NSNR m and σ from Table 3 on page 83 are marked on the left vertical axis with large tick marks. Note that for C = 0, F_{snr}, the average SNR with respect to the probability weighting function $w(q_{ij})$, is being maximized. Note that case yields signal vectors $\underline{s}$ close to the maximum MAMF output SNR signal vectors given in Table 1 on page 51. The contour plots for the first, fourth, and eleventh signal vectors are given in Figure 46 to Figure 48 for the lowpass system and Figure 49 to Figure 51 for the bandpass system. Once again, the more robust filters have NSNR contour plots that have wide maximums over the areas of the correlation histograms (Figure 26 for the lowpass system and Figure 34 for the bandpass system).

Table 5. Lowpass signal vectors for different C.

C	Signal Vectors		
0.0	-.4262	0.7980	-.4262
0.1	-.3970	0.8289	-.3940
0.2	0.0856	-.9926	0.0856
0.3	0.0856	-.9926	0.0856
0.4	0.0631	-.9960	0.0631
0.5	0.0856	-.9926	0.0856
0.6	0.0856	-.9926	0.0856
0.7	-.6987	0.0295	0.7148
0.8	-.5850	-.5618	-.5850
0.9	-.5839	-.5640	-.5839
1.0	-.5822	-.5675	-.5822

Table 6. Bandpass signal vectors for different C.

C	Signal Vectors		
0.0	-.4931	0.7167	-.4931
0.1	-.4715	0.7453	-.4714
0.2	-.4437	0.7787	-.4435
0.3	-.4436	0.7787	-.4436
0.4	-.4086	0.8162	-.4086
0.5	-.5755	-.5818	-.5747
0.6	-.5751	-.5818	-.5751
0.7	-.5751	-.5818	-.5751
0.8	-.5750	-.5818	-.5752
0.9	-.5752	-.5818	-.5750
1.0	-.5751	-.5818	-.5751

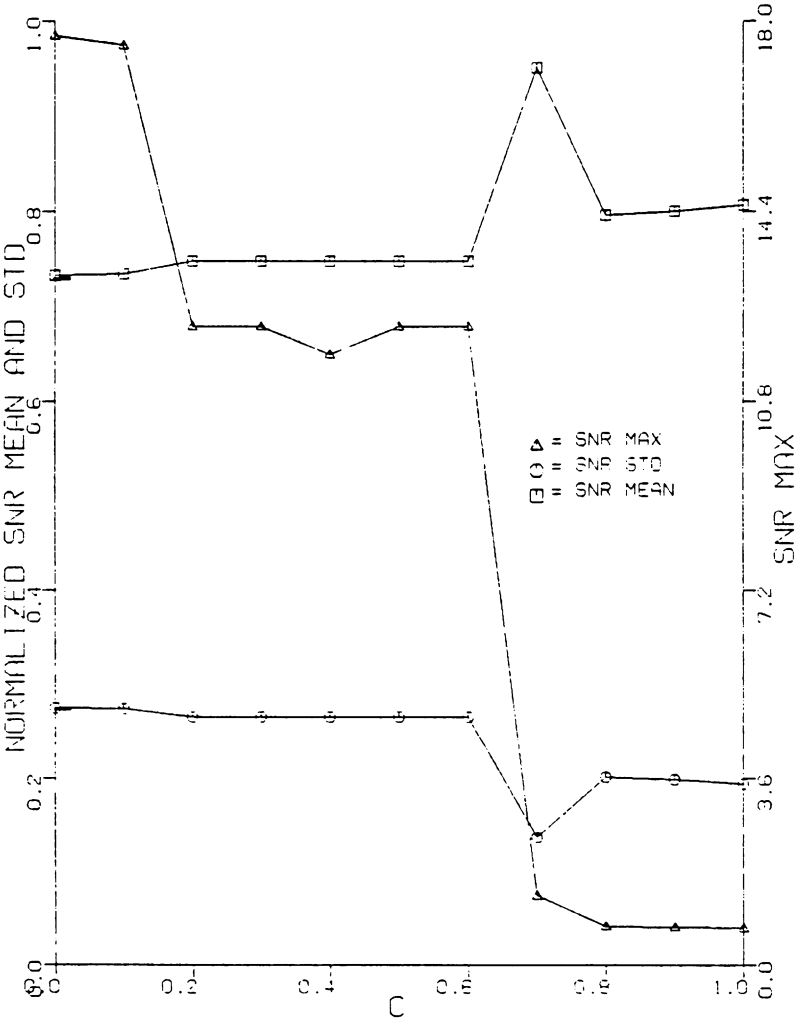

Figure 44. Lowpass performance as C is varied.

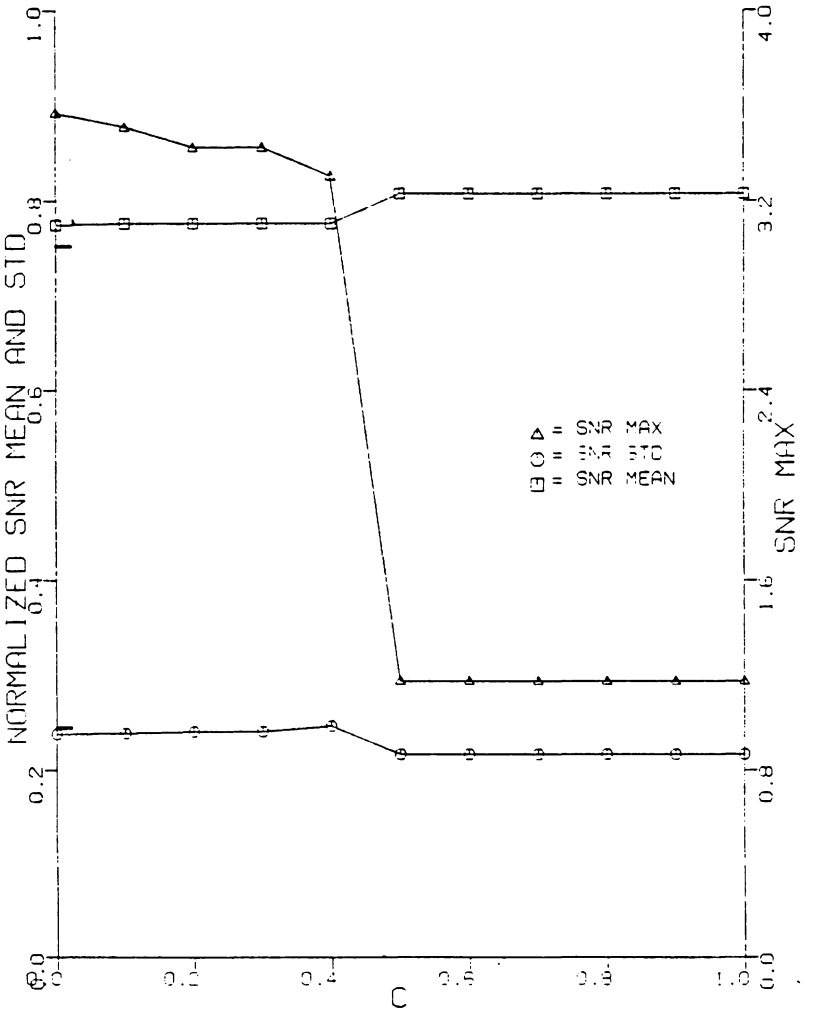

Figure 45. Bandpass performance as C is varied.

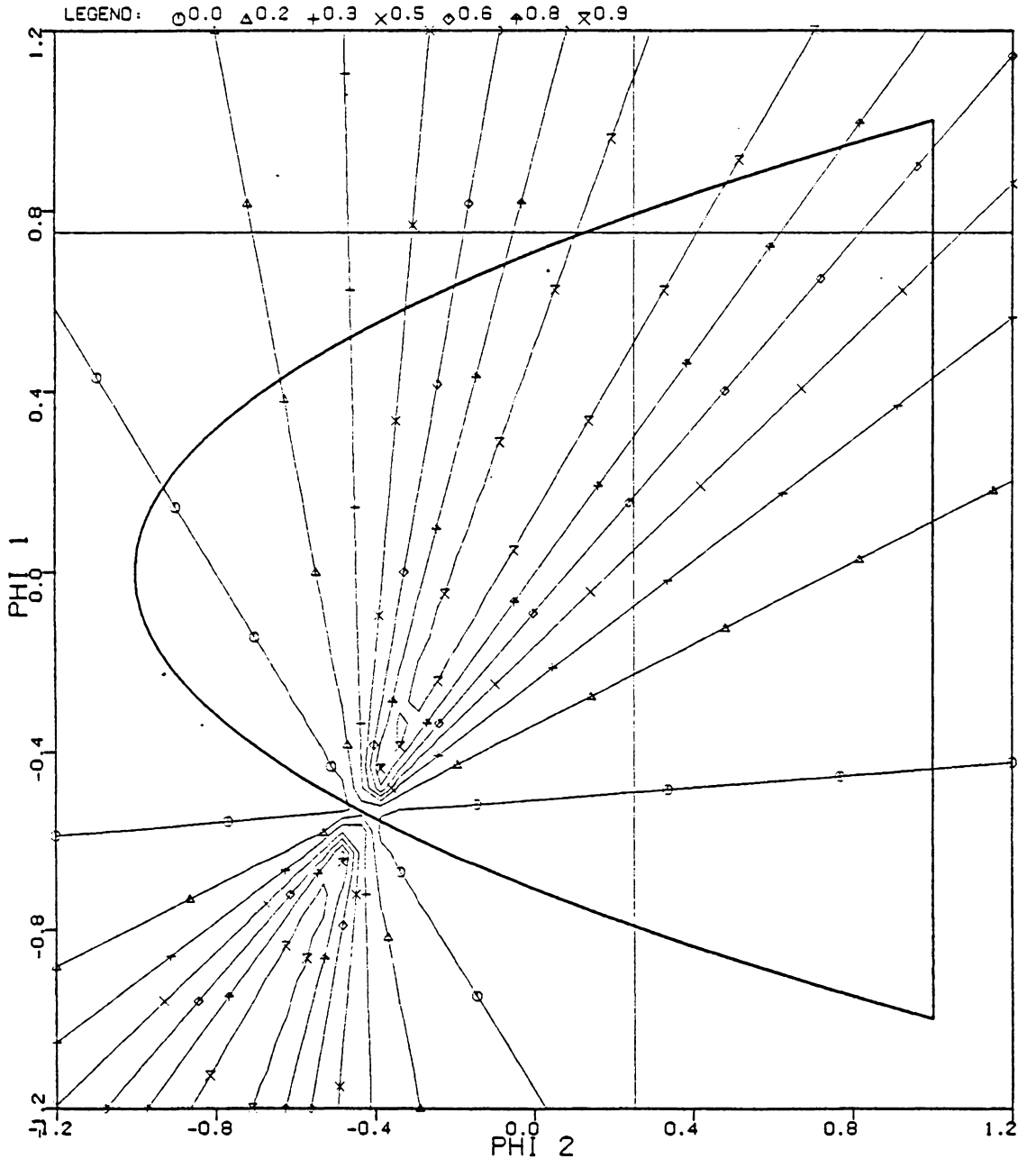

Figure 46. Lowpass for C, 1st signal vector.

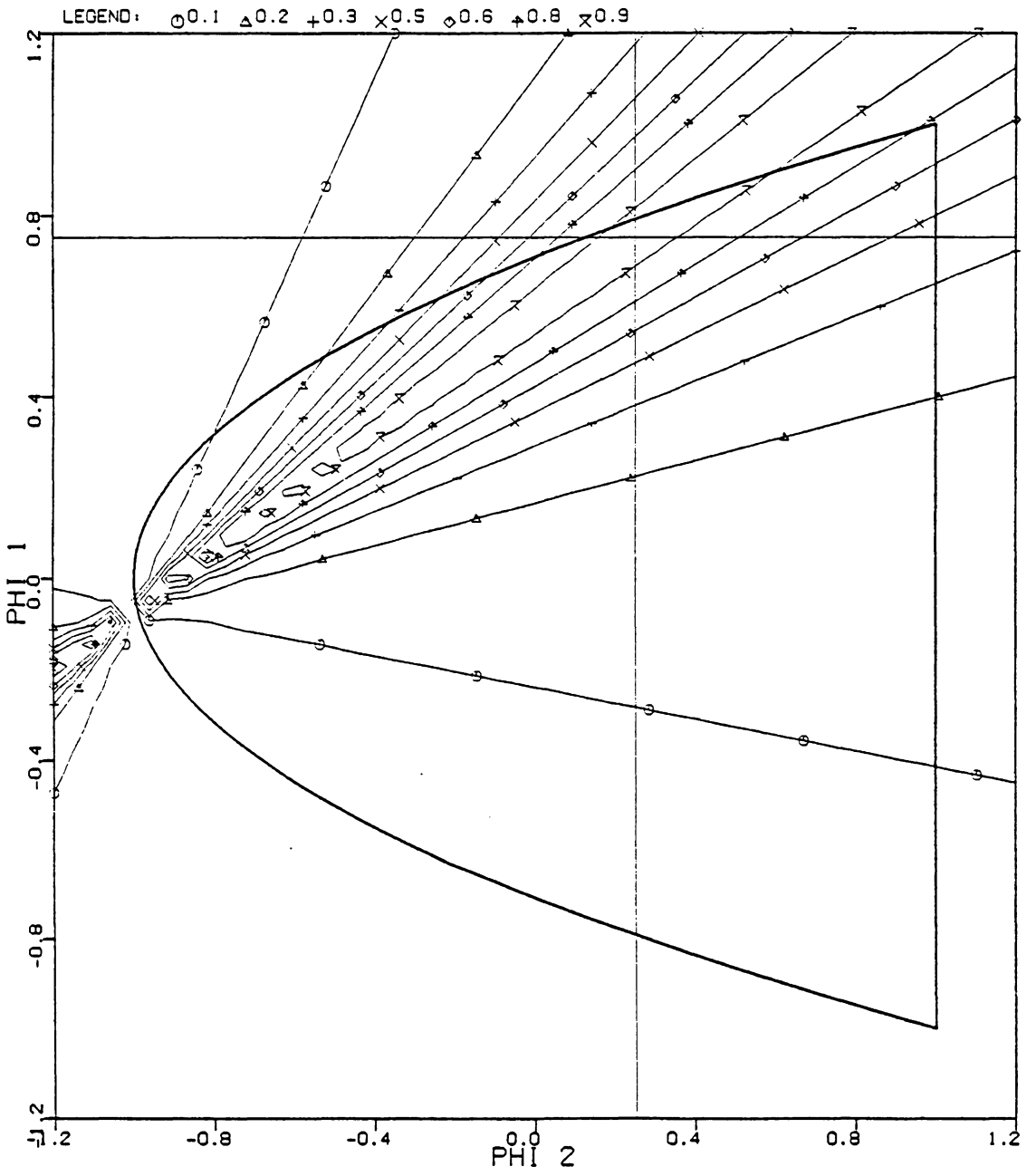

Figure 47. Lowpass for C, 4th signal vector.

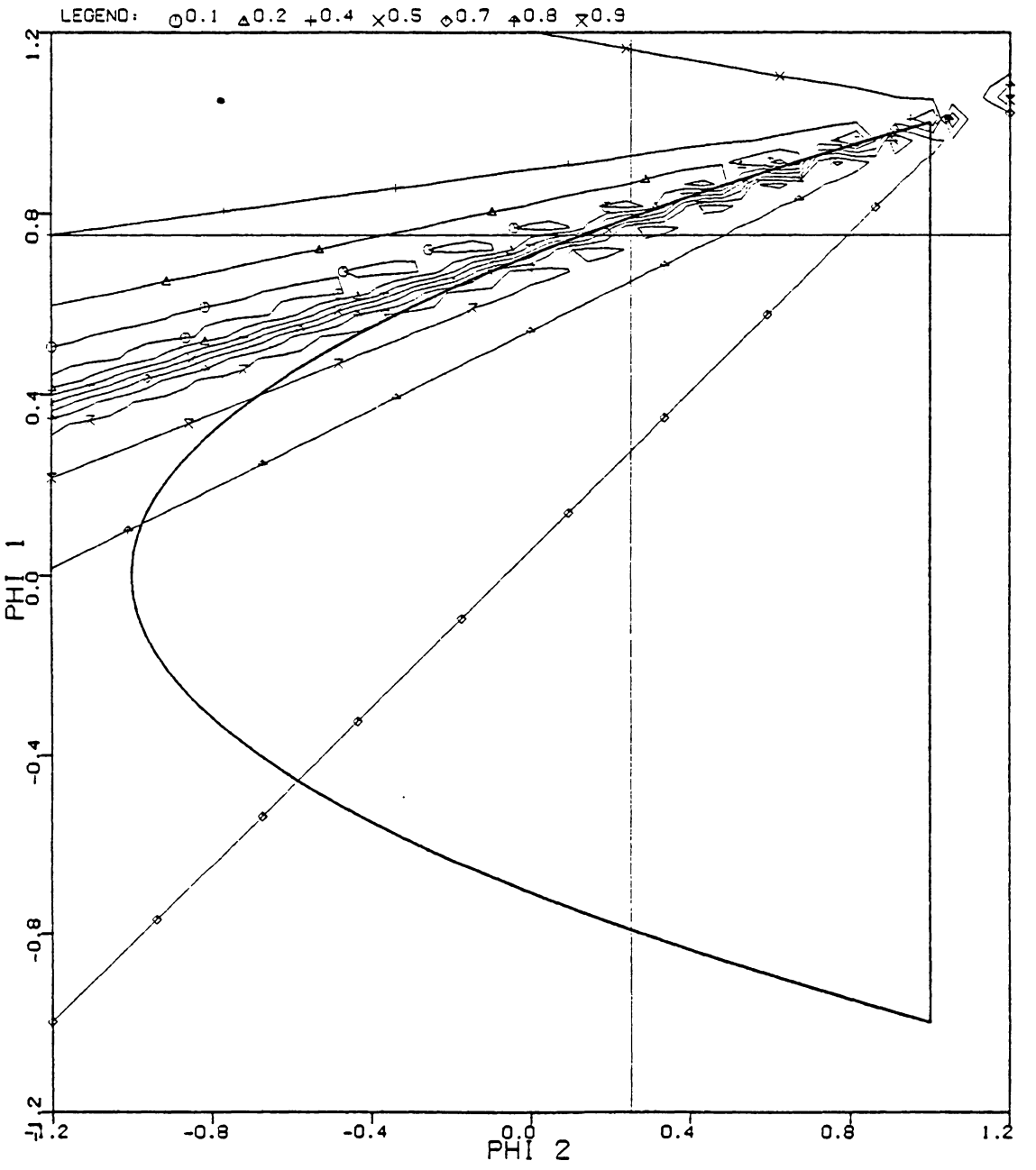

Figure 48. Lowpass for C, 11th signal vector.

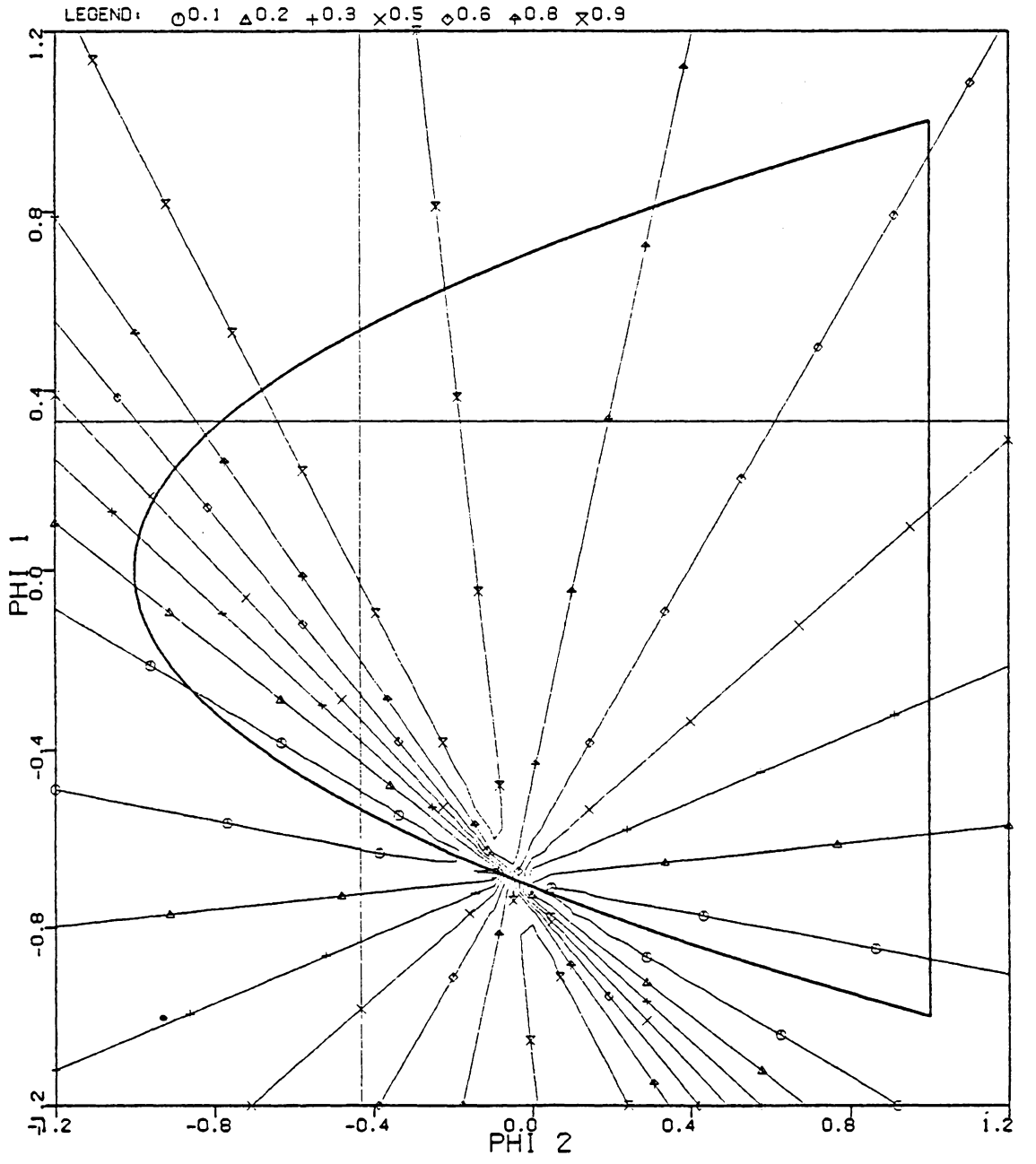

Figure 49. Bandpass for C, 1st signal vector.

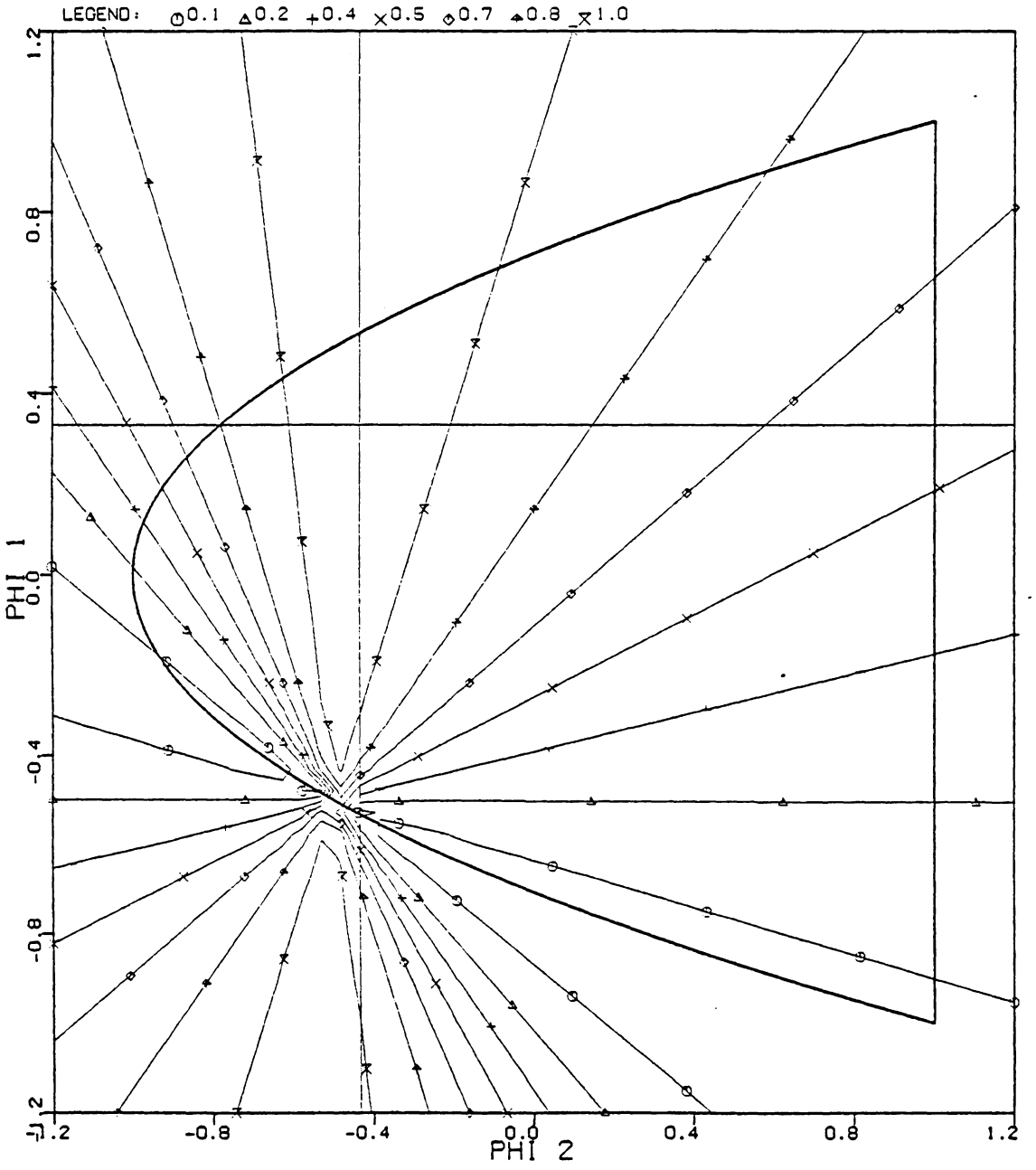

Figure 50. Bandpass for C, 4th signal vector.

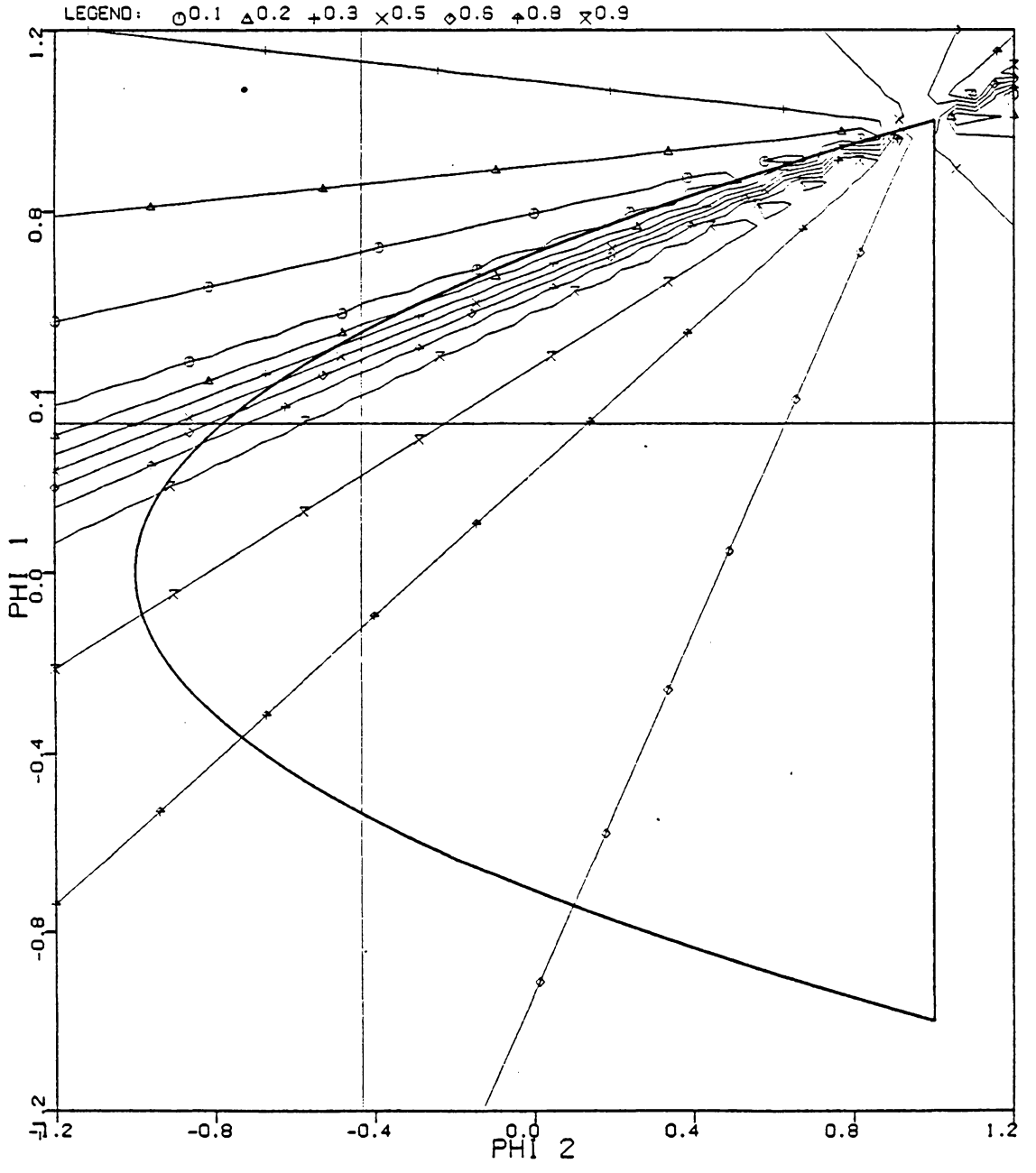

Figure 51. Bandpass for C, 11th signal vector.

5.0 CONCLUSION.

In this thesis, a thorough study of the theoretical characteristics of MAMF's and spectral estimators was performed. A simulation system was then devised that allowed the performance of MAMF's using several different spectral estimators to be compared. Comparisons of MAMF's in different noise environments and with different spectral estimators were executed and analyzed. Finally, several methods of generating robust MAMF's on the basis of correlation estimator histograms were devised and tested. Some conclusions can now be drawn.

When designing a MAMF in a low input SNR environment, it is important to avoid the use of spectral estimators that are not guaranteed to be NND. In fact, it is probably better to use a spectral estimator that biases estimated correlation sequences away from the NND boundary. If an estimated correlation sequence that is near the NND boundary is used to design a MAMF, it is possible for that MAMF to have a very poor output SNR, as was shown in Chapter 3.2. Further, if the estimate is on the NND boundary, problems will be encountered inverting the Toeplitz correlation matrix, since that matrix will be singular [GMS]. Conversely, using correlation estimates that are bounded away from the NND boundary does not necessarily reduce the output SNR of a

MAMF, since many correlation sequence estimates may still result in a MAMF with maximum output SNR (Equation 93 on page 39). Finally, it is seen that signal selection is important in designing a MAMF for a noisy environment, the more so as the actual correlation approaches the NND boundary. Since the maximum output SNR of a MAMF is $1/\lambda_N$, where λ_N is the minimum eigenvalue of the correlation matrix Φ (Equation 85), the closer Φ approaches the NND boundary where λ_N is zero, the greater the maximum MAMF output SNR. If a signal is chosen that is greatly different from the eigenvector associated with the minimum eigenvalue of Φ in such a case, the MAMF output SNR can be seriously degraded. If, in the above case, the noise environment is non-stationary, it would be advisable to provide a means of changing the signal vector as time progresses.

A possible solution to the problem of a non-stationary noise environment can now be outlined as follows: during operation of a system using a MAMF, correlation sequence estimates could be made intermittently. After normalization, these estimates could be placed into a correlation histogram whose older members are forgotten. Short correlation sequences could be used; further note that the histogram would be in N-1 dimensions, where N is the length of the signal vector. If the environment became more noisy, the histogram would be expected to spread out; if the noise environment changed the histogram would shift towards the new

Φ_a, eventually reaching Φ_a as the older correlation sequences were forgotten. If a signal vector generated by one of the methods given in Chapter 4.2.2 were used to design the MAMF, a robust system would result. While the maximum output SNR of such an adaptive system would drop initially upon the change in actual correlation, it would probably not drop as far as a system which simply uses an average of the correlation estimates.

A future project to be considered would be the efficient implementation of such an adaptive system, and comparison of the performance of this system with other methods of generating robust filters that have appeared in the literature.

BIBLIOGRAPHY.

[AFS] G.A. Arrendondo, J.C. Feggeler, and J.I. Smith, "Advanced Mobile Phone Service: Voice and Data Transmission," Bell System Technical Journal, vol. 58, no.1, pp. 97-122, Jan. 1979.

[AOS] A. Oppenheim and R. Schafer, Digital Signal Processing, New Jersey: Prentice Hall, 1975.

[BCB] K.A. Becker and A.A. Beex, "The Effects of Spectral Estimation on Matched Filter Design," 27th Midwest Symposium on Circuits and Systems, June 11-12, 1984, Morgantown, WV, pp. 211-214.

[BEB] A.A. Beex and K.A. Becker, "Spectral Estimation and Matched Filter Performance," IEEE International Conference on Acoustics, Speech, and Signal Processing (ICASSP '84), March 19-21, San Diego, CA., pp. 31.4.1-4.

[CGS] C. Gueguen and M. Sidahmed, "Sur la prediction lineaire dans le cas singulier," Colloque CNRS, Aussois, Sept. 1981.

[CMG] Cooper, G.R. and McGillem, C.D., Probabilistic Methods of Signal and System Analysis, New York: Holt, Rinehart and Winston, 1971, pp. 146.

[CTC] C. Chen, Introduction to Linear System Theory, New York: Holt, Rinehart and Winston, 1970, pp. 409.

[DBS] J.P.Dugre, A.A. Beex, and L.L. Scharf, "Generating covariance sequences and the calculation of quantization and rounding error variances in digital filters," IEEE Transactions on Acoustics, Speech, and Signal Processing, vol. ASSP-28, pp. 102-104, Feb. 1980.

[DMB] D.M. Boroson, "Sample Size Considerations for Adaptive Arrays," IEEE Transactions on Aerospace and Electronic Systems, vol. AES-16, no. 4, pp. 446-451, Jul. 1980.

[DON] D.O. North, "Analysis of the factors which determine signal/noise discrimination in radar," RCA Labs., Princeton, N.J., Rep. PTR-6C, June 1943; reprinted in Proc. IRE, vol. 51, pp. 1016-1028, July 1963.

[HVP] H.V. Poor, "Robust Matched Filters," IEEE Transactions on Information Theory, vol. IT-29, no. 5, pp. 677-687, Sept. 1983.

[IML] User's Manual, IMSL Library, Houston: IMSL, Edition 9.2, Chapters 'G' and 'M', Nov. 1984.

[GHM] B.S. Garbow, K.E. Hillstrom, and J.J. More, "Implementation Guide for MINPACK-1," Argonne, Ill.: Argonne National Laboratory, ANL-80-68, July, 1980.

[GMS] C. Gueguen and M. Sidahmed, "The singular case and robust linear prediction," 1982 IEEE International Conference on Acoustics, Speech, and Signal Processing (ASSP-82), May 3-5, Paris, France.

[JAC] J. A. Cadzow, "Generalized Digital Matched Filtering," 12th Annual Southeastern Symposium on System Theory, Virginia Beach, VA, May 19-20, 1980, pp. 307-312.

[JGA] J.G. Allen, "Maximum Entropy Spectral Analysis," Astronomy and Astrophysics Supplemental Series, vol. 15, pp. 383-393, 1974.

[JMA] J. Makhoul, "On the Eigenvectors of Symmetric Toeplitz Matrices," IEEE Transactions on Acoustics, Speech, and Signal Processing, vol. ASSP-29, no. 4, pp. 868-872, August 1981.

[JMB] J. Makhoul, "Stable and Efficient Lattice Methods for Linear Prediction," IEEE Transactions on Acoustics, Speech, and Signal Processing, vol. ASSP-25, No. 5, pp. 423-428, October 1977.

[KVM] T. Kailath, A. Vieira, and M. Morf, "Inverses of toeplitz operators, innovations, and orthogonal polynomials," Siam Review, vol. 20, no. 1, pp. 106-119, Jan. 1978.

[KVP] S.A. Kassam and H.V. Poor, "Robust Signal Processing for Communications Systems," IEEE Communications Magazine, Jan. 1983, pp. 20-28.

[MBT] A.B. Martinez and J.B. Thomas, "Finite Length Discrete Matched Filters," Nineteenth Annual Allerton Conference on Communication, Control, and Computing, Sept. 30 - Oct. 2, 1981.

[MGC] C.D. McGillem and G.R. Cooper, Continuous and Discrete Signal and System Analysis, New York: Holt, Rinehart and Winston, 1984, pp. 149.

[MIS] M.I. Skolnik, Introduction to Radar Systems, New York: McGraw-Hill, 1980, 369-375.

[MJH] M.J. Hopper, The Harwell Subroutine Library, A Catalogue of Subroutines (1973), Harwell, England: Theoretical Physics Division U.K.A.E.A. Research Group, Atomic Energy Research Establishment, Harwell, July, 1973.

[MSB] M.S. Bartlett, An Introduction to Stochastic Processes, 2nd ed., New York: Cambridge University Press, 1966.:

[PAP] A. Papoulis, Probability, Random Variables, and Stochastic Processes, New York: McGraw-Hill, 1984, pp. 298-310.

[RBG] L. Rabiner and B. Gold, Theory and Application of Digital Signal Processing, New Jersey: Prentice-Hall, 1975, pp.748-751.

[RMB] I.S. Reed, J.D. Mallett, and L.E. Brennan, "Rapid Convergence Rate in Adaptive Arrays," IEEE Transactions on Aerospace and Electronic Systems, vol. AES-10, no. 6, pp. 853-863, Nov. 1974.

[SBU] S. Buchner, Harmonic Analysis and the Theory of Probability, Berkeley: University of California Press, 1955, pp. 57-59.

[VPK] V.P. Kuznetsov, "Stable Detection When the Signal and the Spectrum of Normal Noise are Inaccurately Known," Telecommunications and Radio Engineering, vol. 30/31, pp. 58-64, March 1976.

[WBT] M.D. Wood and J.B. Thomas, "A Computationally Efficient Approximation to a Discrete-Time Matched Filter," IEEE Transactions on Aerospace and Electronic Systems, vol. AES-16, no. 5, pp. 648-655, Sept. 1980.

[WVS] W.V. Snyder, "Algorithm 531 Contour Plotting, [J6]," ACM Transactions on Mathematical Software, vol. 4, no. 3, pp. 290-294, Sept. 1978.

[ZHT] R.E. Ziemer and W.H. Tranter, Principles of Communications, Boston: Houghton Mifflin, 1976, pp. 308-346.

The vita has been removed from the scanned document